PHILOSOPHICAL TRANSACTIONS OF THE ROYAL SOCIETY A MATHEMATICAL, PHYSICAL & ENGINEERING SCIENCES

Transport and Heat Flux of the Florida Current at 27 degrees N Derived from Cross-Stream Voltages and Profiling Data: Theory and Observations

J. C. Larsen

Phil. Trans. R. Soc. Lond. A 1992 **338**, 169-236
doi: 10.1098/rsta.1992.0007

Transport and heat flux of the Florida Current at 27° N derived from cross-stream voltages and profiling data: theory and observations

By J. C. Larsen

Pacific Marine Environmental Laboratory, National Oceanic and Atmospheric Administration, Seattle, Washington 98115, U.S.A.

Contents

The variability in the volume transport of the Florida Current at 27° N has been observed from the voltage measured between a point 16 km east of Jupiter Inlet, Florida and Settlement Point, Grand Bahama Island by the use of an abandoned communications cable. The voltage is caused by the separation of electric charges in the ocean that are caused by the Florida Current crossing the Earth's magnetic field (motional induction), by the electric currents induced in the ocean caused by time

Phil. Trans. R. Soc. Lond. A (1992) **338**, 169–236
Printed in Great Britain

varying ionospheric and magnetospheric electric currents (geomagnetic induction), and by the voltage bias between the cable–ocean contacts caused by differences in the temperature, salinity and electrochemical state of the contacts. The geomagnetic-induced voltage was removed by the use of shore-based magnetic data and transfer functions. Changes in the voltage bias of the cable–ocean contact at Settlement Point were minimized by the use of a silver–silver-chloride electrode. The comparison of the daily mean motion-induced voltages with 137 daily profiling-derived transports, yields a voltage calibration factor of 24.42 ± 0.56 Sv V^{-1}, a correlation squared of 0.94, and a root mean square misfit of 0.77 Sv (1 Sv = 10^6 m^3 s^{-1}). The misfit is consistent with an error of 0.9 Sv in the voltage-derived transport estimated from the velocity and temperature profiling data, the electric current effects, and the profiling derived transport error. Hence the voltages accurately monitor the transport variations.

The mean voltage-derived transports for the Florida Current at 27° N is 32.3 ± 3.2 Sv based on 4862 daily mean values from 1969 to 1990. The annual variation has a range of 4.4 Sv. There is no evidence since 1969 for any long-term trend in the transport but there are numerous shorter term variations as large as 15 Sv lasting from days to months. The mean northward heat flux is 1.30 ± 0.13 PW derived from 130 days of profiling the velocity and temperature of the Florida Current and assuming the North Atlantic has a southward, velocity-weighted temperature of 9.4 °C. The variations in heat flux are, essentially, due to the variations in transport because the velocity weighted temperature estimated by the profiling data has a nearly constant value of 19.1 ± 0.6 °C.

Notation

The following is a list of symbols frequently used in the text.

x, y, z	rectangular coordinates with origin at the Florida coast for x horizontal and perpendicular to the stream, y downstream and parallel to the stream, and z vertically up from the sea surface
x_n	distance of nth profiling site from Florida Coast
L	width of strait
X	stream width
Y	downstream wavelength
H, H_0	water depth, effective water depth
V	downstream velocity
A	cross-sectional area of strait
$\Delta\phi$	cross-stream voltage
C, C_T	voltage and tidal calibration factors
$W, \boldsymbol{W}$	cable weighting factor, horizontal vector cable weighting factor
$\theta, \bar{\theta}, \tilde{\theta}$	*in situ* temperature, strait temperature, flow temperature
$S, \bar{S}, \tilde{S}$	salinity, strait salinity, flow salinity
σ, σ'	electrical conductivity of the ocean, and the sediments and conducting crust
$I', I*$	electric currents in the sediments and conducting crust, and in the land and ocean outside the stream
T, T_θ, T_S	volume transport, time varying temperature flux, time varying salinity flux

E	horizontal electric field
F_z	magnitude of vertical component of Earth's magnetic field
τ, τ', τ^*	conductance of the ocean, sediments and conducting crust; the sediments and conducting crust; and the land areas
ν	conductance ratio equal to the conductance of the ocean divided by the conductance of the ocean, sediments and conducting crust
$\bar{(\ )}$	depth-averaged value equal to $H(x)^{-1}\int_{-H(x)}^{0}(\ )\,\mathrm{d}z$ for $H \neq 0$ and zero otherwise
$\tilde{(\ )}$	velocity-weighted value equal to $[H(x)\,\bar{V}(x,t)]^{-1}\int_{-H(x)}^{0}(\ )\,V(x,z,t)\,\mathrm{d}z$ for $H\bar{V} \neq 0$ and zero otherwise
$\langle\ \rangle$	time-averaged value
ϵ	relative change in seawater conductivity due to changes in temperature and salinity
ϵ^*	relative change in cross-stream voltage due to electric current I^*

1. Introduction

The Florida Current is a major contributor to the circulation of the North Atlantic and to the transport of heat from the equator to higher latitudes (Hall & Bryden 1982). Monitoring the transport variations will therefore provide an important time series for the verification of ocean circulation models and for the study of climate variability.

Cross-stream voltages are equal to a spatial integral over the flow and are observable on a continuous basis. They can provide, for suitable cable positions, accurate estimates of the variations in transport. Current meter mooring and profiling observations require, however, a dense sampling in time and space for accurate transport measurements. They are, therefore, generally not feasible for monitoring transport but are extremely valuable for evaluating the cable site and for calibrating the voltages.

Recordings of the voltage variations across the Straits of Florida began in 1969 and ended in 1974 (Sanford 1982) making use of an abandoned cable between Jupiter Inlet, Florida and Settlement Point, Grand Bahama Island (figure 1). The recordings were then resumed in late 1981 as part of the Subtropical Atlantic Climate Studies program (STACS). The voltages since 1981 have been measured between the exposed, centre copper conductor of the abandoned cable at the cable break, 16 km east of Jupiter Inlet and a silver–silver-chloride electrode at Settlement Point. Nearly 14 years of data have been obtained.

The purpose of this paper is to describe the procedures used to reduce the observed cross-stream voltages to daily mean transports, to give a physical interpretation of the different terms that can produce temporal variations in the cross-stream voltages, to experimentally justify the linear relation used to convert voltage to transport, and to describe the temporal variations in the transport and heat flux of the Florida Current.

The problems that have discouraged the use of voltage measurements for monitoring transport variations have been: the contamination of the voltages by geomagnetic-induced variations; the lack of independent estimates of the transport variations for determining the voltage calibration factor and for validating the voltage-transport relation; the instability of the cable–ocean contacts; the possible sensitivity of the voltages to meanders of the stream; the role of the electric currents;

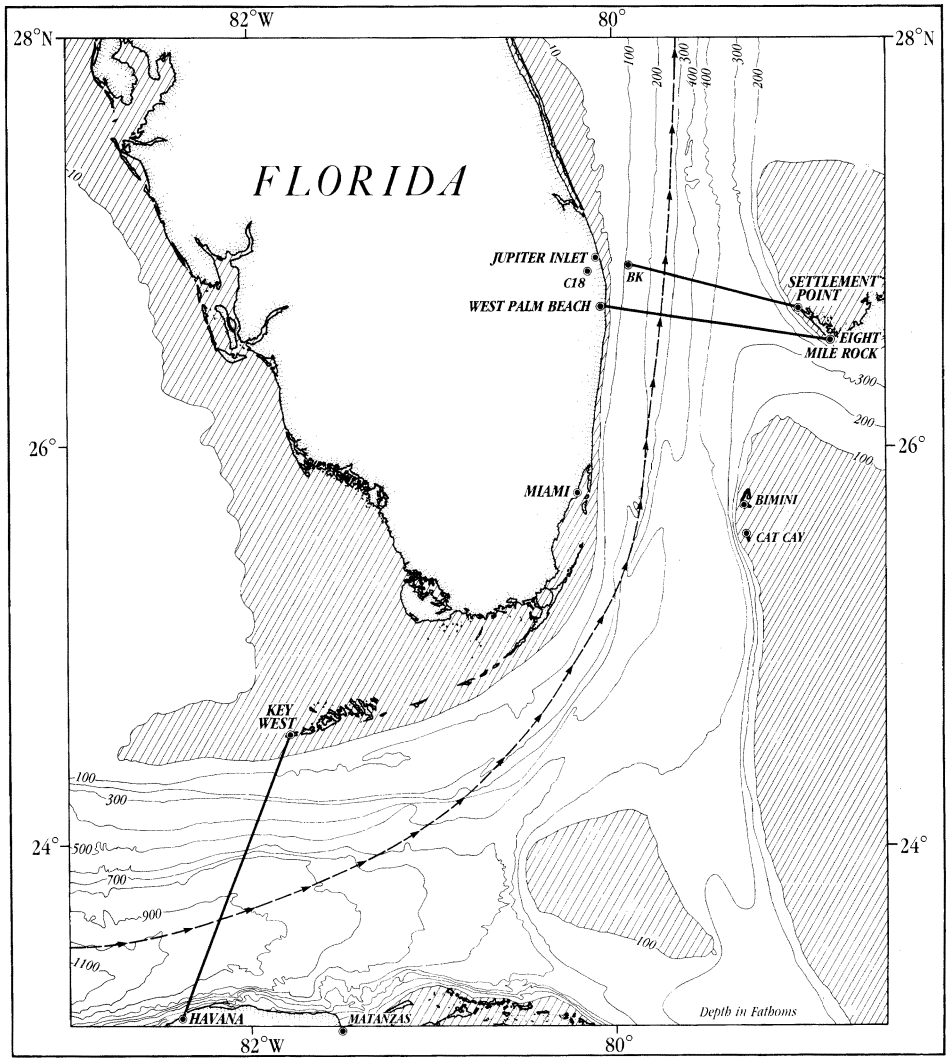

Figure 1. Cables connect Key West to Havana, West Palm Beach to Eight Mile Rock, Jupiter Inlet to BK, and BK to Settlement Point (solid lines). Profiling sections are from Key West to Matanzas, Miami to Bimini and Jupiter Inlet to Grand Bahama Island. Tides stations have been at Key West, Havana, Miami, Cat Cay and Settlement Point. Axis of Florida Current is dashed line with arrows. Depth in fathoms.

and the influence of the conducting sediments and crust. Section 2 derives the voltage-transport equation used for the interpretation of the motion-induced voltages. Section 3 discusses the profiling-derived transports and temperatures of the Florida Current. These are used to estimate the error in the voltage-derived transports. This section also describes the various voltage measurements made across the Straits of Florida; discusses the corrections needed to reduce the voltages to the daily mean, motion-induced voltages; and estimates the voltage calibration factors and voltage bias of the various voltage time series. The voltage-derived transports are then compared with the current meter mooring derived transports,

PHILOSOPHICAL TRANSACTIONS OF THE ROYAL SOCIETY A MATHEMATICAL, PHYSICAL & ENGINEERING SCIENCES

the sea level data, and the general circulation model transports driven by monthly winds over the Atlantic. Section 4 gives estimates of the conductance of the sediments, the tidal induced horizontal electric currents and the tidal downstream wavelengths. Section 5 describes the various temporal variations found in the Florida Current transports and estimates the heat flux of the Florida Current.

2. Electromagnetic theory

The electromagnetic theory of motional induction applied to ocean streams has been developed over the past 40 years by Stommel (1948), Longuet-Higgins (1949), Malkus & Stern (1952), Longuet-Higgins *et al.* (1954), Wertheim (1954), Cox *et al.* (1970), Larsen (1968, 1973), Sanford (1971, 1982), Sanford & Schmitz (1971), Sanford & Flick (1975), Robinson (1976, 1977), Baines & Bell (1987), Larsen & Sanford (1985), Spain & Sanford (1987) and Chave & Luther (1990).

These studies show that the voltage $\Delta\phi$ measured between the two cable–ocean contacts consists of three time-varying parts

$$\Delta\phi(t) = \Delta\phi_V(t) + \Delta\phi_G(t) + \Delta\phi_N(t). \tag{2.1}$$

The motion-induced voltage $\Delta\phi_V$ is caused by the separation of electric charges in the ocean that are caused by the Florida Current crossing the Earth's magnetic field. These charges concentrate along the gradients in the conductivity and fluid motion and create a cross-stream electric field. If the charges are not uniform in the downstream direction, then a downstream electric field is also created. The geomagnetic-induced voltage $\Delta\phi_G$ is caused by electric currents induced in the ocean by the time varying horizontal electric currents in the ionosphere and magnetosphere. The bias voltage $\Delta\phi_N$ is caused by the differences and changes in the temperature, salinity and electrochemical state of the cable–ocean contacts.

(*a*) *Local motion-induced voltages*

The motion-induced voltages can be split into two parts (Sanford 1971) as

$$\Delta\phi_V(t) = \Delta\phi_{\mathrm{L}}(t) + \Delta\phi_I(t), \tag{2.2}$$

where $\Delta\phi_{\mathrm{L}}$ is the local motion-induced voltage caused by the fluid motion near the cable and $\Delta\phi_I$ is caused by the horizontal electric current I*. It is created by a downstream electric field due to downstream changes in the direction and speed of the fluid motion, changes in the conductivity and topography of the ocean and sediments, or by remote fluid motion. The interpretation of $\Delta\phi_I$ therefore requires a study of the fluid motion over a region surrounding the cable–ocean contacts (Sanford 1971; Robinson 1976; Baines & Bell 1987).

(i) *Sanford voltage equation*

The local motion-induced, cross-stream voltages for wide ocean streams (Sanford 1971) is

$$\Delta\phi_{\mathrm{L}}(t) = \int_0^L [F_z(x)/\tau(x,t)] \int_{-H(x)}^0 \sigma(x,z,t)\, V(x,z,t)\, \mathrm{d}z\, \mathrm{d}x \tag{2.2a}$$

that can be written as

$$\Delta\phi_{\mathrm{L}}(t) = \int_0^L [F_z(x)\, \tilde{\sigma}(x,t)/\tau(x,t)]\, H(x)\, \bar{V}(x,t)\, \mathrm{d}x \tag{2.3}$$

where L is the width of the strait at the cable location. The various terms in (2.3) are: F_z, the magnitude of the vertical component of the Earth's magnetic field;

$$\bar{V}(x,t) = H(x)^{-1} \int_{-H(x)}^{0} V(x,z,t)\,\mathrm{d}z, \tag{2.4}$$

the depth-averaged downstream velocity;

$$\tilde{\sigma}(x,t) = [H(x)\ \bar{V}(x,t)]^{-1} \int_{-H(x)}^{0} \sigma(x,z,t)\,V(x,z,t)\,\mathrm{d}z, \tag{2.5}$$

the time-dependent, velocity-weighted value of the conductivity σ of the ocean;

$$\tau(x,t) = \bar{\sigma}(x,t)\,H(x) + \tau'(x) \tag{2.6}$$

the time-dependent conductance of the ocean, sediments and upper conducting crust; $\bar{\sigma}$, the time-dependent, depth-averaged conductivity of the ocean; and τ', the conductance of the sediments and upper conducting crust beneath the ocean down to a resistive zone at depth H'. Throughout this paper the use of the term sediments by itself implies the sediments and the conducting crust beneath the sediments.

The Sanford voltage equation (2.2a) assumes that the downstream spatial wavelengths Y of the time varying fluid motion, the depth, the conductivity, and the Earth's magnetic field, are all much larger than the stream width X. The vertical velocity and horizontal component of the Earth's magnetic field can then be ignored. Equation (2.2a) also assumes that the frequency and spatial scales are small so that self and mutual induction can be ignored. This assumption is valid for most ocean currents excluding deep ocean tides and basin-wide planetary motions (Larsen 1968; Chave & Luther 1990). Finally, equation (2.2a) assumes that the stream is wide compared with the depth H' of the resistive zone but not so wide that the amount of electric current flowing into the resistive zone cannot be ignored. The resistive zone can then be approximated by an insulator.

Recent evidence in the eastern Pacific (Cox *et al.* 1986; Chave *et al.* 1990) indicates that a highly resistive zone occurs beneath the ocean crust at a depth of 7 km with a conductivity smaller than $\sigma'' = 1 \times 10^{-5}$ S m^{-1} and layer thickness $H'' \approx 30$ km. The analysis of the electric current by the circuit model in §2c shows that the resistive zone approximates an insulator if the stream width is smaller than

$$X_{\max} = 2[(\sigma_0/\sigma'')\,H_0\,H'']^{\frac{1}{2}}.$$

It has the value $X_{\max} \approx 13400$ km for the open ocean where $\sigma_0 \approx 3$ S m^{-1} is a typical ocean conductivity and $H_0 \approx 5$ km is a typical ocean depth and the value $X_{\max} \approx 5250$ km for the Straits of Florida where $\sigma_0 = 4.6$ S m^{-1} and $H_0 = 0.5$ km. Thus equation (2.2a) can be used for most ocean streams as they are usually much wider than 7 km and much narrower than 5000 km. Then the attenuation of the local motion-induced voltage by the electric current depends only on the ocean and sediment conductances.

In summary, the Sanford voltage equation (2.2a) states that there is a cross-stream voltage that depends on the depth-averaged velocity, the vertical component of the Earth's magnetic field, the stream width, the electrical conductivity of the ocean, and the conductance of the sediments above a resistive zone approximated by an insulator. If $F_z(x)\,\tilde{\sigma}(x,t)/\tau(x,t)$ is a constant then the cross-stream voltages will be related to the transport via the depth-averaged velocity. The depth-averaged

PHILOSOPHICAL TRANSACTIONS OF THE ROYAL SOCIETY A MATHEMATICAL, PHYSICAL & ENGINEERING SCIENCES

velocity could be called the barotropic component of the velocity, but this term should not be used in motion induction studies because there are different commonly used definitions of barotropic (Rosenfeld *et al.* 1989). For a two-layered ocean, she states: 'The baroclinic velocity is defined as the upper layer minus the lower layer velocity. The barotropic velocity may be defined as either the lower layer velocity V_2, the depth-averaged velocity $(V_1H_1+V_2H_2)/(H_1+H_2)$, or the amplitude of the external mode $(V_1H_1+V_2H_2)/H_1$ where V and H are the velocity and layer depths, respectively, and the subscripts 1 and 2 refer to the upper and lower layers.' The use of the first definition for barotropic velocity in motional induction studies implies, incorrectly, that the voltages will be zero if the bottom layer has zero velocity.

(ii) *Time-varying temperature and salinity*

The factor $\tilde{\sigma}(x,t)/\tau(x,t)$ in (2.3) has a constant part and a time varying part derived as follows. The temporal variations in the depth-average conductivity of seawater can be approximated by

$$\bar{\sigma}(x,t) = \sigma_0\{1+a_\theta[\bar{\theta}(x,t)-\theta_0]+a_S[\bar{S}(x,t)-S_0]\} \tag{2.7}$$

where $\bar{\ }$ represents the depth averaged value, for example,

$$\bar{\theta}(x,t) = H(x)^{-1}\int_{-H(x)}^{0}\theta(x,z,t)\,\mathrm{d}z$$

for $H \neq 0$ and zero otherwise. Here θ_0 and S_0 will be called, respectively, the mean strait temperature and the mean strait salinity. They are derived from $\theta_0 = \langle\bar{\theta}\rangle$ and $S_0 = \langle\bar{S}\rangle$ where

$$\bar{\theta}(t) = A^{-1}\int_0^L\int_{-H(x)}^{0}\theta(x,z,t)\,\mathrm{d}z\,\mathrm{d}x$$

and

$$\bar{S}(t) = A^{-1}\int_0^L\int_{-H(x)}^{0}S(x,z,t)\,\mathrm{d}z\,\mathrm{d}x$$

are, respectively, the time varying strait temperature and strait salinity, A is the cross-sectional area of the strait, and $\langle\ \rangle$ represents the time-averaged value.

The velocity-weighted conductivity can be approximated by

$$\tilde{\sigma}(x,t) = \tilde{\sigma}_0\{1+\tilde{a}_\theta[\tilde{\theta}(x,t)-\tilde{\theta}_0]+\tilde{a}_S[\tilde{S}(x,t)-\tilde{S}_0]\}. \tag{2.8}$$

where $\tilde{\ }$ represents the vertical, velocity-weighted value, for example,

$$\tilde{\theta}(x,t) = [H(x)\,\bar{V}(x,t)]^{-1}\int_{-H(x)}^{0}\theta(x,z,t)\,V(x,z,t)\,\mathrm{d}z$$

for $H\bar{V} \neq 0$ and zero otherwise. Here $\tilde{\theta}_0$ and $\tilde{S}_0$ will be called, respectively, the mean flow temperature and the mean flow salinity. They are derived from $\tilde{\theta}_0 = \langle\tilde{\theta}\rangle$ and $\tilde{S}_0 = \langle\tilde{S}\rangle$ where

$$\tilde{\theta}(t) = T_0^{-1}\int_0^L\int_{-H(x)}^{0}\theta(x,z,t)\,V(x,z,t)\,\mathrm{d}z\,\mathrm{d}x$$

and

$$\tilde{S}(t) = T_0^{-1}\int_0^L\int_{-H(x)}^{0}S(x,z,t)\,V(x,z,t)\,\mathrm{d}z\,\mathrm{d}x$$

are, respectively, the time varying flow temperature and flow salinity and T_0 is the mean transport.

The empirical relation between temperature, salinity and conductivity (Fofonoff & Millard 1983) yield estimates of the temperature coefficient a_θ and the salinity coefficient a_S that lie within the limits

$$0.021 < a_\theta < 0.025 \text{ mV } ^\circ\text{C}^{-1} \text{ and } 0.025 < a_S < 0.026 \text{ mV ppt}^{-1}$$

for $10 < \theta < 20$ °C, $34 < S < 36$ ppt, and $0 <$ pressure < 800 decibar†. Since the temperature and salinity variations will be small, the coefficients will be treated here as constants defined by the mean temperature, salinity, and pressure.

The conductance of the ocean and sediments, combining (2.6) and (2.7), becomes

$$\tau(x,t) = [1+\nu(x)\,\epsilon(x,t)]\,[\sigma_0 H(x)+\tau'(x)\}, \tag{2.9}$$

where $$\epsilon(x,t) = a_\theta[\bar\theta(x,t)-\theta_0]+a_S[\bar S(x,t)-S_0]$$

represents the relative change in the depth-averaged conductivity due to temperature and salinity changes and

$$\nu(x) = \sigma_0 H(x)/[\sigma_0 H(x)+\tau'(x)] \tag{2.10}$$

is the conductance of the ocean divided by the conductance of the ocean and sediments. Since $\nu(x) < 1$ because $\tau' > 0$ and $\epsilon(x,t) \ll 1$ because a_θ and a_S are small, the term $\epsilon(x,t)$ can be approximated by

$$\epsilon(t) = a_\theta[\bar\theta(t)-\theta_0]+a_S[\bar S(t)-S_0] \tag{2.11}$$

and $\nu(x)$ by the cross-stream average ν_0. The effective water depth H_0 is defined by

$$\nu_0 = \sigma_0 H_0/[\sigma_0 H_0+\tau'_0], \tag{2.12}$$

where τ'_0 is the average conductance of the sediments. The conductance can then be approximated by

$$\tau(x,t) = [1+\nu_0\,\epsilon(t)]\,[\sigma_0 H(x)+\tau'(x)]. \tag{2.13}$$

(iii) *Local motion-induced voltage*

The local motion-induced voltage equation (2.3), making use of (2.8) and (2.13), becomes

$$\Delta\phi_L(t) = [1+\nu_0\,\epsilon(t)]^{-1}\int_0^L W(x)\,H(x)[\bar V(x,t)+\tilde a_\theta\,\bar V_\theta(x,t)+\tilde a_S\,\bar V_S(x,t)]\,\mathrm{d}x \tag{2.14}$$

for $\nu(x)\,\epsilon(x,t) \approx \nu_0\,\epsilon(t)$, where

$$W(x) = \tilde\sigma_0 F_z(x)/[\sigma_0 H(x)+\tau'(x)] \tag{2.15}$$

is the cable weighting factor

$$\tilde V_\theta(x,t) = H(x)^{-1}\int_{-H(x)}^0 [\theta(x,z,t)-\tilde\theta_0]\,V(x,z,t)\,\mathrm{d}z$$

is the time variation in the depth-averaged, temperature times velocity, and

$$\bar V_S(x,t) = H(x)^{-1}\int_{-H(x)}^0 [S(x,z,t)-\tilde S_0]\,V(x,z,t)\,\mathrm{d}z$$

is the time variation in the depth-averaged, salinity times velocity.

(b) *Motion-induced electric currents*

The interpretation of the motion-induced voltages in terms of the fluid motion is complicated by the presence of electric currents. For example, the mean Jupiter Inlet

† 1 bar = 10^5 Pa.

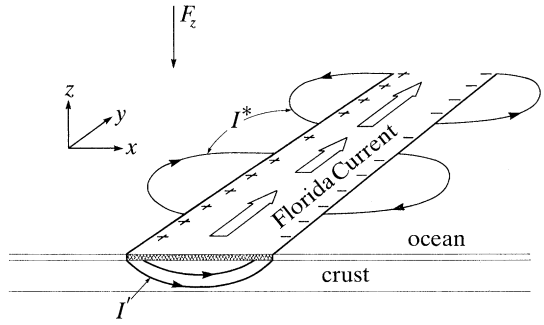

Figure 2. A sketch of horizontal (I^*) and vertical (I') electric currents (lines with arrows), electric charges (+ and −), and fluid motion (broad arrows). F_z is vertical magnetic field. Crust includes sediments beneath ocean.

minus Settlement Point voltage without the electric currents is estimated to be 2.8 V but is observed to be 1.3 V owing to the shunting effect of the electric currents.

The electric currents caused by motional induction are sketched in figure 2. The source for these electric currents is the separation of electric charges in the ocean caused by the stream crossing the Earth's magnetic field. These charges concentrate along the boundaries of the stream and produce a cross-stream electric field that results in an electric current I' flowing in a vertical closed loop connected to the stream. These electric currents return beneath the stream through the conducting region of thickness H' situated above the highly resistive zone. They do not extend horizontally out beyond the stream and therefore do not produce an electric field at land sites.

The downstream changes in the electric charges caused by downstream changes in velocity or conductivity generates a downstream electric field that produces an electric current I^* flowing in a horizontal closed loop connected to the stream. These electric currents flow outside the ocean stream by a horizontal distance roughly equal to Y, the wavelength of the downstream variations, and will therefore produce an electric field at land sites within a distance Y from the stream. Thus I^* for the deep ocean tides extends far into the continents because Y has an ocean-wide dimension. This explains why tidal-induced I^* are seen in the electric field at Tucson (Larsen 1980).

The horizontal electric current $\boldsymbol{I}^*$ is related to the fluid motion by Ohm's law for a moving conductor. For a wide stream, it becomes

$$\boldsymbol{I}^*/\tau = \boldsymbol{E} - (F_z\tilde{\sigma}/\tau)\,H(\hat{\boldsymbol{k}}\times\bar{\boldsymbol{V}}), \tag{2.16}$$

where $\hat{\boldsymbol{k}}$ is the unit vector in the vertical up direction, τ is the conductance of the ocean and sediments, and

$$\boldsymbol{I}^*(x,y,t) = \int_{-H'}^{0} \boldsymbol{i}^*(x,y,z,t)\,\mathrm{d}z$$

is the vertical integral of the electric current density $\boldsymbol{i}^*$ down to the insulating zone within the crust. This expression, from which (2.3) can be derived, assumes that the horizontal electric field $\boldsymbol{E}$ is uniform from the sea surface to the insulating zone because the stream is wide compared with the depth to the resistive zone and that the resistive zone can be approximated by an insulator because the stream is not too wide.

Taking the curl of equation (2.16) and letting $\boldsymbol{I}^* = -\hat{\boldsymbol{k}} \times \nabla\psi$ where ∇ is the horizontal gradient operator and ψ is the electric current stream function, (2.16) becomes

$$\nabla \cdot (\nabla\psi/\tau) = \nabla \cdot [(F_z \tilde{\sigma}/\tau) H \bar{\boldsymbol{V}}] \tag{2.17}$$

where self and mutual induction effects have been ignored. Solutions of (2.17) show that I^* is related to a spatial integral over the term on the right-hand side of (2.17), the electric current source (Sanford 1971; Chave & Luther 1990). Since the long wavelength approximation of fluid continuity, $\nabla \cdot (H\bar{\boldsymbol{V}}) = -\partial\zeta/\partial t$, is valid for wide ocean streams where ζ is the sea level displacement, the electric current source can be written as

$$-(F_z\tilde{\sigma}/\tau)\,\partial\zeta/\partial t + H\bar{\boldsymbol{V}} \cdot \nabla(F_z\,\tilde{\sigma}/\tau).$$

For constant σ, τ', and F_z, one has $\tilde{\sigma} = \sigma$ and the electric current source becomes

$$-(\nu F_z/H)\,\partial\zeta/\partial t - \nu^2 F_z\,\bar{\boldsymbol{V}} \cdot \nabla\,(\ln H),$$

where $\nu = \sigma H/\tau$. Thus I^* is generated by temporal changes in the sea level, and by downstream spatial changes in the water depth, the vertical Earth's magnetic field, the conductivity of the ocean, and the conductance of the sediments. If the conducting sediments are thick, then $\nu \ll 1$ and the effect of downstream changes in the water depth will be reduced. Thus voltage sites over highly conducting sediments are less contaminated by the effects of I^*.

The cross-stream voltage caused by the electric current I^* is given by

$$\Delta\phi_I(t) = -\int_0^L \frac{I^*(x,t)}{\tau(x,t)}\,\mathrm{d}x \tag{2.18}$$

based on (2.23). Substituting (2.13) into (2.18) yields

$$\Delta\phi_I(t) = -[1+\nu_0\,\epsilon(t)]^{-1}\int_0^L \frac{I^*(x,t)}{\tau(x)}\,\mathrm{d}x \tag{2.19}$$

for $\nu(x)\,\epsilon(x,t) \approx \nu_0\,\epsilon(t)$.

(c) *Circuit model of electric currents*

The effect of the electric currents I' and I^* on the voltage between the cable–ocean contacts A and B can be evaluated by an equivalent resistive circuit (figure 3) that models the Florida Current by an ocean stream having a nearly rectangular cross section of width X and depth

$$H_v(x) = H_m\,[1-\{2(x-X_0)/X-1\}^5]^{\frac{1}{5}}$$

for $H_v(x) \leqslant H(x)$ or $H_v(x) = H(x)$ otherwise for $X_0 < x < X_0 + X$, a flow conductivity $\tilde{\sigma}_0$, and a velocity V_0 constant in the cross-stream direction but variable in the downstream direction with wavelength Y; the strait by a depth H_0 and conductivity σ_0; the coastal shelf by a layer of width X_S, depth H_S, and conductivity σ_S; the land area by a surface layer of conductance τ^*; the sediments beneath the strait by a layer of conductance τ_0'; and the resistive crust beneath the sediment and land area by an insulating halfspace. The fixed parameters for the Jupiter Inlet to Settlement Point (JI–SP) circuit model are: $X = 60$ km, $H_m = 600$ m, $\tilde{\sigma}_0 = 4.8$ S m^{-1}, $\sigma_0 = 4.6$ S m^{-1}, $X_S = 8$ km, $H_S = 15$ m, $\tau_0' = 1900$ S, $\tau^* = 700$ S, and $F_z = 41100$ nT. The fixed parameters for the Key West to Havana (KW–HV) circuit model are: $X = 80$ km, $H_m = 600$ m, $\tilde{\sigma}_0 = 4.8$ S m^{-1}, $\sigma_0 = 4.1$ S m^{-1}, $X_S = 30$ km, $H_S = 102$ m, $\tau_0' = 1400$ S, $\tau^* = 700$ S, and $F_z = 43200$ nT.

PHILOSOPHICAL TRANSACTIONS OF THE ROYAL SOCIETY A MATHEMATICAL, PHYSICAL & ENGINEERING SCIENCES

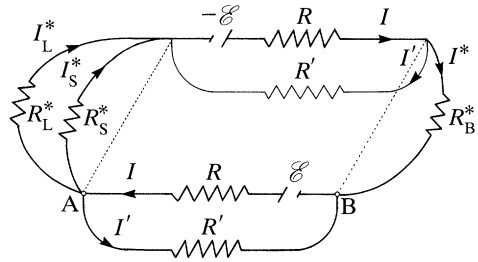

Figure 3. Circuit model of the motion-induced electric currents, where the $\mathscr{E}$s are voltage sources, the Rs are resistors, the Is are electric currents, L = land, S = shelf, and B = ocean east of stream.

The resistive elements of the circuit (figure 3), for a stream width, X, large compared with the depth, H_0, and a downstream wavelength, Y, large compared with the stream width, are equal to the length of the electric current path divided by the cross-sectional area of the electric current and the conductivity of the medium (see Longuet-Higgins *et al.* 1954; Sanford & Flick 1975). Thus the ocean resistance is approximated by $R = 2X/(Y\sigma_0 H_0)$ for the ocean electric currents I flowing horizontally across the stream. The sediment resistance is $R' = 2X/(Y\tau'_0)$ for the sediment electric currents I' flowing horizontally in the cross-stream direction beneath the stream. The shelf resistance is $R^*_S = (Y/2X_S)/(\sigma_0 H_S + \tau'_0)$ for the shelf electric currents I^*_S flowing parallel to the stream. The land resistance is $R^*_L = \pi/2\tau^* + (2X_S/Y)/(\sigma_0 H_S + \tau'_0)$ for the land electric currents I^*_L flowing horizontally in the cross-shelf direction and then into the land in a semi-circular path. The resistance of the ocean east or south of the stream is R^*_B for electric currents I^*.

When the stream is very wide, then the cross-stream voltages experience an additional attenuation caused by the electric currents that pass through the resistive zone and into the conducting mantle. The resistive zone has a circuit resistance approximated by $R'' = 8H''/(\sigma'' XY)$ for the electric currents flowing vertically through the resistive zone. Relative to the ocean resistance, one has $R/R'' = (X/X_{\max})^2$, where $X_{\max} = 2[(\sigma_0/\sigma'')H_0 H'']^{\frac{1}{2}}$. The resistive zone then approximates an insulator when $R/R'' \ll 1$, that is, when $X \ll X_{\max}$. Because $\sigma_0 = 4.6\ \mathrm{S\ m^{-1}}$, $\sigma'' = 1\times10^{-5}\ \mathrm{S\ m^{-1}}$, $H_0 = 0.5$ km, and $H'' = 30$ km, then $X_{\max} \approx 5250$ km. Thus if $X = 100$ km, then $R/R'' = 3.6\times10^{-4}$ and the resistive zone clearly approximates an insulator. The resistive zone is therefore taken as an insulator for the circuit model.

The voltage source $\mathscr{E}$ in figure 3 is equal to the cross-stream voltage when $\tau'_0 = 0$. Ignoring temperature and salinity flux variations, it is determined from

$$\mathscr{E} = \tilde{\sigma}_0 F_z V_0 \int_{X_0}^{X_0+X} [\sigma_0 H(x)]^{-1} H_v(x)\,\mathrm{d}x \tag{2.20}$$

for the stream lying between X_0 and X_0+X and the water depths $H(x)$ derived by a taut cubic spline fit to the Malloy and Hurley bathymetry. These agree quite well with recent depth soundings (figure 4*a*).

The local motion-induced voltage (2.3) between points A and B, ignoring time variations in the temperature and salinity, is

$$\Delta\phi_L = \mathscr{E}_L$$

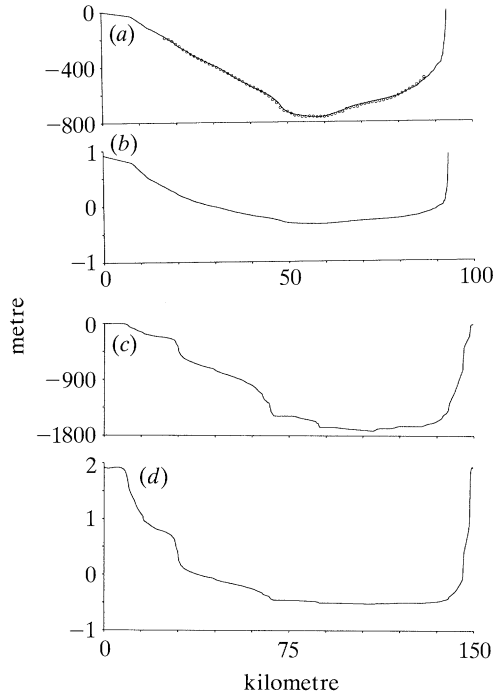

Figure 4. Channel depth $H(x)$ and relative cable weighting factor W/W_0-1. (*a*) Channel depth east of Jupiter Inlet to Grand Bahama Island from Malloy and Hurley map (solid curve) and 1990 sounding for 1518 m s^{-1} sound speed (dots). Fit confirms accuracy of map. (*b*) Relative weighting factor east of Jupiter Inlet for $\sigma_0 = 4.6$ S m^{-1}, $\tau_0' = 1900$ S, and $W_0 = 0.52$. (*c*) Channel depth south of Key West to Cuba. (*d*) Relative weighting factor south of Key West for $\sigma_0 = 4.1$ S m^{-1}, $\tau_0' = 1400$ S, and $W_0 = 0.34$.

where
$$\mathscr{E}_{\mathrm{L}} = \tilde{\sigma}_0 F_z V_0 \int_{X_0}^{X_0+X} [\sigma_0 H(x) + \tau_0']^{-1} H_v(x)\,\mathrm{d}x \tag{2.21}$$

is determined from (2.3) for a constant sediment conductance τ_0'.

In general $|\mathscr{E}_{\mathrm{L}}|/|\mathscr{E}| < 1$ because of the attenuation of the cross-stream voltage by I'. This ratio will be used to represent the conductance ratio $\nu_0 = |\mathscr{E}_{\mathrm{L}}|/|\mathscr{E}|$ for the circuit model. Then
$$\Delta\phi_{\mathrm{L}} = \nu_0 \mathscr{E}$$
and the effective ocean depth for the circuit model is given by
$$H_0 = (\tau_0'/\sigma_0)\,(1/\nu_0 - 1)^{-1}.$$

The cross-stream voltage caused by I^* (2.19) is
$$\Delta\phi_I = -I^* \int_0^{X_{\mathrm{S}}+X_I} [\sigma_0 H(x) + \tau_0']^{-1}\,\mathrm{d}x, \tag{2.22}$$

because I^* can be approximated locally by a value independent of x since the downstream wavelengths are large compared with the stream width. The effective shelf depth H_{S} is then defined by
$$[\sigma_0 H_{\mathrm{S}} + \tau_0']^{-1} = X_{\mathrm{S}}^{-1} \int_0^{X_{\mathrm{S}}} [\sigma_0 H(x) + \tau_0']^{-1}\,\mathrm{d}x$$

and the effective ocean depth H_I is defined by

$$[\sigma_0 H_I + \tau_0']^{-1} = X_I^{-1} \int_{X_S}^{X_S+X_I} [\sigma_0 H(x) + \tau_0']^{-1}\, \mathrm{d}x.$$

Thus (2.22) can be written as

$$\Delta\phi_I = -I^*[X_S/(\sigma_0 H_S + \tau_0') + X_I/(\sigma_0 H_I + \tau_0')],$$

or, in terms of the effective ocean depth H_0,

$$\Delta\phi_I = -I^*[X_S/(\sigma_0 H_S + \tau_0') + \nu_I X_I/(\sigma_0 H_0)],$$

where $\nu_I = \sigma_0 H_0/(\sigma_0 H_I + \tau_0')$ is a pseudo conductance ratio because H_I is not, in general, equal to H_0. The circuit model therefore only approximates the voltage effects of I^*.

The motion-induced voltage between points A and B when $I^* \neq 0$ can be written as

$$\Delta\phi_V = (1-\epsilon^*)\,\nu_0 \mathscr{E}. \tag{2.23}$$

The cross-stream voltage caused by I^* is then

$$\Delta\phi_I = -\epsilon^* \nu_0 \mathscr{E}, \tag{2.24}$$

where

$$\epsilon^* = \nu_0 R/R^*\ (1+\nu_0 R/R^*)^{-1}$$

summarizes the voltage effects of I^*. The term $R^* = R_L^*\, R_S^*/(R_S^* + R_L^*)$ is the total resistance of the shelf and land. If $R^* = 0$, then $\epsilon^* = 1$ and if $R^* = \infty$, then $\epsilon^* = 0$. Thus $0 \leqslant \epsilon^* \leqslant 1$ and $0 \leqslant \Delta\phi_V \leqslant \nu_0 \mathscr{E}$ provided the stream lies between the points A and B. Thus if $\epsilon^* = 1$ then I^* completely shorts out the cross-stream voltage and if $\epsilon^* \ll 1$ then the voltage effects of I^* disappear. This only occurs if the sediments are highly conducting so that $\nu_0 \ll 1$ or if the wavelength is very large compared with the stream width, that is, $Y \gg 4\tau^* X/(\pi\sigma_0 H_0)$, so that $R/R^* \ll 1$.

The attenuation of the cross-stream voltage $\Delta\phi_V$ by I' is ν_0 when $I^* = 0$ and is found, when $I^* \neq 0$ to be

$$\nu_0' = \nu_0 + \epsilon^*(1-\nu_0).$$

Hence the attenuation of the cross-stream voltage by I' depends in general on the sediment conductance and on the value of ϵ^*.

The voltage calibration factor $C = T_0/\Delta\phi_V$ is

$$C = (1-\epsilon^*)^{-1}\, T_0/\mathscr{E}_L, \tag{2.25}$$

transport where the

$$T_0 = V_0 \int_{X_0}^{X_0+X} H_v(x)\, \mathrm{d}x.$$

The tidal calibration factor is

$$C_T = (1-\epsilon^*)^{-1}\, T_T/\mathscr{E}_T \tag{2.26}$$

for tidal transport $T_T = A\, V_0$ and tidal voltage source

$$\mathscr{E}_T = \sigma_0 F_z V_0 \int_0^L [\sigma_0 H(x) + \tau_0']^{-1} H(x)\, \mathrm{d}x, \tag{2.27}$$

based on (2.2) for $H_v(x) = H(x)$ and $X = L$. The tidal calibration factor computed for

the JI–SP model with $\epsilon^* = 0$ is $C_T = 23.6\,\mathrm{Sv\ V^{-1}}$† and for the KW–HV model it is $C_T = 37.2\,\mathrm{Sv\ V^{-1}}$.

The analytical expression for ϵ^* when $X_S = 0$ is

$$\epsilon^* = [1 + (\pi Y/4X)\,(\sigma_0 H_0 + \tau_0')/\tau^*]^{-1}.$$

Hence the reduction in the cross-stream voltage by I^* is dependent on X and Y. Since these will, in general, be time varying, the voltage calibration factor C can only be a time independent constant if $\epsilon^* \ll 1$ or if ϵ^* is a constant.

The onshore electric field E^* caused by I^* is found to be

$$E^* = 2(\tau^* R^* Y)^{-1}\,(1-\epsilon^*)\,\nu_0 \mathscr{E}. \tag{2.28}$$

Hence the electric field calibration factor $C^* = T_0/E^*$ in terms of the voltage calibration factor C is

$$C^* = \tfrac{1}{2}\tau^* R^* Y\, C.$$

The analytical expression for C^* when $X_S = 0$ is

$$C^* = \tfrac{1}{4}\pi Y\, C. \tag{2.29}$$

Thus the electric field calibration factor C^* is strongly dependent on Y which means that the onshore electric field measurements cannot, in general, be used to monitor transport variations. One exception is the observation of the tidal flow from a shore electric field site (Harvey *et al.* 1977) because Y is then be a time independent constant for each tidal constituent.

(i) *Downstream wavelength effects*

The value of ϵ^* for different downstream wavelengths Y are estimated for the JI–SP voltages, the Cable Break minus Settlement Point voltages (16–SP), the KW–HV and the Florida shelf break minus Havana voltages (30–HV) when the stream is outside the shelf region (table 1). The ϵ^* for the JI–SP and KW–HV voltages are found by moving the cable–ocean contact A along the path R_L^* (figure 3).

As the cable–ocean contacts A and B move away from the edge of the stream or Y decreases, the electric current effect ϵ^* increases and the observed voltage $\Delta\phi_V$ decreases. If the cable–ocean contacts A and B are both greater than a distance Y from the edge of the stream, then $\epsilon^* \approx 1$ and the voltage $\Delta\phi_V$ between A and B is reduced to zero because I^* essentially shorts out the voltage within a band of approximately width Y surrounding the stream. One way to visualize the attenuation is to consider the distribution of electric charges in figure 2 after subtracting the electric charges due to the mean flow. Then the electric charges created by the time varying flow will have a downstream distribution that alternates between positive and negative values over the distance Y. If the cable–ocean contacts are close to the edges of the stream, then the voltage is due to the nearby electric charges since the distant electric charges can be ignored. If the cable–ocean contracts are much farther than Y from the stream, then the voltages due to the electric charges of one sign will be cancelled by the voltages due to the electric charges of the opposite sign. Thus voltages observed from long cables cannot observe the transport variations of narrow streams if the cable–ocean contacts are a distance much greater than Y from the edges of the stream.

The effect of I^* on the 16–SP and 30–HV voltages is, however, small for

† In this paper, 1 Sv = $10^6\ \mathrm{m^3\ s^{-1}}$. The Sverdrup (Sv) was proposed by Dunbar (1962).

Table 1. *Dependency of ϵ^* on downstream wavelength Y for Jupiter Inlet minus Settlement Point (JI–SP), Florida shelf break minus Settlement Point (16–SP), Key West minus Havana (KW–HV), Florida shelf break minus Havana (30–HV) voltages when the stream is outside the Florida shelf region*

Y/km	JI–SP	16–SP	KW–HV	30–HV
100	0.28	0.22	0.48	0.31
200	0.13	0.10	0.25	0.15
300	0.09	0.06	0.17	0.10
500	0.05	0.03	0.10	0.05
1000	0.02	0.02	0.05	0.03

$Y \geqslant 300$ km (table 1) because the cable–ocean contacts are close to the edges of the stream and the cable–ocean contact on the Florida side is outside the shelf break. The KW–HV voltages are much more sensitive to I^* and hence changes in Y because of the wide shelf region (30 km) south of Key West.

The results of the circuit model show that I^* becomes smaller when the sediments become more conducting, when the continental regions become more resistive, and when the downstream wavelength Y become larger. The voltage effect of I^* can never be eliminated, however, because Y will always be finite since the time variations in transport will have a finite propagation speed and the region surrounding the stream will always be conducting. The voltage effect of I^* can be minimized, however, if the cable–ocean contacts are on opposite sides of the stream and close to the edges of the stream but outside the coastal shelf region.

(ii) *Meandering effects*

Estimates of the voltage changes caused by meanders of the stream can be assessed by introducing a lateral shift in the stream axis. This causes the calibration factor C to vary because of changes in the cable weighting factor W and in the electric current factor ϵ^*.

Figure 4*b*, *d* shows the relative cable weighting factor $W/W_0 - 1$ as a function of the cross-strait position for the circuit model parameters where W_0 is the cross-strait average that has the value $W_0 = 0.52$ for JI–SP and $W_0 = 0.34$ for KW–HV. This figure shows the importance of locating the cable–ocean contacts outside the shelf regions. For the JI–SP model $|W/W_0 - 1| \leqslant 0.33$ for 17.3 km $< x <$ 91.5 km and for the KW–HV model, $|W/W_0 - 1| \leqslant 0.52$ for 29.2 km $< x <$ 145.7 km. Hence the KW–HV voltages will be more sensitive to meanders than the JI–SP voltages.

For the JI–SP model with $I^* = 0$, the values of $C_{\text{JI–SP}}$, for cable–ocean contacts at 0 and 93 km, and $C_{\text{16–SP}}$, for cable–ocean contacts at 16 and 93 km, are: $C_{\text{JI–SP}} =$ 22.0 Sv V^{-1} and $C_{\text{16–SP}} = 22.6$ Sv V^{-1} when the stream lies between 8 and 68 km (stream axis = 38 km); $C_{\text{JI–SP}} = C_{\text{16–SP}} = 23.2$ Sv V^{-1} when the stream lies between 18 and 78 km (stream axis = 48 km); and $C_{\text{JI–SP}} = C_{\text{16–SP}} = 24.1$ Sv V^{-1} when the stream lies between 28 and 88 km (stream axis = 58 km). There is thus a 5.5% reduction in $C_{\text{JI–SP}}$ and a 2.7% reduction in $C_{\text{16–SP}}$ from the nominal value 23.2 Sv V^{-1} when the stream moves onshore by 10 km and a 3.9% increase in $C_{\text{JI–SP}}$ and $C_{\text{16–SP}}$ when the stream moves offshore by 10 km. Hence the meandering induced variability is ± 4.8% for $C_{\text{JI–SP}}$ and ± 3.3% for $C_{\text{16–SP}}$ when there is a ± 10 km lateral shift in the stream. The corresponding errors in the voltage-derived transports are, respectively, ± 1.6 Sv and ± 1.1 Sv for a mean transport of 32.3 Sv. Thus the JI–SP and 16–SP voltages are relatively insensitive to meanders.

Table 2. *Dependency of calibration factor C on downstream wavelength Y and position of stream axis x for Jupiter Inlet minus Settlement Point (JI–SP) and Key West minus Havana (KW–HV) voltages*

	C(JI–SP)/(Sv V^{-1})			C(KW–HV)/(Sv V^{-1})		
Y/km	x = 38 km	x = 48 km	x = 58 km	x = 50 km	x = 70 km	x = 90 km
100	31.3	32.8	31.6	41.4	58.2	60.3
200	25.7	26.9	27.3	31.5	40.4	46.8
300	24.2	25.5	26.2	27.8	35.3	42.4
500	23.2	24.5	25.3	25.5	32.3	39.2
1000	22.6	23.8	24.7	24.1	30.4	37.1

For the KW–HV model with $I^* = 0$, the values of $C_{\text{KW–HV}}$, for cable–ocean contacts at 0 and 150 km, and $C_{30\text{–HV}}$, for cable–ocean contacts at 30 and 150 km, are: $C_{\text{KW–HV}} = 22.9$ Sv V^{-1} and $C_{30\text{–HV}} = 26.1$ Sv V^{-1} when the stream lies between 10 and 90 km (stream axis = 50 km); $C_{\text{KW–HV}} = C_{30\text{–HV}} = 28.9$ Sv V^{-1} when the stream lies between 30 and 110 km (stream axis = 70 km); and $C_{\text{KW–HV}} = C_{30\text{–HV}} = 35.4$ Sv V^{-1} when the stream lies between 50 and 130 km (stream axis = 90 km). There is thus a 26.2% reduction in $C_{\text{KW–HV}}$ and a 10.7% reduction in $C_{30\text{–HV}}$ from the nominal value 28.9 Sv V^{-1} when the stream moves onshore by 20 km and a 22.5% increase in $C_{\text{KW–HV}}$ and $C_{30\text{–HV}}$ when the stream moves offshore by 20 km. Hence the meandering-induced variability is ± 27.3% for $C_{\text{KW–HV}}$ and ± 17.8% for $C_{30\text{–HV}}$ when there is a ± 20 km lateral shift in the stream. The corresponding errors in the voltage-derived transport are, respectively, ± 7.5 Sv and ± 4.8 Sv for a mean transport of 27.3 Sv. Thus the KW–HV and 30–HV voltages are sensitive to meanders.

For the JI–SP model with $I^* \neq 0$, a lateral shift of the stream axis from 38 km to 48 km and 58 km eastward from the Florida coast for $Y = 300$ km changes ϵ^* from 0.09 to 0.09 and 0.08, and C from 24.2 Sv V^{-1} to 25.5 Sv V^{-1} and 26.2 Sv V^{-1} respectively. The JI–SP voltages are therefore relatively insensitive to changes in Y when $Y \geqslant 300$ km because $\epsilon^* < 0.1$. The value of the calibration factor C varies by ± 7.4% for $Y \geqslant 300$ km and a ± 10 km lateral shift in the stream (table 2). This corresponds to a voltage-derived transport error of ± 2.4 Sv. The JI–SP and 16–SP voltages are therefore relatively insensitive to both meanders and changes in the down stream wavelengths and the value of ϵ^* is relatively insensitive to meanders.

For the KW–HV model with $I^* \neq 0$, a lateral shift of the stream axis from 50 km to 70 km and 90 km southward from the Key West shelf break for $Y = 300$ km changes ϵ^* from 0.18 to 0.18 and 0.16, and C from 27.8 Sv V^{-1} to 35.3 Sv V^{-1} and 42.4 Sv V^{-1} respectively. The values of ϵ^* are much larger for the KW–HV voltages than for the JI–SP voltages which indicates that the KW–HV voltages are more sensitive to I^* than the JI–SP voltages. The calibration factor varies by ± 27.5% for a ± 20 km lateral shift in the stream when $Y \geqslant 300$ km (table 2). This corresponds to a voltage-derived transport error of ± 7.5 Sv. Hence the KW–HV voltages are much more sensitive to meanders and changes in the downstream wavelengths than the JI–SP voltages. The value of ϵ^* is, however, relatively insensitive to meanders.

In summary, the circuit model shows the following. (1) The dominant effect of the meanders is to change the calibration factor C while the electric current effect ϵ^* remains relatively constant for a fixed Y. Hence estimates of the voltage meandering effect can be obtained by simply considering the Sanford voltage equation (2.2a) and ignoring the effects of the electric current I^*. (2) The BK–SP voltages are suitable for

monitoring transport variations because the errors in the voltage-derived transports are expected to be less than ± 1 Sv. (3) The KW–HV voltages may not be suitable for monitoring transport because the calibration factor decreases significantly when the Florida Current moves closer to Florida and increases significantly when the Florida Current moves away from Florida. The meanders could cause a $\pm 28\,\%$ variability in the calibration factor which would lead to errors in the voltage-derived transports of ± 8 Sv. Moving the cable–ocean contact from Key West to 30 km from Key West would reduce the errors in the voltage-derived transports to ± 5 Sv, which is not as small as one would like. Before the sensitivity of the KW–HV voltages to meanders can be accurately assessed, however, the dimension of the stream and the conductance of the sediments need to be determined.

(*d*) *Voltage attenuation by the electric currents*

The local motion-induced voltage is

$$\Delta\phi_{\mathrm{L}} = (1+\nu_0\,\epsilon)^{-1}\,\nu_0\,\mathscr{E} \tag{2.30}$$

when the conductivity variation ϵ is included. Expanding the voltage source term $\mathscr{E}$ into normal modes $\mathscr{E}_{nm}$ such that

$$\mathscr{E} = \sum_{n=1}^{N}\sum_{m=1}^{M} \mathscr{E}_{nm}\,,$$

where $\mathscr{E}_{nm}$ corresponds to $X_n = X/n$ for the cross-stream width X and $Y_m = Y/m$ for the maximum downstream wavelength Y, the electric current voltage $\Delta\phi_I$ (2.24) for the n and m normal mode is

$$\Delta\phi_{Inm} = -(1+\nu_0\epsilon)^{-1}\,\nu_0\,\epsilon^*_{nm}\,\mathscr{E}_{nm}$$

when the conductivity variation ϵ is included. The total voltage $\Delta\phi_I$ is

$$\Delta\phi_I = -(1+\nu_0\,\epsilon)^{-1}\sum_{n=1}^{N}\sum_{m=1}^{M}\epsilon^*_{nm}\mathscr{E}_{nm}\,.$$

Thus $\Delta\phi_I$ can be related to the voltage source term by

$$\Delta\phi_I = -(1+\nu_0\,\epsilon)^{-1}\tilde{\epsilon}^*\,\nu_0\,\mathscr{E}, \tag{2.31}$$

where $\tilde{\epsilon}^*$ is the source-weighted value given by

$$\tilde{\epsilon}^* = \mathscr{E}^{-1}\sum_{n=1}^{N}\sum_{m=1}^{M}\epsilon^*_{nm}\,\mathscr{E}_{nm}\,.$$

The motion-induced voltages are then related to the local voltage source term by

$$\Delta\phi_V = (1+\nu_0\,\epsilon)^{-1}\,(1-\tilde{\epsilon}^*)\,\mathscr{E}_{\mathrm{L}} \tag{2.32}$$

for $\mathscr{E}_{\mathrm{L}} = \nu_0\,\mathscr{E}$.

(*e*) *Voltage-transport equation*

The motion-induced voltage $\Delta\phi_V$ (2.32), for the local voltage source

$$\mathscr{E}_{\mathrm{L}} = \int_0^L W(x)\,H(x)\,[\bar{V}(x,t)+\tilde{a}_\theta\,\bar{V}_\theta(x,t)+\tilde{a}_{\mathrm{S}}\,\bar{V}_{\mathrm{S}}(x,t)]\,\mathrm{d}x,$$

given by (2.14), is related to the volume transport via the voltage-transport equation

$$C(t)\,\Delta\phi_V(t) = T(t)+T_{wm}(t)+\tilde{a}_\theta\,T_\theta(t)+\tilde{a}_{\mathrm{S}}\,T_{\mathrm{S}}(t), \tag{2.33}$$

where
$$C(t) = [1+\nu_0\,\epsilon(t)]\,[1-\tilde{\epsilon}^*(t)]^{-1}\,\tilde{W}_0^{-1} \tag{2.34}$$
is the voltage calibration factor,
$$\tilde{W}_0 = T_0^{-1}\int_0^L W(x)\,H(x) < \bar{V}(x,t) > \mathrm{d}x \tag{2.35}$$
is the velocity-weighted value of the cable weighting factor, $\bar{V}$ is the depth-averaged velocity,
$$T(t) = \int_0^L H(x)\,\bar{V}(x,t)\,\mathrm{d}x \tag{2.36}$$
is the volume transport with mean T_0,
$$T_\theta(t) = \int_0^L H(x)\,\bar{V}_\theta(x,t)\,\mathrm{d}x \tag{2.37}$$
is the time varying temperature flux,
$$T_S(t) = \int_0^L H(x)\;\;\bar{V}_S\,(x,t)\,\mathrm{d}x \tag{2.38}$$
is the time varying salinity flux, and
$$T_{wm}(t) = \int_0^L H(x)\,[W(x)/\tilde{W}_0 - 1]\,\bar{V}(x,t)\,\mathrm{d}x \tag{2.39}$$
is the voltage meandering effect related to the relative weighting factor $W(x)/\tilde{W}_0 - 1$ times the depth-averaged velocity $\bar{V}$. The terms
$$\tilde{a}_\theta\int_0^L H(x)\,[W(x)/\tilde{W}_0 - 1]\,\bar{V}_\theta(x,t)\,\mathrm{d}x$$
and
$$\tilde{a}_S\int_0^L H(x)\,[W(x)/\tilde{W}_0 - 1]\,\bar{V}_S(x,t)\,\mathrm{d}x$$
have been dropped because they are small.

The relation (2.33) between the voltage and the transport is nonlinear because the calibration factor C depends on ϵ and $\tilde{\epsilon}^*$. These have temporal variations caused by, respectively, variations in the temperature and salinity of the ocean and variations in the downstream wavelength. The voltage calibration factor will only have a constant value
$$C_0 = (1-\tilde{\epsilon}_0^*)^{-1}\,\tilde{W}_0^{-1} \tag{2.40}$$
if the temperature and salinity variations are small so that ϵ can be neglected, if the wavelengths of the time variations are relatively large and constant, and if the cable ocean contacts are close to the edges of the stream so that $\tilde{\epsilon}^*$ can be approximated by a small constant $\tilde{\epsilon}_0^*$.

(i) *Meanders*

The voltage variations caused by meanders of the Florida Current can be assessed by separating the depth-averaged velocity into two parts as
$$\bar{V}(x,t) = \alpha(t) < \bar{V}(x) > + \bar{V}_m(x,t), \tag{2.41}$$
where $\alpha(t)$ is the amplitude modulation of the time- and depth-averaged velocity

$\langle \bar{V}(x) \rangle$ and $\bar{V}_m(x,t)$ is the depth-averaged meandering part. The transport is then equal to

$$T(t) = \alpha(t)\, T_0 + T_m(t), \tag{2.42}$$

where $\alpha(t)$ is the amplitude modulation of the mean transport T_0 and $T_m(t)$ is the transport of the meanders. The voltage meandering effect T_{wm} then reduces to

$$T_{wm}(t) = \int_0^L H(x)\,[W(x)/\tilde{W}_0 - 1]\,\bar{V}_m(x,t)\,\mathrm{d}x \tag{2.43}$$

that is a function of the meandering velocities alone because the contribution of $\alpha(t)\langle \bar{V}(x) \rangle$ vanishes for $\tilde{W}_0$ defined by (2.35). Thus T_{wm} is related to the spatial cross-stream correlation between the changes in the relative transport weighting factor and the meandering part of the depth-averaged velocity.

The amplitude modulation $\alpha(t)$ is found from the profiling data by a spatial least squares fit between $\langle \bar{V}(x) \rangle$ and the depth-averaged velocities $\bar{V}(x,t)$. It is given by

$$\alpha(t) = \int_0^L H(x)\ \ \bar{V}(x,t)\langle \bar{V}(x) \rangle\,\mathrm{d}x \Big/ \int_0^L H(x)\langle \bar{V}(x) \rangle^2\,\mathrm{d}x \tag{2.44}$$

for $\langle \alpha(t) \rangle = 1$.

(ii) *Tidal variation*

The voltage-transport equation (2.33) can be used to interpret tidal flow in straits or estuaries but not in the deep ocean, where self and mutual induction effects can no longer be ignored (Chave & Luther 1990). For tidal flow in straits, $V(x,z,t) = V_{\mathrm{T}}(t)$, $\tilde{\theta}_0 = \theta_0$, and $\tilde{S}_0 = S_0$, and thus $\tilde{a}_\theta\, T_\theta(t) + \tilde{a}_s\, T_s(t) = \epsilon(t)\, T_{\mathrm{T}}(t)$, where $T_{\mathrm{T}}(t) = A\, V_{\mathrm{T}}(t)$ is the tidal transport and $T_{wm} = 0$ because there is no meandering effect. The voltage-transport equation then becomes the voltage-tidal equation

$$C_{\mathrm{T}}(t)\,\Delta\phi_V(t) = T_{\mathrm{T}}(t), \tag{2.45}$$

where the tidal calibration factor is

$$C_{\mathrm{T}}(t) = [1 + \nu_0\,\epsilon(t)]\,[1 + \epsilon(t)]^{-1}\,[1 - \epsilon^*(t)]^{-1}\,W_0^{-1} \tag{2.46}$$

for $\nu(x)\,\epsilon(x,t) \approx \nu_0\,\epsilon(t)$ and

$$W_0 = A^{-1} \int_0^L H(x)\, W(x)\,\mathrm{d}x$$

is the cross-stream spatial average of the cable weighting factor. The ratio C_{T}/C_0, from (2.34) and (2.46) for $\epsilon = 0$, is

$$C_{\mathrm{T}}/C = [(1 - \tilde{\epsilon}^*)/(1 - \epsilon^*)]\,(\tilde{W}_0/W_0). \tag{2.47}$$

Hence C_{T} will not, in general, be equal to C_0 because $\tilde{W}_0 \neq W_0$, and $\tilde{\epsilon}^* \neq \epsilon^*$.

(iii) *Transatlantic voltages*

The voltage-transport equation for transatlantic voltage measurements reduces to

$$C(t)\,\Delta\phi_V(t) = T_{wm}(t) + \tilde{a}_\theta\, T_\theta(t)$$

because T_{S} will be small and T can be neglected because the transport into the Atlantic via the Bering Straits is small.

The voltage-transport equation in terms of the heat flux Q is

$$C(t)\,\Delta\phi_V(t) = T_{wm}(t) + \tilde{a}_\theta\,(\rho C_p)^{-1} Q(t), \tag{2.48}$$

where the time varying heat flux Q, in terms of the time varying temperature flux, is given by

$$Q(t) = \rho C_p T_\theta(t),$$

for ρ, the density, and C_p, the specific heat per constant pressure.

The voltage calibration factor C for the North Atlantic is estimated to be 100 Sv V^{-1} for $\tilde{\epsilon}^* = 0$ and $\tilde{a}_\theta(\rho C_p)^{-1}$ is estimated to be 5.1 Sv PW^{-1} for $\rho C_p =$ 0.00409 PW $°C^{-1}$ Sv^{-1} (Cox & Smith 1959). Hence a change of 1 PW in heat flux will cause a 51 mV change in voltage that is readily detectable. The cable weighting factor W (2.15) will be relatively constant in an east–west direction across the Atlantic and the time variations in the ocean conductivity are likely to be small. If the flow is broadscaled, then the effects of meanders and I^* will be small and it might then be possible to use east–west transatlantic cables for monitoring the broad scaled meridional heat flux variations.

(iv) *Estuaries*

The time dependent conductance of the ocean and sediments (2.6) in an estuary

$$\tau(x,t) = \bar{\sigma}(x,t)\,[H(x)+\zeta(t)]+\tau'(x) \tag{2.49}$$

includes the variations in sea level ζ. For small temperature, salinity and sea level variations the conductance can be approximated, in a manner similar to deriving (2.13), by

$$\tau(x,t) = [1+\nu_0\,\epsilon(t)+\nu_0\{1+\epsilon(t)\}\,\zeta(t)/H_0]\,[\sigma_0\,H(x)+\tau'(x)]. \tag{2.50}$$

The voltage-transport equation then becomes

$$C(t)\,\Delta\phi_V(t) = T(t)+\tilde{a}_S\,T_S(t) \tag{2.51}$$

because meandering effects and temperature flux can be ignored as they are likely to be small for most estuaries. The voltage calibration factor is

$$C = [1+\nu_0\,\epsilon+\nu_0(1+\epsilon)\,(\zeta/H_0)]\,[1-\tilde{\epsilon}^*]^{-1}\,\tilde{W}_0^{-1}. \tag{2.52}$$

For barotropic tidal flow, the voltage-tidal equation (2.45) has the tidal calibration factor

$$C_T = [(1+\nu_0\,\epsilon)(1+\epsilon)^{-1}+\nu_0\,\zeta/H_0]\,[1-\epsilon^*]^{-1}\,W_0^{-1}. \tag{2.53}$$

Thus the calibration factors C and C_T will vary due to changes in the sea level ζ and changes in the term ϵ caused by changes in salinity.

Monitoring the salt flux in an estuary might be accomplished in the following manner. Observations of the tidal-induced voltages will yield estimates of the changes in the tidal calibration factor C_T and these changes could be used to estimate changes in the voltage calibration factor C. These changes could then be interpreted as changes in salinity via the term ϵ if the sea level variations are also observed and the conductance ratio ν_0 determined from resistivity studies. The cross-stream voltages, corrected for temporal changes in the calibration factor C, will then yield estimates of the changes in the salt flux T_S provided the fresh water influx T is simultaneously observed. Whether it will be possible to accurately monitor salt flux in an estuary by this method will depend on the magnitude of the voltage variations, on the accuracy of the tidal variations determined from short record lengths, and on whether the voltage effects of I^* can be ignored.

(*f*) *Electric field*

Short span electric field devices have been used to observe geomagnetic- and motion-induced electric fields in the ocean (Cox 1980; Lilley *et al.* 1986; Filloux 1987; Luther *et al.* 1987; Chave *et al.* 1989). The motion-induced electric field E in the cross-stream direction for wide streams is related to the fluid motion by

$$E(x,t) = [\bar{\sigma}(x)\,H(x)+\tau'(x)]^{-1}\,[-\tilde{\sigma}(x)\,F_z(x)\,H(x)\,\bar{V}(x,t)+I^*(x,t)], \tag{2.54}$$

which is based on (2.16) where I^* is the electric current in the cross-stream direction.

The electric field E beneath a strong ocean stream will therefore be related to the depth-averaged velocity $\bar{V}$ modified by I^* but E observed outside the stream will only be related to I^*. If the boundary of the stream is known or can be determined, then E measured just outside the stream can be used to remove the effects of I^* from E measured beneath the stream because I^* in the cross-stream direction will essentially be independent of x for downstream wavelengths large compared with the stream width.

The low frequency, geomagnetic-induced electric fields are related, by Ohm's law, to the geomagnetic-induced electric currents I by

$$E(x,t) = [\bar{\sigma}(x)\,H(x)+\tau'(x)]^{-1}\,I(x,t). \tag{2.55}$$

(*g*) *Robinson voltage equation*

The theory for the interpretation of motion-induced voltages between widespread cable–ocean contacts in the ocean has been developed by Robinson (1976, 1977). He derived an expression for the voltage that is a spatial integral over the fluid velocity $\boldsymbol{V}$

$$\Delta\phi_V = \int\!\!\int\!\!\int \boldsymbol{W}'\cdot\boldsymbol{V}\,\mathrm{d}x\,\mathrm{d}y\,\mathrm{d}z. \tag{2.56}$$

This expression includes the effects of $\boldsymbol{I}^*$ but ignores the effects of self and mutual induction. The vector cable weighting factor is $\boldsymbol{W}' = \boldsymbol{F}\times\boldsymbol{i}'$, where $\boldsymbol{F}$ is the Earth's magnetic field and $\boldsymbol{i}'$ is the virtual electric current density produced in the ocean by the injection of a current of unit strength from the cable ends. The spatial distribution of the virtual electric current is derived from $\boldsymbol{i}' = -\sigma\nabla\phi'$ for a layered Earth, where the potential ϕ' is the numerical solution of $\nabla\cdot(\sigma\nabla\phi') = q$ for q zero everywhere except at the cable–ocean contacts. Solutions have been found for cables spanning the Irish Sea (Robinson 1976), the English Channel (Robinson 1977) and the Tasman Sea (Baines & Bell 1987).

The Robinson equation can be reduced to a surface integral when the cable length and the stream width are large compared with the ocean depth. The horizontal electric field caused by the virtual electric current is then approximately uniform over the water column and the virtual horizontal electric current becomes $\boldsymbol{i}' = \sigma\bar{\boldsymbol{E}}'$, where $\bar{\boldsymbol{E}}'$ is the depth-averaged, virtual horizontal electric field. The Robinson equation then reduces to

$$\Delta\phi_V(t) = [1+\nu_0\,\epsilon(t)]^{-1}\int\!\!\int H(x,y)\;\boldsymbol{W}(x,y)\cdot[\,\bar{\boldsymbol{V}}(x,y,t)+\tilde{a}_\theta\,\tilde{\boldsymbol{V}}_\theta(x,y,t)+a_S\,\bar{\boldsymbol{V}}_S(x,y,t)]\,\mathrm{d}x\,\mathrm{d}y \tag{2.57}$$

for a linear expansion of seawater conductivity about the mean temperature and salinity. The term on the right-hand side of (2.57) is the horizontal vector form of the

voltage source for (2.14) with a vector cable weighting factor $\boldsymbol{W} = \tilde{\sigma}_0 \boldsymbol{F} \times \boldsymbol{E}'$. Equation (2.57) is, basically, the two-dimensional version of the local motion-induced voltage (2.14) combined with the voltage effects of the motion-induced electric currents (2.19).

3. Transport estimates

(*a*) *Profiling Measurements*

(i) *Transport*

Transports of the Florida Current estimated by velocity profiling data collected before the STACS program include 85 days (1964–1970) without tidal correction (Niiler & Richardson 1973) and 41 days (1974) with tidal correction (Brooks 1979) from Miami, Florida to Bimini Island, and 13 days (1972) of profiling data to 200 m depths without tidal correction (Brooks & Niiler 1975) from Key West, Florida to 35 km north of Matanzas, Cuba. Profiling data from locations north of Jupiter Inlet and between Miami and Key West have been excluded.

The profiling-derived velocities were obtained by a freely falling dropsonde described by Richardson & Schmitz (1965). The data were then integrated horizontally to produce the transports. All the published values are plotted in figure 5*a* along with the 95% confidence limits derived from the monthly range in transport for the 1981–1990 voltage-derived transport of the Florida Current east of Jupiter Inlet. The partial transports by Brooks & Niiler (1975) have been multiplied by the factor 1.22 and increased by 5 Sv to compare them with the transport east of Jupiter Inlet. One sees that most of the profiling-derived transports lie within the range of the voltage-derived transport except for some low values between October and January. Because of these low values, the Niiler & Richardson (1973) annual variation (figure 5*a*) is inconsistent with the annual cycle derived from the voltage-derived transports. These low values could be caused by errors or by undersampling but an alternative explanation is that the transport east of Miami is smaller than the transport east of Jupiter Inlet due to flow into the Straits via the Northwest Providence Channel north of Miami. This flow could add a few Sverdrups to the profiling-derived transports east of Miami making them more consistent with the range in the voltage-derived transports east of Jupiter Inlet.

The recent profiling estimates of the transport for the Florida Current east of Jupiter Inlet started with the STACS program and consists of 130 days of velocity and temperature data from 19 different cruises (1982–1984) obtained by a profiling device (Pegasus) tracked by two bottom acoustic transponders at nine sites (table 3) approximately 10 km apart (Leaman *et al.* 1987) and 14 days (1985–1990) obtained, at the same sites, by the velocity profiler in the dropsonde mode. The variations in these transports, corrected for the barotropic tidal velocity, are consistent with the range in the voltage-derived transports (figure 5*b*). It is clear, however, that the number of profiling-derived transports is still not sufficient to accurately determine the annual variation in the transport.

The profiling-derived transports for the STACS program were computed from the depth-averaged velocities observed at the nine sites in the following manner. (1) The barotropic tidal velocity, based on the tidal constituents estimated from the hourly mean voltages and applying a tidal calibration factor, was first removed from each depth-averaged velocity value. (2) Missing depth-averaged velocity values were then filled by a linear time interpolation for gaps less than three days and extrapolated

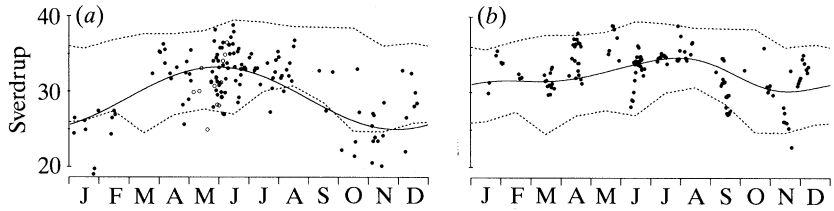

Figure 5. Profiling-derived transports. (*a*) 1964–1974 transports east of Miami (dots) and partial transports south of Key West times 1.22 plus 5 Sv (circles). Values are mostly consistent with the 95% confidence limits based on the 1981–1990 BK–SP voltage-derived transports (pair of dashed curves) but the annual variation (solid curve) from Niiler & Richardson (1973) is inconsistent with the 1982–1990 profiling-derived transports and the 1981–1990 voltage-derived transports. (*b*) 1982–1990 transports east of Jupiter Inlet. Values are consistent with the 95% confidence limits. Solid curve is annual variation based on the 1981–1990 voltage-derived transports.

Table 3. *Jupiter Inlet to Grand Bahama Island profiling site locations x_n, depths H_n, weights A_n, depth-averaged and velocity-weighted conductivities $\bar{\sigma}_n$ and $\tilde{\sigma}_n$, least squares estimated weights U_n, and estimates of sediment and upper crustal conductance τ'_n and τ'_{ns} (Spain & Sanford 1987) for $n = 1, \ldots, 9$ sites*

n	x_n/km	H_n/m	A_n/km^2	$\bar{\sigma}_n$/(S m^{-1})	$\tilde{\sigma}_n$/(S m^{-1})	U_n	std	τ'_n/(S)	std/(S)	τ'_{ns}/(S)
1	12.9	121	1.03	5.02	5.28	0.37	0.47			
2	19.7	225	1.81	4.74	5.13	1.48	0.48	2050	980	1630
3	28.1	363	3.30	4.59	4.98	0.86	0.39	3570	2270	2560
4	37.7	503	4.26	4.50	4.81	1.66	0.53	340	800	3070
5	45.4	612	6.14	4.47	4.73	0.88	0.31	2120	1650	3170
6	56.6	763	7.81	4.40	4.72	0.94	0.21	1150	980	2560
7	66.3	705	7.19	4.59	4.84	0.96	0.34	1280	1520	2800
8	77.0	634	6.31	4.75	4.87	0.65	0.33	3710	3240	2740
9	86.2	523	5.46	4.97	4.95	0.77	0.23	3200	1670	3220

one day beyond for gaps greater than three days. (3) Daily mean velocities were then constructed by a linear interpolation in time between the values. (4) The remaining missing values were then filled, for those days that had at least one observation, by a linear interpolation in space between the nearest sites having at least one observed velocity. Weights ranging from 0 to 9 were then assigned to each daily mean transport equal to the number of sites occupied for that day. The values with zero weights were then excluded. In all there were 144 daily mean transports based on 743 observed depth-averaged values, 446 time interpolated values, and 125 spatially interpolated values.

The volume transport

$$T(t) = \sum_{n=1}^{10} \int_{x_{n-1}}^{x_n} H(x)\, \tilde{V}(x,t), \mathrm{d}x$$

is computed for the depth $H(x)$ given by a cubic spline fit to the bottom topography and the depth-averaged velocity $\bar{V}(x,t)$ assumed to be linearly related to the observed profiling velocities $\bar{V}(x_n,t)$ by

$$\bar{V}(x,t) = (x_n - x_{n-1})^{-1}[(x_n - x)\, V(x_{n-1},t) + (x - x_{n-1})\, V(x_n,t)]$$

for $x_{n-1} \leqslant x \leqslant x_n$, where x_0 is on the western side of the strait, x_{10} is on the eastern

Figure 6

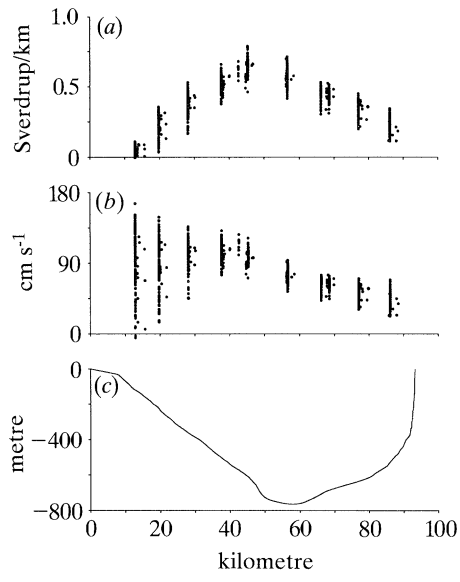

Figure 7

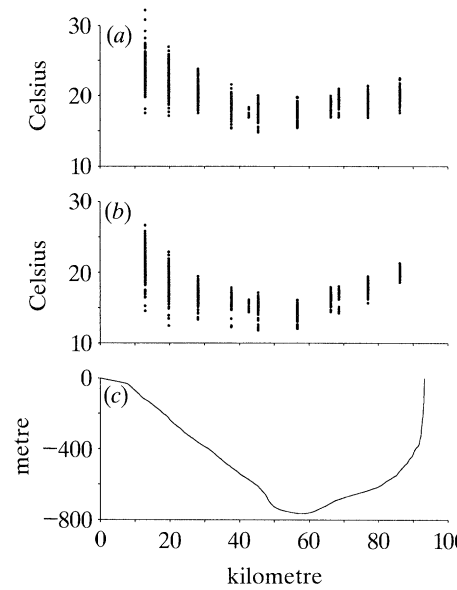

Figure 6. Profiling-derived transports east of Jupiter Inlet. (*a*) Transport per kilometre width. Range in values is similar at each site. (*b*) Depth-averaged velocity. Largest range in values are near Florida. (*c*) Channel depth east of Jupiter Inlet to Grand Bahama Island.

Figure 7. Profiling-derived temperatures east of Jupiter Inlet. (*a*) Flow temperature. (*b*) Strait temperature. Values are smaller than the flow temperature. The range in values is similar for both temperatures with largest range near Florida. (*c*) Channel depth east of Jupiter Inlet to Grand Bahama Island.

side of the strait, $V(x_0, t) = V(x_1, t)$ and $V(x_{10}, t) = V(x_9, t)$. The computed transport is then related to the observed depth-averaged velocities by

$$T(t) = \sum_{n=1}^{9} A_n \bar{V}(x_n, t) \tag{3.1}$$

for weights $A_n, n = 1, \ldots, 9$ (table 3) derived by evaluating integrals over $H(x)$ and $xH(x)$. Leaman *et al.* (1987), in their processing of the profiling data, estimate the error in the profiling-derived transport to be 0.4 Sv.

The largest range in the depth-averaged velocity (figure 6) occurs in the shallow coastal region but the transport per kilometre width, $H(x_n)\,\bar{V}(x_n, t)$ for $n = 1, \ldots, 9$, has a maximum value in the central portion of the strait with a range in values similar at each site except for the coastal site where the range is much smaller. Thus the coastal site makes only a small contribution to the temporal variations in the total transport and therefore the total transport variations can be observed with the cable–ocean contacts lying outside the Florida shelf region.

(ii) *Temperature*

The strait temperature and the flow temperature have a similar range in values at each site (figure 7) with the largest range occurring in the shallow coastal region. The strait temperature $\bar{\theta}(t)$ and the flow temperature $\tilde{\theta}(t)$ (see §2*a*(ii)) are slightly warmer from July to November (figure 8) but the large day-to-day variability makes it impossible to accurately determine the annual variation. The mean strait and

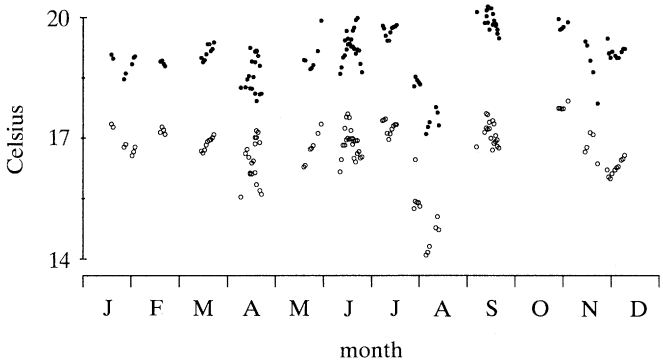

Figure 8. 1982–1985 profiling-derived temperatures. Dots are flow temperature and circles are strait temperature. The flow temperature is warmer than the strait temperature. The temperatures are slightly warmer from June to November, but the largest variations occur on a day-to-day timescale.

flow temperatures are $\theta_0 = 16.88 \pm 0.66\,^{\circ}\mathrm{C}$ and $\tilde{\theta}_0 = 19.10 \pm 0.63\,^{\circ}C$. Hence the Florida Current is, on average, $2.39 \pm 0.91\,^{\circ}\mathrm{C}$ warmer than the strait temperature.

The strait conductivity, for $\theta_0 = 16.9\,^{\circ}\mathrm{C}$ and $S_0 = 36$ ppt is, empirically, $\sigma_0 = 4.60\ \mathrm{S\ m^{-1}}$ with a temperature coefficient $a_\theta = 0.022\,^{\circ}\mathrm{C}^{-1}$ and a salinity coefficient $a_s = 0.025\ \mathrm{ppt}^{-1}$. The flow conductivity, for $\tilde{\theta}_0 = 19.1\,^{\circ}C$ and $\tilde{S}_0 = 36.0$ ppt, is $\tilde{\sigma}_0 = 4.83\ \mathrm{S\ m^{-1}}$ with coefficients $\tilde{a}_\theta = 0.022\,^{\circ}\mathrm{C}^{-1}$ and $\tilde{a}_S = 0.025\ \mathrm{ppt}^{-1}$. Hence the conductivity ratio is $\tilde{\sigma}_0/\sigma_0 = 1.050$.

(iii) *Meanders*

The meandering part of the transport per kilometre width, $H(x_n)\,\bar{V}_m(x_n, t)$ for $n = 1, \ldots, 9$ has a range of $0.3\ \mathrm{Sv\ km^{-1}}$ (figure 9*a*) that is similar to the range in the total transport per kilometre width, $H(x_n)\,\bar{V}(x_n, t)$ at each site (figure 6*a*). The transport $T_m(t)$ of the meanders has, however, a root mean square (rms) deviation of 0.53 Sv that is small compared with the rms deviation of 3.13 Sv for the total transport $T(t)$ (figure 10*a*).

A measure of the 'transport efficiency', defined here as the cross-stream variance of $\alpha(t)\langle\bar{V}(x)\rangle$ divided by the cross-stream variance of $\bar{V}(x, t)$, is given, for the profiling data, by

$$\gamma^2(t) = \sum_{n=1}^{9} A_n\,\bar{V}(x_n, t)\langle\bar{V}(x_n)\rangle \Big[\sum_{n=1}^{9} A_n\,\bar{V}(x_n, t)^2 \sum_{n=1}^{9} A_n\langle\bar{V}(x_n)\rangle^2\Big]^{-1} \tag{3.2}$$

for the least squares estimate $\alpha(t)$ (2.44) given by

$$\alpha(t) = \sum_{n=1}^{9} A_n\,\bar{V}(x_n, t)\langle\bar{V}(x_n)\rangle / \sum_{n=1}^{9} A_n\langle\bar{V}(x_n)\rangle^2.$$

The term γ^2 is, in fact, the spatial correlation squared between $\bar{V}(x, t)$ and $\langle\bar{V}(x)\rangle$. Thus when $\gamma^2 = 1$ there is no meandering and when $\gamma^2 = 0$ the flow is dominated by the meandering of the stream.

The 144 days of profiling-derived, depth-averaged velocities yield a median transport efficiency of 0.26. Johns & Schott (1987), in an analysis of the current meter data from an array of five subsurface moorings approximately 20 km apart with four instruments per mooring, find a transport efficiency, defined slightly differently by

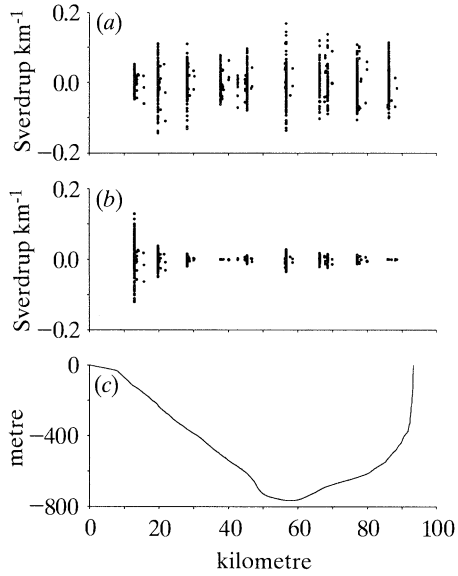

Figure 9. Profiling-derived meanders east of Jupiter Inlet. (*a*) Meandering transport per kilometre width. (*b*) Voltage meandering effect per kilometre width. It has a much smaller range in values than the range in the meandering transports. (*c*) Channel depth east of Jupiter Inlet to Grand Bahama Island.

them, that is generally less than 0.2. Thus the transport efficiency is even smaller for the velocities than for the depth-averaged velocities. This explains why it is not possible to compute accurate transport estimates of the Florida Current from a few current meter moorings. All five moorings are needed.

(iv) *Estimated error in voltage-derived transports*

The error in the voltage-derived transport, caused by various non-transport terms in the voltage-transport equation (2.33) and variations in the voltage calibration factor (2.34), can be estimated by making use of the profiling data and the circuit model. The various sources of error are as follows. (1) The term T_{wm}. The profiling data yield values that are usually smaller than 1 Sv (figure 10*b*) with a rms deviation of 0.45 Sv. The voltage meandering effect per kilometre width, $[W(x_n)/\tilde{W}_0 - 1]\, H(x_n)\, \bar{V}_m(x_n, t)$ for $n = 1, \ldots, 9$, yields a range in values that is smaller than 0.1 Sv km^{-1} (figure 9*b*). This is much smaller than the range in values for the meanders $H(x_n)\, \bar{V}_m(x_n, t)$ except for the site closest to Florida. Thus the meandering effects on the BK–SP voltages are small because the cable–ocean contact lies outside the shallow shelf region. (2) The term $\tilde{a}_\theta T_\theta$ for $\tilde{a}_\theta = 0.022\ ^\circ\mathrm{C}^{-1}$. The profiling data yield values that are usually smaller than 1 Sv (figure 10*b*) with a rms deviation of 0.47 Sv. (3) The term ϵ. The profiling data yield values that are usually smaller than 1 % (figure 10*c*) with a rms deviation of 0.7 %. This corresponds to an error of ± 0.23 Sv in the voltage-derived transports for mean transport 32.3 Sv. (4) The term

$$\tilde{a}_\theta \int_0^L H(x)\, [W(x)/\tilde{W}_0 - 1]\, \bar{V}_\theta(x, t)\, \mathrm{d}x$$

dropped in the voltage-transport equation. The profiling data yield a rms deviation

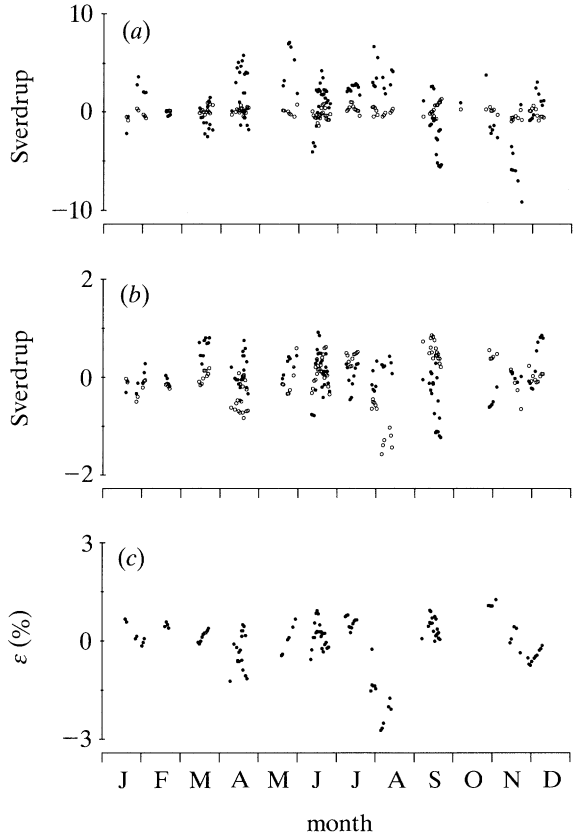

Figure 10. Profiling-derived estimates of errors in the voltage-derived transport. (*a*) Transport minus 32.3 Sv (dots) and transport of meanders T_m (circles). (*b*) Temperature flux $\tilde{a}_\theta T_\theta$ (dots) and voltage meandering effect T_{wm} (circles). (*c*) ϵ (dots) as percent changes in calibration factor. The volume transport has the largest variation; the variation of all other terms are negligible.

of only 0.07 Sv. (5) The term T_S. It was not observed but its effect is expected to be small because $\tilde{a}_S$ is small and the variations in salinity are expected to be small. (6) The term $\tilde{\epsilon}^*$. Its value is estimated by the circuit model, to be smaller than 0.1 for the BK–SP voltages. If 300 km $\leqslant Y \leqslant$ 500 km, then $0.06 \leqslant \tilde{\epsilon}^* \leqslant 0.03$ (table 1) and the estimated error in $\tilde{\epsilon}^*$ is ± 0.015. This corresponds to an error of ± 0.48 Sv in the voltage-derived transports for a mean transport of 32.3 Sv.

In summary, the terms T_{wm}, T_θ, ϵ, and $\tilde{\epsilon}^*$ yield rms deviations of 0.45, 0.47, 0.23, 0.48 Sv and a total rms deviation of 0.84 Sv. These deviations and the total deviation are 1.4%, 1.5%, 0.7%, 1.5%, 2.1% of the mean transport 32.3 Sv. These are small compared with the deviation in the transport that is 3.13 Sv on 9.7% of the mean. Hence the BK–SP cross-stream voltages can be used to determine the transport variations with an accuracy of ± 0.8 Sv.

The voltage-transport equation for the Straits of Florida east of Jupiter Inlet thus reduces to a simple linear relation between voltage and transport

$$C_0 \Delta\phi_V(t) = T(t), \tag{3.3}$$

with a constant voltage calibration factor $C_0 = (1-\tilde{\epsilon}_0^*)^{-1} \tilde{W}_0^{-1}$ (2.40).

Table 4. *Voltage difference between different electrodes relative to* Ag–AgCl (*B*, *1*) *for various durations in hours*
(B = basement of cable station, L = lagoon, 1 = first electrode, and 2 = second electrode.)

bias (mV)	std (mV)	hours	electrode
−0.1	1.8	41405	Ag–AgCl(B, 2)
−48.9	3.9	53170	Ag–AgCl(L)
221.9	20.9	6475	Cu(B)
323.6	32.9[a]	2443	Pb(B)
570.7	13.9	11804	Pb–PbCl(B, 1)
559.9	5.9	7793	Pb–PbCl(B, 2)
401.7	131.2	60225	armour–copper

[a] Error measured relative to armour–copper contact.

(*b*) *Voltage measurements*

The first attempt to observe motion-induced voltages was made by Faraday (1832) who recorded the voltage between two copper plates suspended on opposite ends of the Waterloo Bridge. Erratic variations in voltage made it impossible for him to detect the tidal motion in the Thames but he predicted that the Gulf Stream should produce a measurable signal. He assumed that the erratic variations were caused by electrode noise but these variations may have been caused by geomagnetic-induced voltages since his observations were probably made during the period of sunspot maximum (1827–1831).

(i) *Key West minus Havana voltages*

The first observations of the Florida Current induced voltages were made from 1952 to 1961 by recording the Key West minus Havana (KW–HV) voltages by the use of a telephone cable when it was not in service during weekends (Wertheim 1954; Stommel 1957, 1959, 1961; Broida 1962, 1963) (figure 1). The distance is about 170 km and the cable is orientated 111° east of the stream direction. Only 491 daily mean values were obtained. Good agreement was found in 1952 between five months of voltage variations and sea level difference between Key West and Havana (Wertheim 1954) which means that the voltage variations seemed to be tracking the transport variations. The Key West tide station was discontinued at the end of 1952 so no further comparisons could be made. During the first two years (1952–1953) there were some large voltage variations lasting from days to months that were considered to be unrealistically large and rapid by Schmitz & Richardson (1968) and Wunsch *et al.* (1969). They therefore judged the KW–HV voltages to be hopelessly contaminated by the meandering of the Florida Current and concluded that this was not a suitable site for voltage measurements of transport. This caused most oceanographers to ignore voltage measurements as a means for monitoring transport variations.

The circuit model of the meandering effects for $I^* = 0$ (§2*c*) shows that the error in the voltage-derived transport could be as large as ±27% for the KW–HV voltages if the stream meanders by ±20 km whereas it is only ±3% for the BK–SP voltages if the stream meanders by ±10 km. The voltage meandering effect estimated from the profiling data (§3*a*) is ±1.4% for the BK–SP voltage-derived transports, which shows that the circuit model gives a reasonable estimate of the meandering effect.

The voltage meandering effect is therefore expected to be a significant problem for the KW–HV voltages.

The evaluation of the KW–HV voltages for monitoring transport is complicated, however, by the following. (1) The transport variations were not determined by an independent method and therefore the voltage calibration factor, the bias voltage, and the cross-stream spatial distribution of the depth-averaged velocity are unknown. (2) The voltages were so sparsely sampled that the daily changes in transport were undersampled. The day-to-day changes are now known to be significant. (3) The geomagnetic-induced variation was hand filtered. (4) The bias voltage drifted during April 1958 by an amount estimated to be +560 mV which is equivalent to a 14.4 Sv change. Such a large change was most likely caused by the Ag–AgCl electrode at the cable–ocean contact near Florida changing to copper because the electrode went bad. Sanford observed, for example, a change of +620 mV in the Jupiter Inlet minus Settlement Point voltage when an Ag–AgCl electrode disappeared at Jupiter Inlet. The observed *in situ* voltage difference between various types of electrodes (table 4) also shows that there can be a voltage bias of nearly one volt between different types of electrodes. (5) The conductance of the sediments and the stream's cross-sectional dimensions are unknown and this increases the uncertainty in the model estimates of the voltage changes caused by meanders and horizontal electric currents.

In an attempt to better understand and evaluate the KW–HV voltages, the original strip chart recordings of the voltage variations for one month in 1970 and 10 months during 1972–1973 were obtained from Sanford. Hourly time marks were determined by assuming the chart speed was constant between the time marks entered on the record. Hourly mean values were then determined by the slope technique (Larsen 1974). The time marks were then checked and corrected by comparing the voltage variations with the geomagnetic-induced voltages based on the magnetic variations recorded at San Juan, Puerto Rico and Fredericksburg, Virginia (see §3*c*). The corrections amount to, at most, a 1.7 h shift for the last month of data when timing marks had not been entered.

(ii) *Jupiter Inlet minus Settlement Point voltages*

The Jupiter Inlet minus Settlement Point JI–SP voltages were recorded from 1969 to 1974 (Sanford 1892) by the use of a submarine co-axial communication cable (figure 1) installed in 1954. The distance is about 113 km and the cable is orientated 97° east of the stream direction. The coaxial cable is made up of an inner copper conductor, an insulating layer of polyethylene, a laminated outer copper conductor, a layer of jute serving, armour wires, and a layer of jute and tar. The armour and outer copper conductor are therefore in contact with seawater. A description of the shore facilities is given by Sanford (1982).

Sanford (1982) felt that recording the JI–SP voltages would reduce the meandering effects because the Straits of Florida is so much narrower east of Jupiter Inlet than south of Key West. An analysis of voltage measurements by the method of towed electrodes (Sanford & Schmitz 1971) also showed that the electrical measurements between Miami and Bimini could determine transport to within an uncertainty of 10% of the mean. Sanford suspended his JI–SP voltage measurements in 1974 because of equipment failure.

The JI–SP voltages recorded between January 1970 and October 1972 were hand-filtered by Sanford (1982) to remove the geomagnetic-induced variations and were

PHILOSOPHICAL TRANSACTIONS OF THE ROYAL SOCIETY A MATHEMATICAL, PHYSICAL & ENGINEERING SCIENCES

then analysed by him to extract the annual variation. In this paper objective values of the hourly mean JI–SP voltages were determined by use of the slope technique (Larsen 1974) applied to the original 1969 to 1974 strip chart recordings. The timing marks were then checked and corrected by a comparison with the geomagnetic-induced voltages and the tidal variation.

(iii) *Jupiter Inlet minus Cable Break and Cable Break minus Settlement Point voltages*

Recordings of the Jupiter Inlet minus Settlement Point voltages were started again in December 1981. The cable had been broken, however, in shallow water near Florida during or after 1974. Two attempts in 1981 and 1982 were, however, unsuccessful in repairing the break. Fault localization and insulation tests were then carried out yielding the following conclusions. (1) The break is 16.6 km of cable east of Jupiter Inlet and 98.9 km of cable west of Settlement Point. Since the distance between Jupiter Inlet and Settlement Point is 113 km, the distance from Settlement Point to the break is 96.7 km and the distance from Jupiter Inlet to the break is 16.3 km. (2) The break is complete. (3) The centre conductor and its surrounding polyethylene dielectric, excluding the break, is electrically sound. (4) The mechanical strength of the cable resides in its armour wires. Since the cable has aged it is no longer capable of being handled by a cable ship.

Owing to the cable break, the Jupiter Inlet minus cable break (JI–BK) voltages were recorded at Jupiter Inlet and the cable break minus Settlement Point (BK–SP) voltages were recorded at Settlement Point (figure 1). The sum of the two voltage measurements will be equal to the JI–SP voltages since the cable–ocean contacts are similar because the cable–ocean contacts at Jupiter Inlet and Settlement Point were initially the outer copper conductor of the coaxial cable and the cable–ocean contacts at the cable break were the exposed, inner copper conductor of the cable. The mean JI–BK plus BK–SP voltage was found to be about 1.3 V which agrees with the earlier mean JI–SP voltage when the cable was intact. The bias for the combined voltages will therefore be small but there may be a significant bias voltage for the individual JI–BK and BK–SP voltages because of electrochemical differences between the outer copper conductor and the exposed, inner copper conductor.

Recordings of the JI–BK and BK–SP voltages were initially made by a battery powered, digital Lycor recorder that printed hourly mean values. The times of the hourly values were then checked by a comparison with the geomagnetic-induced voltages based on the magnetic variations at San Juan and Fredericksburg and by a comparison with the tidal variation estimated by ten-day sections. The cable-ocean contact at Settlement Point was changed in January 1984 from the outer copper conductor of the cable to a Ag–AgCl electrode placed beneath the cable station in the basement 2.5 m by 2.5 m flooded with 0.6 m of seawater of 27.7 ppt salinity. The Ag–AgCl electrode is therefore in good electrical contact with the open ocean and provides a cable-ocean contact superior to the outer copper conductor of the cable. A new recorder, installed in November 1984 and powered by solar cells, generated hourly mean values from one minute filtered samples of the voltage. This recorder consisted of a pair of differential amplifiers used at a gain of one with a bias current of 25 pA and a long-term stability of 10 μV a^{-1}. The noise is therefore well below the desired 1 mV accuracy of the voltage measurements. The hourly mean values along with temperature and various battery checks were transmitted via a satellite data link.

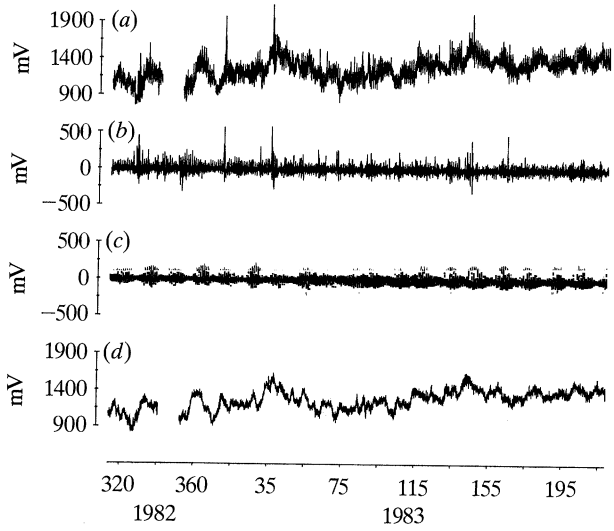

Figure 11. Sample of BK–SP observed voltages. (*a*) Observed voltages. (*b*) Estimated geomagnetic-induced voltages. (*c*) Estimated tidal variation. (*d*) Voltages corrected for geomagnetic-induced voltages, tidal variation, and outliers. Note that the corrected voltages are much smoother than the observed voltages verifying the validity of the corrections.

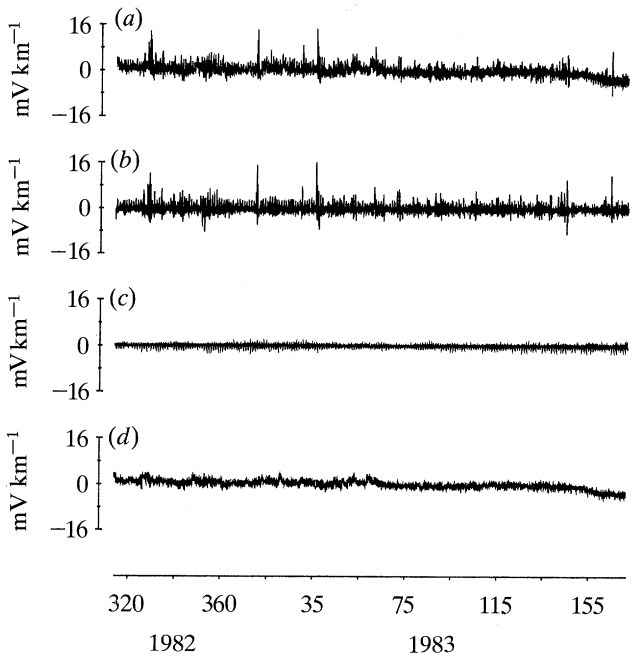

Figure 12. Samples of east JI–BK electric field. (*a*) Observed field. (*b*) Estimated geomagnetic-induced field. (*c*) Estimated tidal variation. (*d*) Corrected electric field. The geomagnetic-induced variation dominates.

The recordings of the voltages at Jupiter Inlet were discontinued in November 1987 because it became clear that the JI–BK voltages showed little relationship to changes in the total transport or to changes in the partial transport near Florida as derived from the near-shore velocity profiling data. It was also clear that the voltage-derived transports could be more accurately determined from the BK–SP voltages alone. In October 1985 a clean cable cut was made to improve the cable-ocean contact at the cable break for the BK–SP voltages. The cut shortened the BK–SP cable by an amount estimated to be less than 0.5 km. A magnetic station was installed at Settlement Point in June 1988 and the observed hourly mean magnetic values were transmitted by satellite.

The cable broke in deep water (640 m) and 33.6 km from Settlement Point on 29 November 1990. This is most likely due to mechanical aging because of the advanced age (37 years) of the cable. The depth precludes a man made fault and points, rather, to corrosion and chafing as the cause of the fault. This means that the cable is likely to be in such a mechanically weakened condition that it is not feasible to repair it.

A sample of the BK–SP voltage variations is given in figure 11*a* and a sample of the JI–BK variations, converted to east electric field by dividing the JI–BK voltage by the distance 16.3 km, is given in figure 12*a*.

(iv) *West Palm Beach minus Eight Mile Rock voltages*

The West Palm Beach, Florida minus Eight Mile Rock, Grand Bahama Island (WP–EM) voltages (figure 1) have been observed by recording the power voltage and power current on an in-service, undersea telephone cable that makes ocean contact near West Palm Beach and Eight Mile Rock (Larsen 1991). This cable, installed in 1972, has 11 repeaters and is located about 25 km south of the Jupiter Inlet to Settlement Point cable. The recorders are similar to those used to record the JI–BK and BK–SP voltages.

The essential elements of an in-service, undersea telephone cable for voltage measurements are: submarine cable, repeaters, power supply, power separation filters and cable sea–earth grounds. The telephone transmission enters and leaves the cable via the power separation filters at the cable ends and is amplified by the repeaters powered by a shore based power station supplying a nearly constant electric current. This current flows down the cable via the inner copper conductor and returns through the ocean via the sea–earth grounds near the cable stations. It is the existence of the sea–earth grounds and the nearly constant power current that makes it possible to deduce the variations in the motion-induced voltages between the sea–earth grounds by accurately recording the power voltage and current variations. The time variations in these voltages, after applying various corrections (Larsen 1991), determines the transport variations but not the mean transport, because of the large, approximately 360 V offset caused by the power current. The monthly mean values of the WP–EM voltage-derived transport are estimated to have an accuracy of 1 Sv (Larsen 1991). This makes the monthly mean values acceptable for transport estimates.

(v) *Canal 18 electric field*

The voltage effects of the electric currents I^* was observed at an electric field land station, C18, installed 12.5 km due west from the Florida coast and 1 km south of Jupiter Inlet (figure 1) at a junction in Canal 18 serving as a drainage system for the area and for maintaining a fresh water barrier to salt water intrusion. The voltages

Figure 13

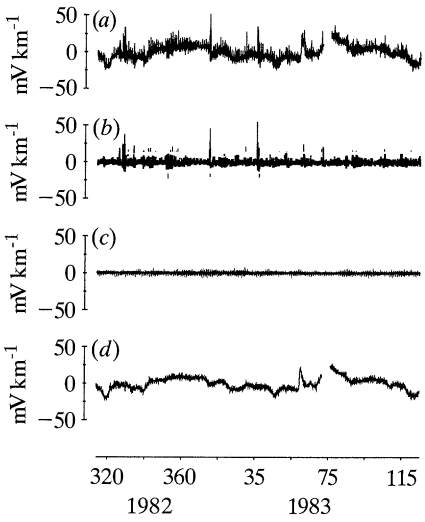

Figure 14

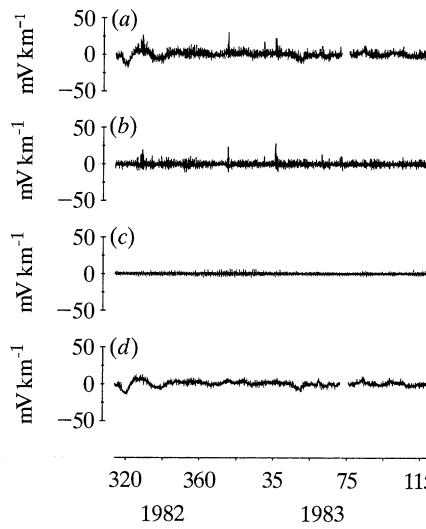

Figure 13. East C18 electric field. (*a*) Observed field. (*b*) Estimated geomagnetic-induced field. (*c*) Estimated tidal variation. (*d*) Corrected electric field. The variations are much larger in the east C18 than in the east JI–BK electric field.

Figure 14. North C18 electric field. (*a*) Observed field. (*b*) Estimated geomagnetic-induced field. (*c*) Estimated tidal variation. (*d*) Corrected electric field. The geomagnetic-induced variation is smaller in the north C18 than in the east C18 electric field because of the large east–west conductivity contrast between the ocean and land.

were measured between two pairs of Ag–AgCl electrodes: one pair along the west leg of Canal 18 in a direction 91° NE with a 817 m spread and the other pair along the east leg of Canal 18 in a direction 176° east of north with a 880 m spread. The recorders were similar to those used for recording the JI–BK and BK–SP voltages. The electric field was determined from the negative of the voltage divided by the distance between the electrodes. The electric field was then transformed into north and east components. The station was maintained for two years but only 200 days of hourly values were recovered due to a severe lightning problem that caused the recording system to repeatedly fail and the electrodes to drift after the system failed. The east component, after removing the long period drift of the electrodes, is given in figure 13*a* and the north component is given in figure 14*a*. Note that the geomagnetic-induced variation is significantly larger in the east component than in the north component. This is due to the large east–west conductivity contrast between the ocean and land.

(*c*) *Voltage corrections*

The power spectrum of the observed hourly 1981–1990 BK–SP voltages (figure 15*a*) shows spectral peaks at 1, 2 and 3 cpd and variations that generally increase in intensity with decreasing frequency. The power spectrum of the geomagnetic-induced voltages (figure 15*b*) shows that the geomagnetic-induced variation is an important part of the observed voltages for frequencies greater than 0.2 cpd and especially for frequencies at 1, 2 and 3 cpd because of the large solar diurnal variation. The geomagnetic-induced voltages must therefore be removed from the observed hourly voltages in order to determine the hourly motion-induced voltages.

PHILOSOPHICAL TRANSACTIONS OF THE ROYAL SOCIETY A MATHEMATICAL, PHYSICAL & ENGINEERING SCIENCES

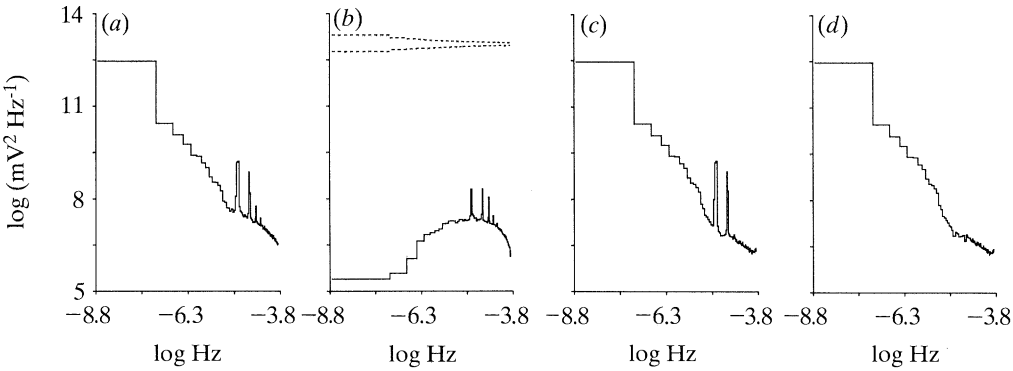

Figure 15. Power spectra of hourly BK–SP voltages against common logarithm of frequency in Hertz. (*a*) Observed voltages. (*b*) Geomagnetic-induced voltages. (*c*) Voltages minus geomagnetic-induced voltages. (*d*) Voltages minus tidal variation, geomagnetic-induced variation, and outliers. Pair of dashed curves (top right panel) are 95% confidence limits that apply to all spectra. The removal of the tidal and geomagnetic-induced variations yields a very smooth residual spectrum.

The various voltage corrections needed for determining the motion-induced voltages are discussed in the following sections.

(i) *Geomagnetic-induced voltages*

The voltage variations induced in the ocean by the time varying ionospheric and magnetospheric electric currents can easily mask the motion-induced voltages for frequencies greater than 0.2 cpd and especially for the tidal-induced voltages having frequencies near 1 and 2 cpd (figure 15*b*). This has been a serious problem for the earlier voltage measurements but experimental evidence presented here shows that it is possible to remove most of the geomagnetic-induced voltages by applying transfer functions to hourly magnetic variations observed at land sites within 100 km of the voltage measurements. This method works because the ionospheric electric currents are coherent over distances much larger than 100 km if the voltage and magnetic sites are outside the auroral zone and away from the magnetic dip equator.

The geomagnetic-induced voltages can also be removed by the use of hourly magnetic variations observed at sites 1000 km or more from the voltage site because the hourly variations, after removing the solar variations, are dominated by the disturbed storm time variations (D_{st}) that are globally coherent (Chapman & Bartels 1940). The solar diurnal variation has to be filtered out because it has a large spatial gradient modulated by a large annual variation. The K_1 and S_2 tidal constituents are therefore lost because they have, respectively, frequencies 1.0027 and 2.0000 cpd, that are similar to the frequencies of the solar diurnal variation.

The transfer functions, used to convert the magnetic variations to the geomagnetic-induced voltages, are defined in the frequency and wavenumber domain by the magnetotelluric relation

$$\hat{E}(\omega, \boldsymbol{k}) = Z(\omega, \boldsymbol{k})\, \hat{B}(\omega, \boldsymbol{k}), \tag{3.4}$$

where $\hat{E}$ is the electric field, $\hat{B}$ is the magnetic field, ω is the radian frequency, $\boldsymbol{k}$ is the horizontal vector wavenumber, and Z is the magnetotelluric transfer function. Experience shows that the small wavenumber approximation, $Z(\omega, \boldsymbol{k}) \approx Z(\omega, 0)$, is

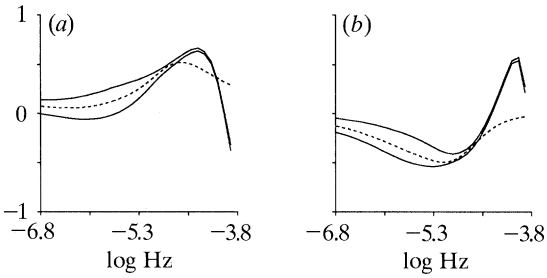

Figure 16. The geomagnetic transfer function as a non-dimensional value $(\mu_0/\omega)^{\frac{1}{2}}\, Z(\omega, 0)$ against the common logarithm of the frequency for the Settlement Point magnetic field in the direction 19.9 east of north where μ_0 is the magnetic permeability of free space and ω is the radian frequency. The pairs of curves are the 95% confidence limits for the real (a) and the imaginary (b) parts. Dashed curves are real and imaginary parts of the transfer function for the best fitting one dimensional conductivity model.

valid for magnetic sites close to the voltage measurements or for D_{st} variations at remote magnetic sites. The approximation is, however, not valid for solar diurnal variations at remote sites because of time variations in $\boldsymbol{k}$.

The geomagnetic-induced voltage is given by

$$\Delta\Phi_G(\omega, y) = -\int_0^L E(\omega, x, y)\,\mathrm{d}x, \tag{3.5}$$

where

$$E(\omega, x, y) = Z(\omega, 0)\, B(\omega, x, y) \tag{3.6}$$

that is the inverse spatial transform of (3.4) for the small wavenumber approximation. The geomagnetic-induced voltage is then

$$\Delta\Phi_G(\omega) = T(\omega)\, B(\omega), \tag{3.7}$$

where $T(\omega) = -Z(\omega, 0)/L$, and

$$B(\omega) = L^{-1}\int_0^L B(\omega, x, y)\,\mathrm{d}x \tag{3.8}$$

is the magnetic field averaged along the cable. The geomagnetic-induced voltage for two magnetic components is given by

$$\Delta\Phi_G(\omega) = T_1(\omega)\, B_1(\omega) + T_2(\omega)\, B_2(\omega), \tag{3.9}$$

where B_1 and B_2 are approximated by the horizontal magnetic components at one site or by the magnetic components at two different remote sites and the T_1 and T_2 are the transfer functions. The time series of the geomagnetic-induced voltages $\Delta\phi_G(t)$ is then given by the inverse Fourier transform of $\Delta\Phi_G(\omega)$.

The transfer functions are determined in the following manner. Theory and experimental evidence (Larsen 1989) indicates that the magnetotelluric transfer function $Z(\omega, 0)$ will be a smooth, continuous function of frequency that can be represented by

$$Z(\omega, 0) = D(\omega)\, Z_{1\mathrm{D}}(\omega), \tag{3.10}$$

where

$$Z_{1\mathrm{D}}(\omega) = -\mathrm{i}\omega \sum_{n=1}^{N-1} a_n[b_n - \mathrm{i}\omega]^{-1} - \mathrm{i}\omega\, a_N, \tag{3.11}$$

is the transfer function for a one dimensional (1D) conductivity model with $a_n \geqslant 0$,

PHILOSOPHICAL TRANSACTIONS OF THE ROYAL SOCIETY A MATHEMATICAL, PHYSICAL & ENGINEERING SCIENCES

$b_n \geqslant 0$, $\mathrm{i} = \sqrt{-1}$, and fields proportional to $\exp(-\mathrm{i}\omega t)$ (Weidelt 1972; Parker 1980); and

$$D(\omega) = \sum_{n=1}^{M} d_n (2\omega/\omega_J - 1)^{n-1} \tag{3.12}$$

is the distortion function that smoothly transforms the 1D transfer function to the observed transfer function. The ω_J is the Nyquist frequency. Generally $M < 10$ is sufficient.

The distortion function D is found iteratively, for an initial Z_{1D}, by a robust least squares method that yields weighted residuals that are nearly independent and identically distributed in the frequency and time domain (Larsen 1989). A new Z_{1D} is then generated from the a_ns and b_ns for $n = 1, \ldots, N$ derived by the D^+ inversion algorithm (Parker & Whaler 1981) of the estimated transfer function given by (3.10). The process is then repeated for five iterations. The representation of the transfer function by (3.10) is important because it allows the iterative process to converge to the 1D representation if most of the data are consistent with a 1D interpretation. The transfer function for the Settlement Point magnetic data is shown in figure 16. It indicates a 1D model for frequencies smaller than 1 cpd.

Samples of the hourly geomagnetic-induced variations for the BK–SP, JI–BK, and C18 data (figures 11*b*, 12*b*, 13*b* and 14*b*) show that the geomagnetic-induced voltages are a significant part of the variations in the BK–SP voltages and a major part of the variations in the C18 and JI–BK electric field data. The power spectrum (figure 15*b*) of the BK–SP geomagnetic-induced voltages show that the diurnal variation has strong spectral peaks at 1, 2 and 3 cpd and that the geomagnetic-induced voltages are important for frequencies greater than 0.2 cpd. The removal of the geomagnetic-induced voltages is therefore necessary to determine accurately the tidal and day-to-day variations.

(ii) *Geomagnetic secular change*

The magnitude of the vertical magnetic field for the Straits of Florida has decreased by 100 nT per year over the past two decades. It had a magnitude of $F_z = 41100$ nT at the end of 1981 for Jupiter Inlet. Since the voltage calibration factor is proportional to the magnitude of the vertical magnetic field, this secular change has caused a 2% decrease in the magnitude of the voltage variations over the past eight years. This decrease is removed by multiplying the motion-induced voltages by a factor inversely proportional to the secular change in F_z.

(iii) *Contact potentials*

The most important experimental detail that affects the accuracy of long-term voltage measurements is the stability of the cable-ocean contacts. This depends on the type of electrode used and on the thermal and chemical changes at the electrodes. The voltage difference between a pair of similar electrodes in seawater is mainly a function of temperature and salinity (Sanford 1967) that can be written as

$$\Delta\phi_N = \phi(\theta_1, S_1) - \phi(\theta_2, S_2), \tag{3.13}$$

where θ and S are, respectively, the temperature and salinity at electrodes 1 and 2. The voltage difference, for the usually small temperature and salinity differences in the ocean, can then be approximated by the linear relation

$$\Delta\phi_N \approx \beta_\theta(\theta_1 - \theta_2) + \beta_S(S_1 - S_2), \tag{3.14}$$

PHILOSOPHICAL TRANSACTIONS OF THE ROYAL SOCIETY A MATHEMATICAL, PHYSICAL & ENGINEERING SCIENCES

where β_θ and β_S are, respectively, the temperature and salinity coefficients for a pair of electrodes.

Silver–silver-chloride (Ag–AgCl) electrodes are a class of electrodes called reference electrodes where the metal is in equilibrium with a saturated solution of a slightly soluble salt. They have been used extensively in the ocean (Filloux 1987). The coefficients for Ag–AgCl electrodes in seawater can be approximated (Sanford 1967) by

$$\beta_\theta \approx a + b(\theta_1 - \theta_2) \tag{3.15}$$

and

$$\beta_s \approx -c\,\theta_2/S_2\,, \tag{3.16}$$

where experimentally

$$a = 0.315\,\text{mV}\ ^\circ\text{C}^{-1}, \quad b = 0.035\,\text{mV}\ ^\circ\text{C}^{-2} \quad \text{and} \quad c = 0.0612\,\text{mV ppt}^{-1}$$

(Sanford 1967). Thus $\beta_\theta \approx 0.35$ mV °C^{-1} and $\beta_s \approx -0.51$ mV ppt^{-1} for $\theta_1 - \theta_2 = 1$ °C, $\theta_2 = 298$ K and $S_2 = 36$ ppt.

The voltage variations caused by the effects of temperature and salinity variations on the type of Ag–AgCl electrodes used at Settlement Point and described by Filloux (1987) were determined by experiments carried out on three Ag–AgCl electrodes in an 80 gallon tank containing seawater and a reference Ag–AgCl electrode in an 80 gallon tank containing a NaCl solution of 35 ppt. The tanks were connected by a salt bridge consisting of a 1.2 cm diameter plastic tube. The voltage variations of the three different electrodes in the seawater tank relative to the electrode in the NaCl tank were measured for various temperatures and salinities of the seawater tank over a temperature range 4.6 °C to 40.0 °C and salinity range 4.7 ppt to 36.7 ppt. There was no significant difference between the three electrodes and the experimental results yielded coefficients $a = 0.525 \pm 0.093$ mV °C^{-1} and $b = -0.0077 \pm 0.0039$ mV °C^{-2} for temperatures between 10 °C and 34 °C. These coefficients appear to be independent of salinity variations.

The temperature coefficient is thus $\beta_\theta = 0.517$ mV °C^{-1} for a temperature difference of 1 °C. This temperature coefficient combines the temperature effects caused by the Ag–AgCl : seawater junction potential and the thermocouple effect of the Cu : Ag junction potential where the electrode is spliced onto the copper wire leading to the recorder. The effects of the liquid : liquid junction potential within the salt bridge is not expected to be important.

The experimental results yielded a salinity coefficient

$$\beta_s = -1.145 \pm 0.035\,\text{mV ppt}^{-1}$$

for salinities between 6.9 ppt and 36.7 ppt. The salinity coefficient appears to be independent of temperature variations.

The above experimental results are only approximately consistent with the results of Sanford (1967) but show, nevertheless, that the temperature- and salinity-induced voltage variation in $\Delta\phi_N$ for the Ag–AgCl electrodes will be less than a few millivolts if the variation in the temperature difference between the electrodes is less than a few degrees Celsius and if the variation in the salinity between the electrodes is less than a few ppt salinity. Thus the temperature and salinity effects on the cable–ocean contacts can be ignored for long cables in the deep ocean provided Ag–AgCl electrodes are used. In estuaries the observed voltages will be much smaller because the cable lengths and transports are smaller. The temperature and salinity effects on the electrodes then become very important which means that the Ag–AgCl electrodes

PHILOSOPHICAL TRANSACTIONS OF THE ROYAL SOCIETY A MATHEMATICAL, PHYSICAL & ENGINEERING SCIENCES

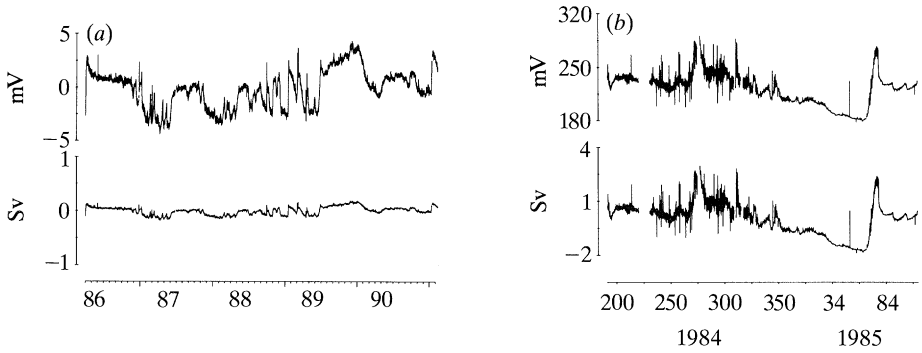

Figure 17. The hourly mean voltage difference observed (*a*) between two similar Ag–AgCl electrodes and (*b*) between a copper wire and a Ag–AgCl electrode. The electrodes were in the seawater basement of the cable station at Settlement Point. The error in the transport (bottom curve for (*a*) and (*b*)) is derived by multiplying the voltages by the voltage calibration factor for the BK–SP voltages. The Ag–AgCl electrode provides an excellent cable–ocean contact but the copper wire does not.

should be buried or placed in wells to reduce the variability in the temperature and salinity at the electrodes.

Different types of metal–seawater contacts have been tested at Settlement Point for various durations to evaluate the stability of the outer copper conductor, the inner copper conductor, and other types of electrodes (table 4). Two Ag–AgCl electrodes, two Pb–PbCl electrodes, a Cu wire, and a Pb wire were therefore placed in the seawater basement of the cable station, and an Ag–AgCl electrode placed in a nearby lagoon. The latter electrode was connected to the electrodes in the basement by a cable installed in the 1970s by Sanford. The voltages between these electrodes, including the outer copper conductor at Settlement Point, were recorded relative to a common Ag–AgCl electrode in the basement.

A summary of the experimental results (table 4) is as follows. (1) The small standard deviations between the Ag–AgCl electrodes, less than 4 mV, indicate that the Ag–AgCl electrode makes the best cable–ocean contact with a long-term drift less than 9 mV (figure 17*a*). This corresponds to a transport error of 0.2 Sv for a voltage calibration factor of 24.42 Sv V^{-1}. The rms deviation of 1.8 mV (table 4) corresponds to a transport error of ± 0.04 Sv. (2) The Pb wire is unacceptable. (3) The Pb–PbCl electrodes were initially quite good but started to drift when the plaster of paris that encased the Pb–PbCl electrode disintegrated after a few months of immersion in seawater. (4) Copper is not a good choice because the long term changes were as large as 112 mV relative to Ag–AgCl (figure 17*b*). The use of copper would therefore yield an unacceptable transport error of 2.7 Sv. The rms deviation of 20.9 mV corresponds to a transport error of ± 0.5 Sv. (5) The outer copper conductor at Settlement Point relative to copper (table 4) was 180 mV which indicates that this contact is mainly copper. It showed, however, erratic changes of 200 mV compared with the Ag–AgCl electrode. This indicates that the outer copper conductor at Settlement Point was changing from copper to a mixture of armour and copper which means the outer copper conductor is a bi-metal armour–copper contact and is therefore unacceptable as a cable–ocean contact.

PHILOSOPHICAL TRANSACTIONS OF THE ROYAL SOCIETY A MATHEMATICAL, PHYSICAL & ENGINEERING SCIENCES

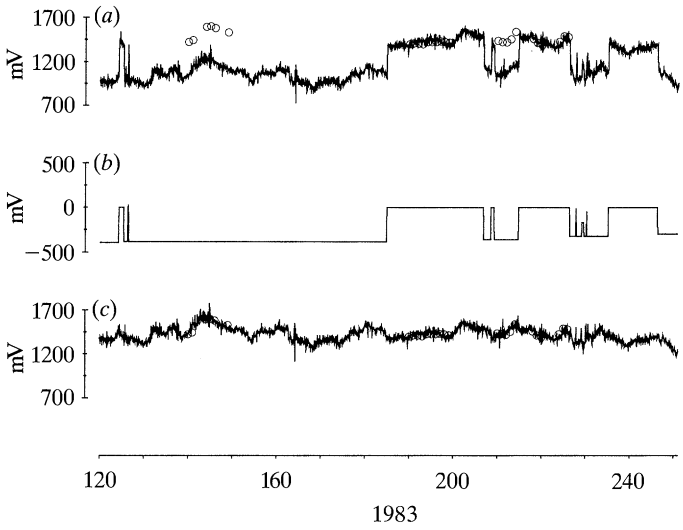

Figure 18. BK–SP voltage corrections. (*a*) Observed voltages minus tidal and geomagnetic-induced variations. Transport from velocity profiling data is converted to voltages (circles) by dividing by the voltage calibration factor. (*b*) Estimated offsets and outliers in cable–ocean contact potential. (*c*) Corrected voltages. The offsets have clearly been removed.

(iv) *Armour–copper contact potential*

The outer copper conductor of the coaxial cable was used as the cable–ocean contact at Settlement Point and Jupiter Inlet for the JI–SP and JI–BK voltages and initially for the BK–SP voltages. The outer copper conductor compared to a bare copper wire in the basement seawater of the cable station at Jupiter Inlet in 1981 was observed to give a voltage difference comparable in magnitude to the voltage of +670 mV observed between copper and armour in salt water of salinity 34.2 ppt and room temperature. Thus the cable–ocean contact at Jupiter Inlet at this time was mainly the steel armour surrounding the coaxial cable and not the outer copper conductor as one might have thought. Thus the outer copper conductor at Jupiter Inlet was in contact with the armour which makes this a bi-metal armour–copper contact. There may therefore be significant electrode noise in the JI–SP and JI–BK voltages.

The cable–ocean contact for the BK–SP voltages at the cable break was the exposed inner copper conductor. Unfortunately, the copper conductor also appeared to be intermittently in contact with the armour, resulting in abrupt voltage offsets of magnitude 100 mV to 440 mV from 3 March 1983 until 1 October 1985. These changes in the voltage are consistent with the 700 mV difference in contact potential inferred between copper and pure iron from tabulated oxidation potentials. The offsets ceased when a clean cut was made in the cable near the cable break on 1 October 1985, but reoccurred from 10 October 1988 to 20 April 1990. The sections of data with the most offsets occurred from 3 March 1983 to 25 January 1984, 6 March 1985 to 1 October 1985, and 5 July 1989 to 20 April 1990. A sample of the offsets (figure 18*a*, *b*) shows that the offsets consist of an abrupt decrease followed by an offset lasting from a few hours to several days and then terminated by an abrupt return of approximately the same magnitude. A visual inspection of the cable break

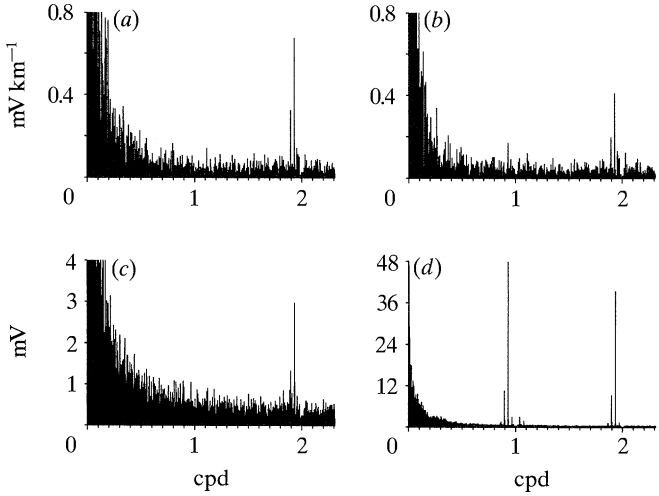

Figure 19. Amplitude spectra of the observed minus geomagnetic induced and solar diurnal variations. (*a*) C18 electric field normal to Straits. (*b*) C18 electric field parallel to Straits. (*c*) JI–BK voltages. (*d*) BK–SP voltages. The diurnal constituents are not present in the C18 normal electric field and in the JI–BK voltages but are prominent in the BK–SP voltages.

Table 5. *Well determined tidal constituents for BK–SP voltages, 8 December 1981 to 29 November 1990, for 10 (355 day) sections*

comp	amp (mV)	std (mV)	spread (mV)	G/deg	std/deg	spread/deg
Q_1	9.92	0.13	0.86	82.2	0.8	5.7
O_1	43.22	0.14	2.27	93.6	0.2	5.7
N_2	10.74	0.11	0.80	220.1	0.6	6.0
M_2	41.86	0.12	0.59	236.0	0.2	0.8

from a submersible showed that the cable break consisted of a tangled mixture of armour and cable confirming the existence of a bi-metal contact.

To locate, estimate and remove these abrupt offsets in the voltages, the geomagnetic-induced and tidal variations were first removed. The spikes in the magnitude squared of the first difference of the voltages were then identified at the 95% confidence level. These spikes were called simple outliers if they clustered in groups of six or less or called offsets otherwise. The magnitude of the offset was then objectively computed by a least squares fit of a sloping straight line to the voltages observed before and after the offset. The offsets were then matched as pairs so that a decrease was always followed by an increase of the same magnitude to prevent any spurious long-term trend. A sample of the correctioned voltages compared with the voltage inferred from the velocity profiling data (figure 18*c*) shows that the corrections have removed the offsets. The JI–BK voltages were also corrected in a similar manner since they were found to be contaminated by erratic changes in the armour–copper contact.

The offsets occurring from October 1988 to April 1990 in the BK–SP voltages have been fewer in number but the offsets have not been as abrupt. This makes it more difficult to accurately remove them. The profiling-derived transports in June 1990 were therefore used to establish the long terms bias voltage. The uncertainty

Table 6. *Well-determined tidal constituents for JI–BK voltages, 8 December 1981 to 21 February 1985, for 3 (355 day) sections*
(Cable length 16.3 km.)

comp	amp (mV)	std (mV)	spread (mV)	G/deg	std/deg	spread/deg
Q_1	0.43	0.07	0.32	125.1	9.9	57.2
O_1	0.21	0.09	0.40	75.9	25.0	113.4
N_2	1.09	0.07	0.25	108.4	3.6	9.4
M_2	3.97	0.09	0.63	108.0	1.2	2.3

Table 7. *Well-determined tidal constituents for JI–SP voltages, 12 March 1969 to 21 July 1974, for 7 (355 day) sections*
(Cable length 113 km.)

comp	amp (mV)	std (mV)	spread (mV)	G/deg	std/deg	spread/deg
Q_1	10.18	0.14	0.74	77.7	0.8	5.8
O_1	44.26	0.20	1.25	89.8	0.3	3.5
N_2	9.31	0.15	0.66	212.3	0.9	3.9
M_2	38.56	0.22	1.17	229.1	0.3	1.9

Table 8. *Well-determined tidal constituents for C18 electric field normal to Straits, 10 November 1982 to 4 May 1983, for 1 (176 day) section*

comp	amp (mV km^{-1})	std (mV km^{-1})	G/deg	std/deg
Q_1	0.026	0.008	125.3	17.9
O_1	0.049	0.008	250.5	9.8
N_2	0.296	0.008	86.8	1.6
M_2	0.668	0.008	116.6	0.7

Table 9. *Well-determined tidal constituents for C18 electric field parallel to Straits, 10 November 1982 to 4 May 1983, for 1 (176 day) section*

comp	amp (mV km^{-1})	std (mV km^{-1})	G/deg	std/deg
Q_1	0.056	0.008	139.2	8.3
O_1	0.169	0.008	91.0	2.8
N_2	0.201	0.009	103.8	2.5
M_2	0.477	0.009	146.6	1.0

Table 10. *Well-determined tidal constituents for KW–HV voltages, 27 April 1972 to 24 March 1973, for 1 (332 day) section*
(Cable length 170 km.)

comp	amp (mV)	std (mV)	G/deg	std/deg
Q_1	17.44	0.38	77.8	1.3
O_1	80.83	0.44	90.4	0.3
N_2	31.90	0.45	266.3	0.8
M_2	141.81	0.52	283.7	0.2

PHILOSOPHICAL TRANSACTIONS OF THE ROYAL SOCIETY A MATHEMATICAL, PHYSICAL & ENGINEERING SCIENCES

Table 11. *Bias voltage adjustments*

bias (mV)	std (mV)	profiling days	dates and comments
−409	27	39	8 Dec 1981 to 15 Dec 1982 cable then disturbed during attempted cable repair
−352	31	39	16 Dec 1982 to 17 Sep 1983 cable then disturbed during attempted cable repair
−373	29	15	18 Sep 1983 to 10 Jan 1984 Ag–AgCl electrode then attached at Settlement Point
404	28	30	11 Jan 1984 to 1 Oct 1985 clean cable cut on 2 Oct 1985
348	39	10	3 Oct 1985 to 10 Oct 1988 offset then started again
524	11	4	11 Oct 1988 to 29 Nov 1990

remaining in the bias of the voltage from July 1989 to February 1990 is probably less than 100 mV or a few Sverdrups based on a comparison with the WP–EM voltage-derived transports.

(*d*) *Tidal variation*

The tidal variation is a major part of the hourly variations in the BK–SP voltages (figure 11*c*) with numerous tidal constituents near 1 and 2 cpd (figure 19*d*). Observations of these tidal variations are used to estimate the tidal velocity needed to correct the profiling velocities, to evaluate the stability of the calibration factor, to estimate the temporal changes in the conductance of the strait, and to estimate and explain the tidal-induced electric current I^*.

The largest tidal constituents that are well separated in frequency from the 1 and 2 cpd frequencies of the solar diurnal variation, for time series longer than a month, are the Q_1, O_1, N_2 and M_2 constituents. These have frequencies 0.8932, 0.9295, 1.8960 and 1.9323 cpd respectively. Estimates of the amplitude and phase of these constituents for the BK–SP, JI–BK, JI–SP, east C18, north C18, and KW–HV data are given in tables 5, 6, 7, 8, 9 and 10, respectively, along with the rms standard deviation based on the continuum in a 0.6 cpd band width about the constituent frequency and the spread in the estimates based on the rms standard deviation of the estimated tidal constituents from overlapping 355-day sections of data relative to their long-term mean.

(*e*) *Conversion of voltage to transport*

The voltage calibration factor C_0 is estimated from the relation $C_0 \Delta\phi_V(t) = T(t)$ (3.3), where T are the profiling derived transports, and $\Delta\phi_V$ are the motion-induced voltages derived from $\Delta\phi_V = \Delta\phi - \Delta\phi_G - \Delta\phi_N$. The $\Delta\phi$ are the observed voltages, $\Delta\phi_G$ are the estimated geomagnetic-induced voltages, and $\Delta\phi_N$ are the estimated corrections to the voltage bias. The calibration factor C_0 is determined by a robust least squares method (Larsen 1989) to improve the statistical significance of the estimated calibration factor, the voltage bias and the error in these estimates.

(i) *Cable Break minus Settlement Point voltages*

The voltage calibration factor, based on 137 daily mean profiling-derived transport values, is found to be $C_0 = 24.42 \pm 0.56$ Sv V^{-1} and the mean voltage bias is $\langle \Delta\phi_N \rangle = -36 \pm 31$ mV after removing the voltage offsets and changes in the bias caused by changes in the cable-ocean contacts for six sections of data (table 11), the geomagnetic-induced voltages, the tidal variations, and the secular change in F_z. The

PHILOSOPHICAL TRANSACTIONS OF THE ROYAL SOCIETY A MATHEMATICAL, PHYSICAL & ENGINEERING SCIENCES

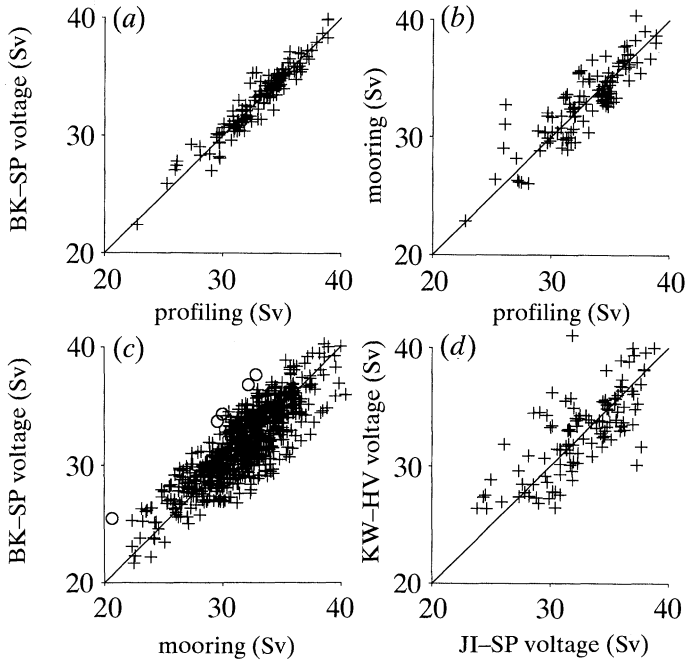

Figure 20. Comparison of different daily mean transports (crosses) excluding outliers (circles). (*a*) Comparison of 137 transports derived from the BK–SP voltage and the velocity profiling data. Correlation squared is 0.94, rms misfit is 0.77 Sv and calibration factor is 24.42 ± 0.56 Sv V^{-1}. (*b*) Comparison of 115 transports derived from current meter and the velocity profiling data. Correlation squared is 0.75 and rms misfit is 1.6 Sv. (*c*) Comparison of 703 transports derived from the BK–SP voltages and the current meter mooring data. Correlation squared is 0.73, rms misfit is 1.7 Sv, and calibration factor is 23.96 ± 0.50 Sv V^{-1}. (*d*) Comparison of 115 transports derived from the KW–HV and the JI–SP voltages. Correlation squared is 0.61, rms misfit is 2.3 Sv, and calibration factor is 26.0 ± 1.7 Sv V^{-1}. The highest correlation and smallest misfit occurs between the BK–SP voltage-derived transports and the profiling-derived transports.

geomagnetic-induced voltage was based on transfer functions and magnetic data from San Juan and Fredericksburg for 1981 to 1988 and magnetic data from Settlement Point for 1988 to 1990. The error in C_0 is $\pm 2.3\%$ and corresponds to a voltage-derived transport error of ± 0.74 Sv for mean transport 32.3 Sv.

The BK–SP voltage-derived transports $C_0 \Delta\phi_V$ compared with the profiling-derived transports (figure 20*a*) yield a correlation squared of 0.94 and a rms misfit of 0.77 Sv. This small misfit is consistent with the 0.93 Sv error based on the 0.84 Sv error in the voltage-derived transport estimated by the profiling data (§3*a*), the circuit model (§2*c*), and the estimated 0.4 Sv error in the profiling-derived transports. This confirms that the BK–SP voltage variations can be used to monitor the transport variations with an accuracy of ± 0.8 Sv.

The BK–SP cable was shortened in October 1985 by an amount less than 0.5 km. A comparison of the dominant tidal constituents in BK–SP before and after October 1985 showed that the amplitude of the M_2 constituent was reduced by $4.8 \pm 0.5\%$, with no significant phase change. The voltage variations after the cable cut were therefore multiplied by the factor 1.048. This 4.8% adjustment is much larger than the 0.3% change in the tidal calibration factor computed by (2.46) for a simple change in length assuming a constant ϵ^* and $\epsilon = 0$. The larger change in the

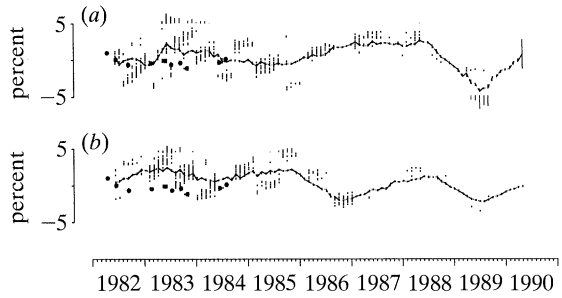

Figure 21. Percentage variation in the amplitude of the (*a*) O_1 tidal and (*b*) M_2 constituents, relative to their long-term average, by 369-day sections advanced by 30-day increments. The vertical bars span two standard deviations. The dots are the percentage variation in the tidal calibration factor inferred from monthly means of the strait temperature based on the profiling temperatures. The stability of the M_2 and O_1 constituents shows that the tidal calibration factor is constant to within a few percent.

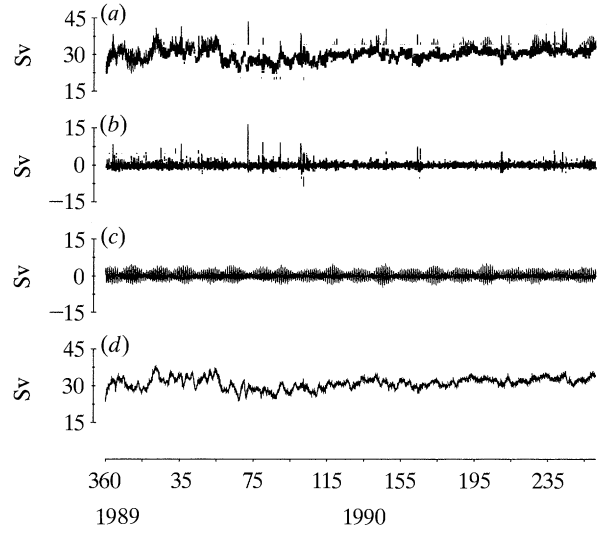

Figure 22. Hourly mean BK–SP voltages in transport units for $C_0 = 24.42\,\mathrm{Sv\ V^{-1}}$. (*a*) Uncorrected values. (*b*) Geomagnetic-induced variations. (*c*) Tidal variation. (*d*) Corrected values. Removing the tidal and geomagnetic-induced variations has significantly smoothed the hourly mean values.

calibration factor can be accounted for, however, by increasing ϵ^* by 0.04. The well determined tidal constituents for the entire corrected BK–SP voltages are given in table 5.

The tidal calibration factor is $C_T = 26.03\,\mathrm{Sv\ V^{-1}}$ derived from C_0 by the use of (2.47) where $\tilde{W}_0/W_0 = 1.066$ based on the profiling data and the circuit model with $\epsilon^* = \tilde{\epsilon}^*$ assumed. The amplitude of the M_2 and O_1 tidal constituents in the BK–SP voltages by 369-day sections advanced by 30 days shows variations that are less than $\pm 2\,\%$ of the long-term mean (figure 21). Thus the tidal calibration factor, C_T, varies by less than $\pm 2\,\%$ over eight years. The changes that do occur could be caused by changes in the temperature of the Straits of Florida but the $\pm 1.4\,\%$ error in the M_2 constituent makes it impossible to deduce the temperature variations with

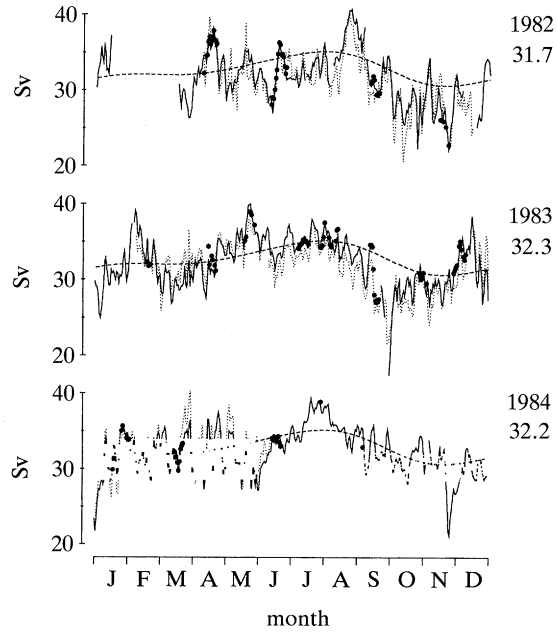

Figure 23. Daily mean transport derived from the BK–SP voltages (solid line), the velocity profiling data east of Jupiter Inlet (dots), and the 40 h low passed current meter data east of Jupiter Inlet (dotted line). The annual variation (dashed line) is based on the 1981–1990 BK–SP voltage-derived transport. The yearly mean is listed to the right of each yearly segment. The three different estimates of the transport are in good agreement.

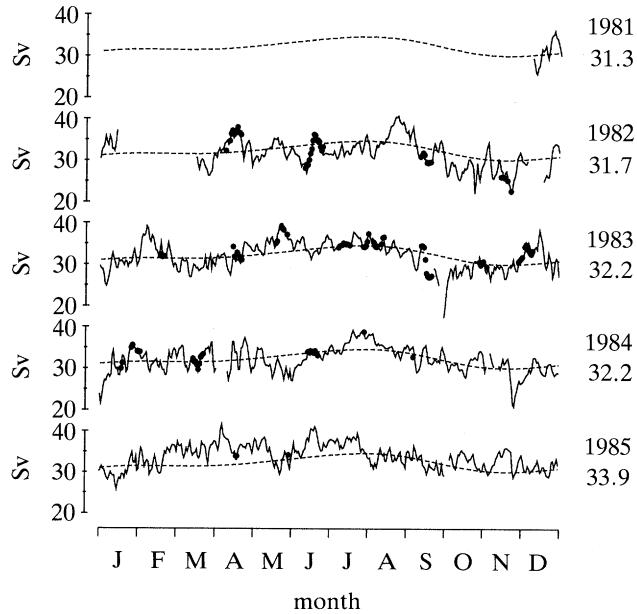

Figure 24. Daily mean transports derived from the BK–SP voltages (solid line) and the velocity profiling data east of Jupiter Inlet (dots) for 1981 to 1985. The annual variation (dashed line) is based on the 1981 to 1990 BK–SP voltage-derived transport. The yearly mean is listed to the right of each yearly segment.

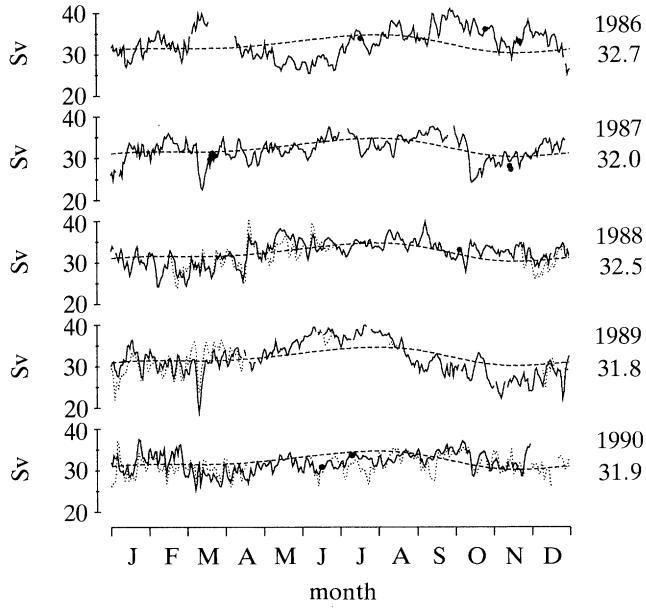

Figure 25. Daily mean transports derived from the BK–SP voltages (solid line), from the velocity profiling data east of Jupiter Inlet (dots), and from the WP–EM voltages (dotted line) for 1981 to 1990. The annual variation (dashed line) is based on the 1981 to 1990 BK–SP voltage-derived transport. The yearly means are listed to the right of each yearly segment.

an accuracy smaller than 1 °C. This is much larger than the 0.6 °C rms deviation found in the profiling temperature data from the Straits of Florida. There is, therefore, only a superficial agreement between the observed changes in the tidal amplitude and the monthly changes inferred from the temperature variations (figure 21). The relative constancy of the tidal calibration factor provides, however, additional confirmation on the accuracy of the BK–SP voltage-derived transports.

The tidal and geomagnetic-induced variations converted to transport units (figure 22) show that these variations dominate the hourly mean values. For the daily mean values, however, the tidal variations vanish but the geomagnetic-induced variations continue to be significant.

The daily mean transports estimated from the BK–SP voltages for 1982 to 1984 are plotted on an expanded scale in figure 23 and all the transports are plotted in figures 24 and 25 together with the annual variation derived from nearly nine years of transport variations. There may be a bias of several Sverdrups in the voltage-derived transports from July 1989 to February 1990 due to an uncertainty in the offset corrections. The mean voltage-derived transport is 32.3 ± 3.0 Sv based on 3124 daily values.

(ii) *Jupiter Inlet minus Settlement Point voltages*

Since there were no profiling-derived transport values east of Jupiter Inlet from 1969 to 1974, the voltage calibration factor for the JI–SP voltages, was set equal to the voltage calibration factor for the BK–SP voltages times a calibration correction factor based on the tidal variation. Daily mean values were computed after removing the geomagnetic-induced voltages, the tidal variation, and the secular change in F_z.

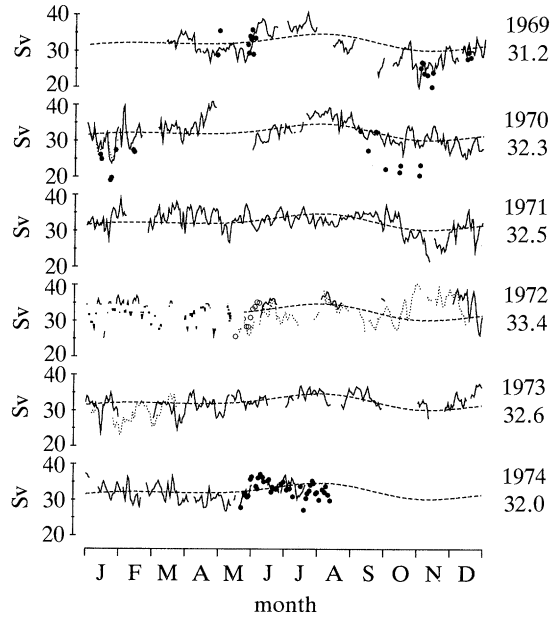

Figure 26. Daily mean transports derived from JI–SP voltages (solid line), KW–HV voltages plus 5 Sv (dotted line), velocity profiling data east of Miami (dots), and velocity profiling data south of Key West (circles). Annual variation (dashed line) based on the 1969–1974 JI–SP voltage-derived transport values. Agreement between the different estimates, although reasonable, is not as good for JI–SP as for BK–SP. The yearly mean is listed to the right of each yearly segment.

The geomagnetic-induced voltages were based on transfer functions and magnetic data from San Juan and Fredericksburg.

Estimates of the calibration correction factor are given by the tidal constituents estimated for the BK–SP voltages divided by the tidal constituents estimated for the JI–BK plus BK–SP voltages (tables 6 and 5). The correction factors for the (Q_1, O_1, N_2, M_2) tidal constituents are (0.97 ± 0.01, 0.995 ± 0.005, 1.03 ± 0.01, 1.059 ± 0.003) with phase differences (-1.6 ± 0.6, 0.1 ± 0.2, 5.6 ± 0.5, 4.5 ± 0.2) degrees respectively. Hence the correction factor is nearly unity with no phase shift for the diurnal constituents but differs from unity for the semi-diurnal constituents because I^* is larger for the semi-diurnal constituents than for the diurnal constituents (§4*b*). The circuit model (§2*c*) yields a correction factor of 0.97. Since the estimates are all approximately one, the calibration correction factor is taken to be unity. Thus the calibration factor for the JI–SP voltages is set equal to 24.42 Sv V^{-1} which is the calibration factor for the BK–SP voltages. The JI–SP voltage-derived transports have then been adjusted to give a mean transport of 32.3 Sv since the bias in the JI–SP voltages is unknown. This amounts to a mean voltage bias correction of $\langle \Delta\phi_N \rangle = -212$ mV.

The variations in the JI–SP voltage-derived transports compare quite well, at times, with the variations in the profiling-derived transport east of Miami (figure 26) but at other times there are large discrepancies. Most of the discrepancy are low values in the profiling-derived transports. The discrepancy could be caused by errors in the voltages and velocity profiling data, by possible transport into the Straits via the Northwest Providence Channel south of Grand Bahama Island, or by the tidal

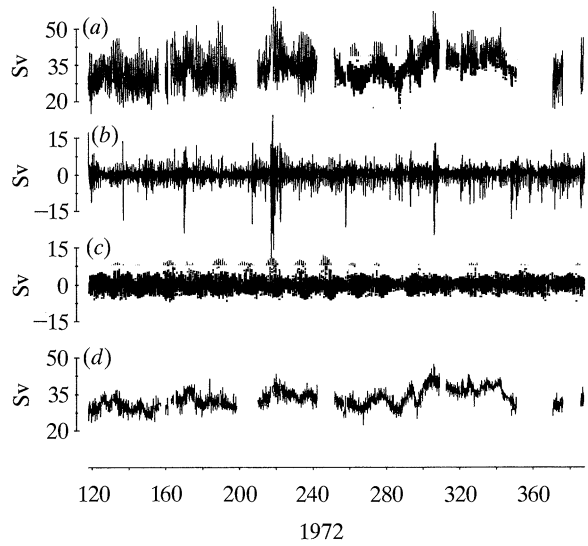

Figure 27. Hourly mean KW–HV voltages in transport units for $C_0 = 26.0$ Sv V^{-1}. (*a*) Uncorrected values. (*b*) Geomagnetic-induced variation. (*c*) Tidal variation. (*d*) Corrected values. The tidal and geomagnetic-induced corrections are much larger for KW–HV than for BK–SP.

variation that was not removed from the profiling data except for the 1974 velocity profiling data. For example, not removing the tidal variation from the 1982–1988 profiling data increased the misfit between the BK–SP voltage-derived transports and the profiling-derived transports by 18%.

(iii) *Key West minus Havana voltages*

Since there were no profiling-derived transport values south of Key West, the voltage calibration factor for the 1972 to 1973 KW–HV voltages was based on the comparison of the KW–HV voltages with the JI–SP voltage-derived transports. The geomagnetic-induced voltages were based on the transfer functions derived for the hourly mean 1972 to 1973 KW–HV voltages and the magnetic data from San Juan and Fredericksburg. The tidal constituents are given in table 10. The hourly mean values of the geomagnetic-induced and tidal variations, converted to transports show that these variations (figure 27*b*, *c*) are approximately three times larger for the hourly mean KW–HV transports than for the hourly mean BK–SP transports (figure 22*b*, *c*). It is therefore important to remove the geomagnetic-induced voltages from the KW–HV voltages.

A comparison of the 1972 to 1973 KW–HV daily mean, motion-induced voltages with the JI–SP voltage-derived transports (figure 20*d*) yields a calibration factor of $C_0 = 26.0 \pm 1.7$ Sv V^{-1}, a correlation squared of 0.61, and a rms misfit of 2.3 Sv. The calibration factor is consistent with the 25.6 Sv V^{-1} assumed by Wertheim (1954) and the values estimated by the circuit model (§2*c*). The value $C_0 = 26.0$ Sv V^{-1} was therefore used to convert the KW–HV voltage to transport. Velocity profiling observations (K. D. Leaman, personal communication) indicate that the transport past Key West is less than the transport past Jupiter Inlet because of flow into the Straits via the Old Bahama Channel north of Cuba and the Northwest Providence Channel south of Grand Bahama Island. The mean KW–HV voltage-derived transports were therefore adjusted to 27.3 Sv which is an arbitrary 5 Sv less than

PHILOSOPHICAL TRANSACTIONS OF THE ROYAL SOCIETY A MATHEMATICAL, PHYSICAL & ENGINEERING SCIENCES

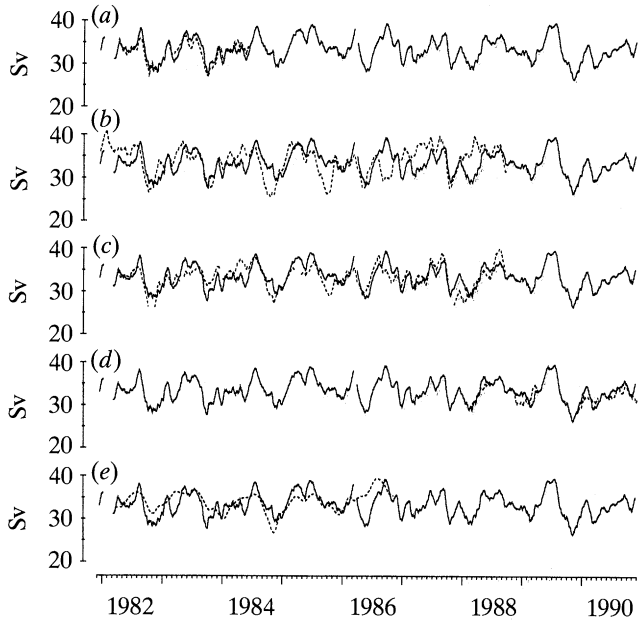

Fig. 28. Monthly mean transports derived from BK–SP voltages (solid curve) compared with the monthly mean transports derived from: (*a*) mooring data; (*b*) Haulover sea level; (*c*) sea level difference based on Cat Cay minus Haulover merged with Settlement Point minus Lake Worth sea level; (*d*) WP–EM voltages; (*e*) and NORDA model driven by monthly winds for transports multiplied by 1.52 and increased by 3.7 Sv (bottom dashed curve). Sea level differences, WP–EM voltages, and mooring data give the best agreement with the BK–SP voltage-derived transports.

the mean BK–SP voltage-derived transport of 32.3 Sv. The mean voltage bias is $\langle \Delta\phi_N \rangle = -371$ mV. The transport variations derived from the 1972 to 1973 KW–HV voltages for $C_0 = 26.0$ Sv V^{-1} and increased by 5 Sv are found to be in reasonably good agreement with the transport variations derived from the 1969 to 1974 JI–SP voltages (figure 26).

The 1952 to 1961 KW–HV published voltage-derived transports (Stommel 1957, 1959, 1961; Broida 1962, 1963) have been revised by removing the daily mean geomagnetic-induced voltages, the tidal variation, and the secular change in F_z, and then applying the calibration factor $C_0 = 26.0$ Sv V^{-1}. The geomagnetic-induced voltages were based on the magnetic data from San Juan alone because the Fredericksburg site was not installed until 1956. The tidal variation was based on the tidal constituents from the 1972 to 1973 KW–HV voltages. The daily mean of the geomagnetic-induced variation lies between -5 Sv and 7 Sv with a rms deviation of 0.9 Sv and the daily mean of the tidal variation lies between -0.4 Sv and 0.4 Sv with a rms deviation of 0.2 Sv. Thus the geomagnetic-induced variation can be an important part of the daily mean estimates of transport but the tidal variation is not. The electrode drift occurring in April 1958 was also removed and the mean transport was then adjusted to yield 27.3 Sv. The mean voltage bias correction is $\langle \Delta\phi_N \rangle = -18$ mV.

Because the KW–HV voltages are sensitive to meanders that could cause a $\pm 28\,\%$ uncertainty in the calibration factor, the KW–HV voltage-derived transport may have an uncertainty as large as ± 8 Sv. They are therefore only marginally useful.

(iv) *West Palm Beach minus Eight Mile Rock voltages*

The voltage calibration factor for the WP–EM voltages is 13.8 ± 0.4 Sv V^{-1} (Larsen 1991) based on comparing the daily mean WP–EM voltages with the daily mean BK–SP voltage-derived transports. The correlation squared between the daily mean values is 0.56 and the correlation squared between the monthly mean values is 0.75. The WP–EM voltage-derived transports were then adjusted so that the mean WP–EM and BK–SP voltages yield the same mean transport.

The WP–EM voltage-derived transports compare favourably, on the long term, with the BK–SP voltage derived transports (figure 25) which means that the WP–EM voltages are reasonably well determined. The monthly mean WP–EM voltage-derived transports have an accuracy of 1 Sv that is adequate for monitoring the transport of the Florida Current (figure 28*e*).

(v) *Jupiter Inlet minus Cable Break voltages and Canal 18 electric field*

A comparison of the motion-induced JI–BK voltages with the profiling derived transports on the shelf east of Jupiter Inlet yields a correlation squared of only 0.07 and a negative voltage calibration factor -0.035 ± 0.005 Sv V^{-1}. This indicates that the JI–BK voltages are unrelated to the transport on the shelf. A comparison of the JI–BK voltages with the BK–SP voltage-derived transports yields a correlation squared of 0.22 and a negative calibration factor of -0.131 ± 0.006 Sv V^{-1}. Thus the JI–BK voltages are essentially unrelated to the total transport and are, in fact, out of phase with the BK–SP voltages. This suggests that the variations in the JI–BK voltages are caused by the variations in the electric current I^*. Hence the JI–BK voltages are not suitable for monitoring the transport variations.

A comparison of the motion-induced C18 electric field normal to the Straits at Jupiter Inlet with the BK–SP voltage-derived transports yields a correlation squared of only 0.14. Since this component of C18 electric field is caused by I^* flowing perpendicular to the stream, the electric field-transport calibration factor C^* (2.28) will be proportional to Y. Thus the small correlation must be caused by variations in Y that are unrelated to variations in the transport. The motion-induced C18 electric field parallel to the Straits at Jupiter Inlet is caused by I^* flowing parallel to the Straits. Since these include I^* generated by remote open ocean sources, the C18 electric field parallel to the Straits will not be directly related to the locally generated I^*. Hence neither components of the shore-based C18 electric field are suitable for monitoring the transport variations.

(*f*) *Voltage-derived transports compared with other estimates*

(i) *Current meter moorings*

Two years (1982–1984) of transport variations east of Jupiter Inlet have been determined from five subsurface current meter moorings approximately 20 km apart with four instruments per mooring (Schott *et al.* 1988; Johns & Schott 1987). The profiling velocities were used to extrapolate the mooring velocities to the surface to obtain the total transport, because the current meters were deeper than 150 m and therefore only sampled 50 % of the transport.

The comparison of 703 daily mean BK–SP voltages with the current meter mooring derived transports (figure 20*c*) gives a voltage calibration factor of 23.92 ± 0.50 Sv V^{-1}. This is consistent with the calibration factor 24.42 ± 0.56 Sv V^{-1} based on the BK–SP voltages and profiling-derived transports. The correlation

PHILOSOPHICAL TRANSACTIONS OF THE ROYAL SOCIETY A MATHEMATICAL, PHYSICAL & ENGINEERING SCIENCES

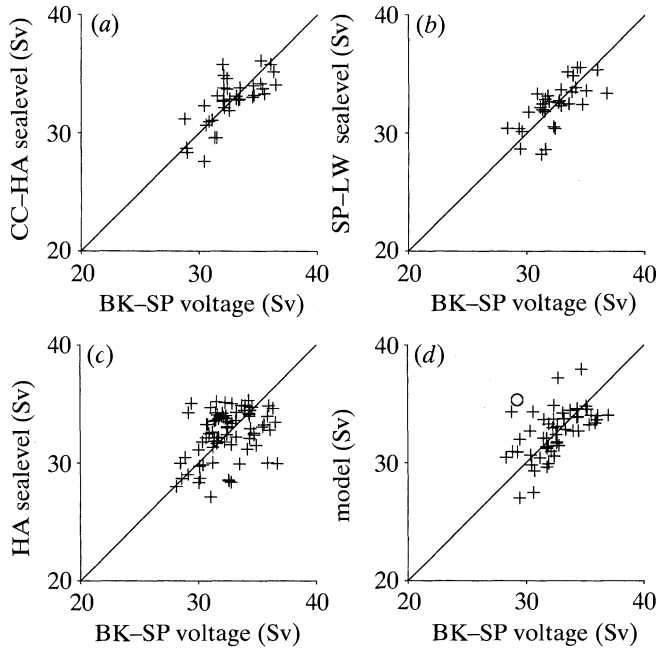

Figure 29. Comparison of various monthly mean transport values (crosses) excluding outliers (circles). (*a*) Comparison of 36 transport values derived from the Cat Cay minus Haulover sea level and the BK–SP voltages. Correlation squared is 0.53, rms misfit is 1.5 Sv, and calibration factor is 24.9 ± 3.1 Sv m^{-1}. (*b*) Comparison of 32 transport values derived from the Settlement Point minus Lake Worth sea level and the BK–SP voltages. Correlation squared is 0.47, rms misfit is 1.6 Sv, and calibration factor is 30.9 ± 4.4 Sv m^{-1}. (*c*) Comparison of 77 transport values derived from the Haulover sea level and the BK–SP voltages. Correlation squared is 0.15, rms misfit is 2.3 Sv, and calibration factor is -25.0 ± 3.2 Sv m^{-1}. (*d*) Comparison of 53 transport values derived from the NORDA model values and the BK–SP voltages. Correlation squared is 0.34 and rms misfit is 1.9 Sv. The variations in the sea level difference correlate better with the voltage-derived transports than the Florida sea level alone.

squared is 0.73 and the rms misfit is 1.74 Sv. The comparison of the mooring-derived transports with the profiling-derived transports (figure 20*b*) yields a correlation squared of 0.75, a rms misfit of 1.62 Sv, and a calibration factor of 1.01 ± 0.05. The smaller correlations and larger rms misfits for the mooring derived transports indicate that these transport estimates are slightly less accurate than the transports derived from the profiling data and the voltages. The mooring derived transports show, for example, a slightly larger daily variation compared to the transports derived from the voltages (figure 23). This is probably due to baroclinic tidal variations not having been completely removed by the vertical averaging of the current meter mooring data. The variations in the monthly mean mooring-derived transports are found, however, to be in excellent agreement (figure 28) with the voltage-derived transports.

In summary, the excellent agreement between the transports derived from the velocity profiling data, the current meter mooring data, and the BK–SP voltages (figure 23) show that these three independent methods for estimating the transport are in excellent agreement. For example, the large 8 Sv change in transport that occurred in June 1982 was accurately tracked by all three estimates of the transport.

(ii) *Sea level*

Sea level variations are related to the transport variations if the variations in the surface flow are correlated with the variations in transport. To determine whether sea level variations are related to transport variations, the sea level differences between Settlement Point, and Lake Worth, Florida, and between Cat Cay, Grand Bahama Island and Haulover, Florida have been compared with the voltage-derived transports. The comparison between the daily mean values for the 1982–1985 Cat Cay minus Haulover sea level difference and the voltage-derived transports yields a correlation squared of 0.44, a rms misfit of 2.6 Sv, and a calibration factor of 27.7 ± 0.7 Sv m^{-1} and, for the 1986–1988 Settlement Point minus Lake Worth sea level difference, a correlation squared of 0.47, a rms misfit of 2.4 Sv, and a calibration factor of 28.8 ± 0.7 Sv m^{-1}. These correlations are much smaller than the correlation between the transports derived from the voltages, profiling, and current meter mooring data. Sea level at Haulover alone yields a correlation squared of 0.22, a rms misfit of 3.4 Sv, and a calibration factor of -28.1 ± 0.6 Sv m^{-1}. Thus the daily mean values of sea level or sea level difference are not very useful for monitoring the daily mean transport. These results agree with Maul *et al.* (1990).

A comparison of the monthly mean values for the 1982–1985 Cat Cay minus Haulover sea level differences yields a correlation squared of 0.53, a rms misfit of 1.5 Sv, and a calibration factor of 24.9 ± 3.1 Sv m^{-1} (figure 29*a*) and, for the 1986–1988 Settlement Point minus Lake Worth sea level differences, a correlation squared of 0.47, a rms misfit of 1.6 Sv, and calibration factor of 30.9 ± 4.4 Sv m^{-1} (figure 29*b*). A comparison of the monthly mean sea level variations at Haulover with the voltage derived transports yields a correlation squared of only 0.17, a rms misfit of 2.3 Sv, and a calibration factor of -25.0 ± 3.2 Sv m^{-1} (figure 29*c*). The monthly mean transports derived from the sea level differences (figure 28*c*) shows that they sometimes track the voltage-derived transports very well but at other times the discrepancy can be as large as 5 Sv. The reasons for the misfit between the sea level difference and the transport may be due to eddies that form along the Florida coast, to lateral shifts in the Florida Current which cause the surface velocity to change because of bottom topography or to changes in the baroclinic structure of the stream.

In summary, the monthly mean sea level difference across the Straits of Florida near Jupiter Inlet or Miami provide monthly mean estimates of transports with a rms accuracy of 1.5 Sv but with discrepancies as large as 5 Sv. The monthly mean transport derived from sea level at Haulover alone (figure 28*b*) shows an even larger misfit with discrepancies as large as 10 Sv. Sea level therefore gives an inferior estimate of the transport compared with the voltage-derived transports.

(ii) *Model transport*

A 1.5 layer general circulation model developed by the Naval Ocean Research and Development Activity (NORDA) (see Rosenfeld *et al.* (1989) for details of model) was spun up by the seasonal winds based on 20 years of Hellerman and Rosenstein winds and 1977–1980 Fleet Numerical Oceanography Center (FNOC) winds. The model was then driven by the monthly mean FNOC winds from 1982 to 1986. The model-derived monthly mean transports for the Straits of Florida, compared with the voltage-derived monthly mean transports (figure 29*d*), yield a correlation squared of 0.34 and a rms misfit of 1.9 Sv. The model transports are too small which requires multiplying them by 1.52 and adding 3.7 Sv to make the model-derived transport

have a mean value of 32.3 Sv. A comparison of the monthly mean values of the rescaled model transport and the voltage-derived transport (figure 28*e*) shows that the variations in the model transport have some similarity to the variations in the voltage-derived transport.

4. Electromagnetic results

Even though the C18 and JI–BK electric fields cannot be used to monitor the transport, they provide valuable information about the conductance of the sediments beneath C18 and JI–BK, the tidal induced electric current I^*, and the downstream wavelengths of the tidal constituents.

(*a*) *Conductance of sediments*

The motion-induced voltage $\Delta\phi_V$, for constant values of sediment conductance τ_0' beneath BK–SP, conductivities σ_0 and $\tilde{\sigma}_0$, electric current effect $\tilde{\epsilon}^*$, and magnitude of the vertical magnetic field F_z, is given by

$$\Delta\phi_V(t) = (1-\tilde{\epsilon}^*)\tilde{\sigma}_0 F_z \int_0^L [\sigma_0 H(x)+\tau_0']^{-1} H(x)\, \bar{V}(x,t)\, \mathrm{d}x \tag{4.1}$$

based on (2.2*a*) and (2.32) for $\epsilon = 0$. The time average of (4.1) can be written as

$$\int_0^L [\sigma_0 H(x)+\tau_0']^{-1} H(x) \langle \bar{V}(x)\rangle\, \mathrm{d}x = T_0[(1-\tilde{\epsilon}^*)\,\tilde{\sigma}_0 F_z C_0]^{-1} \tag{4.2}$$

making use of $C_0\langle\Delta\phi_V\rangle = T_0$. The conductance τ_0' can then be estimated by making use of the profiling derived velocity $\langle\bar{V}(x)\rangle$, the water depth $H(x)$, the observed mean transport $T_0 = 32.3$ Sv, the conductivity values $\sigma_0 = 4.60$ S m^{-1} and $\tilde{\sigma}_0 = 4.83$ S m^{-1} based on the observed temperatures, the calibration factor $C_0 = 24.42 \pm 0.56$ Sv V^{-1}, the magnitude of the vertical magnetic field $F_z = 41\,100$ nT, and an assumed electric current effect $\tilde{\epsilon}^* = 0.1$.

The value of $\tau_0' = 1880 \pm 150$ S was found by successive iterations of (4.2). The average conductivity of the sediments beneath the Straits of Florida east of the cable break is thus $\sigma_0' = 0.47 \pm 0.04$ S m^{-1} if the sediments are 4 km thick as inferred from seismic data for this region (Emery & Uchupi 1984). This relatively high value of the conductivity indicates that the sediments are saturated with seawater. The sediment conductance beneath KW–HV is estimated to be $\tau_0' = 1410$ S based on a conductivity of $\sigma_0' = 0.47$ S m^{-1} and a sediment thickness of 3 km inferred from seismic evidence (Emery & Uchupi 1984).

The conductances beneath JI–BK and C18 relative to the conductance beneath BK–SP are derived from the geomagnetic-induced variations estimated by taking first differences of the time series and removing the tidal variation. An analysis of the electric field components at C18 with the magnetic field components at Jupiter Inlet indicates that the component of the C18 along the direction 102.8° east of north is normal to the Straits east of Jupiter Inlet. The comparison of the C18 electric field normal to the Straits with the BK–SP and JI–BK voltages divided by the cable lengths yields the ratios $E_{\mathrm{C18}}/E_{\mathrm{BK\text{–}SP}} = 7.034 \pm 0.059$ and $E_{\mathrm{C18}}/E_{\mathrm{JI\text{–}BK}} = 3.254 \pm 0.035$. These ratios are related to the conductance ratios between the sites by (2.55). Hence

$$E_{\mathrm{C18}}/E_{\mathrm{BK\text{–}SP}} = \tau_{\mathrm{C18}}'/\tau_0' \quad \text{and} \quad E_{\mathrm{C18}}/E_{\mathrm{JI\text{–}BK}} = \tau_{\mathrm{C18}}'/\tau_{\mathrm{JI\text{–}BK}}'$$

and the sediment conductances are $\tau_{\mathrm{JI\text{–}BK}}' = 1670 \pm 80$ S and $\tau_{\mathrm{C18}}' = 680 \pm 30$ S for

$\tau'_0 = 1880 \pm 150$ S. The value of $\tau'_{\mathrm{JI-BK}}$ agrees with the Spain & Sanford (1987) estimate of 1630 ± 163 S near the Florida coast.

The value of $\tau'_{\mathrm{JI-BK}}$ indicates that the sediments are 3.6 km deep near the Florida coast for $\sigma'_0 = 0.47$ S m^{-1}. This is consistent with the seismic evidence that the sediments close to Florida are less thick (Emery & Uchupi 1984). The value of τ'_{C18} indicates that the sediments beneath the C18 land site, for 3.6 km thickness, have an average conductivity of $\sigma' = 0.19$ S m^{-1}. The smaller conductance of the sediments beneath the land site is due, presumably, to less seawater content and accounts for the onshore electric field normal to the Straits being larger than the offshore electric field normal to the Straits.

The conductance of the sediments beneath each profiling site can be estimated by

$$\Delta\phi_V(t) = (1-\tilde{\epsilon}^*)\, F_z \int_0^L \tilde{\sigma}(x)\,[\bar{\sigma}(x)\,H(x)+\tau'(x)]^{-1}\,H(x)\,\bar{V}(x,t)\,\mathrm{d}x \tag{4.3}$$

modified from (4.1) to allow for variable conductivities and conductance but constant F_z and $\tilde{\epsilon}^*$, and $\epsilon = 0$. Then for $C_0\,\Delta\phi_V(t) = T(t)$ and a linear interpolation of the profiling velocities, one has

$$T(t) = \sum_{n=1}^{9} A_n\,U_n\,\bar{V}(x_n,t) \tag{4.4}$$

that is similar to (3.1) except for the weights

$$U_n = C_0\,(1-\tilde{\epsilon}^*)\,F_z\,\tilde{\sigma}_n[\bar{\sigma}_n\,H_n+\tau'_n]^{-1}, \tag{4.5}$$

where $\tilde{\sigma}_n\,[\bar{\sigma}_n\,H_n+\tau'_n]^{-1}$ approximates $\tilde{\sigma}(x)\,[\tilde{\sigma}(x)\,H(x)+\tau'(x)]^{-1}$.

The weights U_n for the $n = 1, \ldots, 9$ profiling sites are found by a least squares fit between the BK–SP voltage-derived transports $T(t)$ and the depth-averaged profiling velocities $\bar{V}(x_n,t)$ for $C_0 = 24.42$ Sv V^{-1} and water depths $H(x)$. The small value of U_1 indicates that the BK–SP voltages are not sensitive to the velocity variations near the Florida coast because the cable break is 16 km offshore. The $n = 1$ site will therefore be ignored. The conductances τ'_n for $n = 2, \ldots, 9$ (table 3) are derived from (4.5) for $F_z = 41100$ nT and $\tilde{\epsilon}^* = 0.1$. The depths H_n, conductivities $\bar{\sigma}_n, \tilde{\sigma}_n$, and U_n, are listed in table 3. The estimates of τ'_n on the western and eastern sides (table 3) agree with the estimates $\tau'_{n\mathrm{S}}$ by Spain & Sanford (1987) but the estimates in the central part $n = 4, \ldots, 7$ are much smaller. The agreement is considered adequate, however, because the errors in the estimates of τ'_n are quite large due to the poorly determined U_n. In fact, the large errors in the estimates of U_n show that one can assume that $U_n = 1$ for nearly all the sites, which means that the sediments can be approximated by a layer of constant conductance τ'_0.

(*b*) *Tidal induced electric currents*

A comparison of the tidal variation in the JI–BK and C18 data shows that the tidal constituents in the JI–BK voltages (table 6) are nearly in phase with the tidal constituents in the C18 electric field normal to the Straits (table 8). This means that the JI–BK tidal voltages are dominated by the voltage effects of I^*. The actual amount of the tidal-induced electric current I^* in the JI–BK and BK–SP voltages can be estimated from the C18 electric field normal to the Straits because the electric current I^* perpendicular to the stream is essentially continuous, that is, $I^*(x,t) = I^*(t)$; the tidal flow is uniform, $\bar{V}(x,t) = \bar{V}(t)$; and $\tilde{\sigma}_0 = \sigma_0$. The value of ϵ^* is then estimated by the use of (2.54).

The estimated values of ϵ^* for the BK–SP tidal constituents (Q_1, O_1, N_2, M_2) are (0.036 ± 0.021, 0.060 ± 0.004, 0.142 ± 0.016, 0.105 ± 0.005) and the ϵ^* for the JI–BK tidal constituents are (0.08 ± 0.16, 0.74 ± 0.12, 2.02 ± 0.45, 1.67 ± 0.19). Thus the tidal constituents in the BK–SP voltages are almost free of the effects of I^*, but the tidal constituents in the JI–BK voltages are strongly dependent on I^*, especially for the semi-diurnal constituents. A value of ϵ^* greater than unity for JI–BK indicates that I^* is caused by fluid motions outside the region spanned by JI–BK.

The small values of ϵ^* for the tidal motion in the BK–SP voltage, generally less than 10% for the dominant tidal constituents, suggests that the voltage effect of I^* will also be small for the non-tidal, motion-induced BK–SP voltages.

(*c*) *Tidal downstream wavelengths*

The C18 electric field normal to the Straits and the JI–BK voltages are observed to have diurnal tidal constituents that are small compared to the semi-diurnal constituents (figure 19*a*, *c*) but the BK–SP voltages are observed to have diurnal and semi-diurnal tidal constituents that are of nearly equal magnitude (figure 19*d*). The small diurnal variations in C18 normal and JI–BK has the following explanation.

The phase difference between the BK–SP and KW–HV voltages for the (Q_1, O_1, N_2, M_2) tidal constituents (tables 5 and 10) are (4.5 ± 2.1, 3.2 ± 0.5, -46.2 ± 1.4, -47.7 ± 0.4) degrees. Hence the diurnal tidal variations are nearly in phase between the two sites but the semi-diurnal variations are not. Since the C18 electric field E^* normal to the Straits is due to I^*, it is proportional to the transport divided by the downstream wavelength (2.28). Thus a smaller E^* means a larger Y for a given transport. The ratio of the wavelengths between the different tidal constituents is then $Y_1/Y_2 = (\Delta\phi_1 E_2^*)/(\Delta\phi_2 E_1^*)$ where the $\Delta\phi$s are the tidal amplitudes for the BK–SP voltages (table 5) and the E^*s are the tidal amplitudes for the C18 electric field normal to the Straits (table 8). The estimated ratios of the wavelengths are $Y(Q_1)/Y(M_2) = 6 \pm 2$, $Y(O_1)/Y(M_2) = 14 \pm 2$, and $Y(N_2)/Y(M_2) = 0.58 \pm 0.02$. The values of these ratios show that the downstream wavelengths are much larger for the diurnal than for the semi-diurnal constituents. Thus the diurnal variation in C18 normal to the Straits and in the JI–BK voltages are much smaller than the semi-diurnal variation because Y is much larger for the diurnal than for the semi-diurnal tidal variation.

5. Oceanographic results

The analysis in the preceding sections showed that the cross-stream voltages between the cable break 16 km east of Jupiter Inlet and Settlement Point can be used to monitor the transport variations of the Florida Current at 27° N with an error smaller than ± 0.8 Sv. Over 14 years of daily mean values of the transport have been obtained from 1969 to 1974 and 1981 to 1990, which makes this a unique oceanographic time series. This section gives an overview of the transport variations.

(*a*) *Temporal variability in the volume transport*

The frequency content of the transport variations in the Florida Current from 1981 to 1990 has been estimated by comparing the spectra of the daily mean transports for 93 segments of 500 days duration, where each segment is advanced 30 days compared to the previous segment. Each time segment was detrended and then multiplied by a π prolate window. The 95% confidence interval is 0.4 for the lowest frequency band and is 0.2 for the highest frequency band. The common logarithm of the spectra for

PHILOSOPHICAL TRANSACTIONS OF THE ROYAL SOCIETY A MATHEMATICAL, PHYSICAL & ENGINEERING SCIENCES

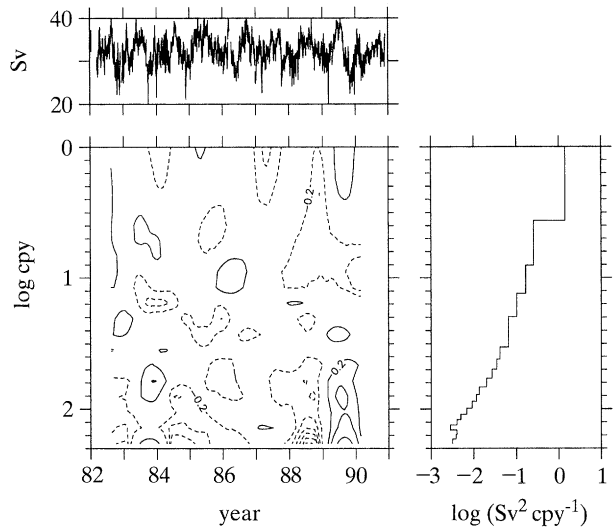

Figure 30. Monthly changes in the power spectra of the transports (bottom left panel) relative to its long term average derived from the 1981 to 1990 BK–SP daily mean voltages (top panel) for 500-day sections multiplied by a π prolate window and advanced by 30-day increments. The common logarithm of the spectrum for each section divided by the averaged spectra (right panel) are contoured by 0.2 increments (bottom left panel) that are equivalent to a 20% change in the spectra relative to the average spectrum and roughly equivalent to the 95% confidence interval. Solid contours are positive and dashed contours are negative. The spectral values vary between −100% and 80%.

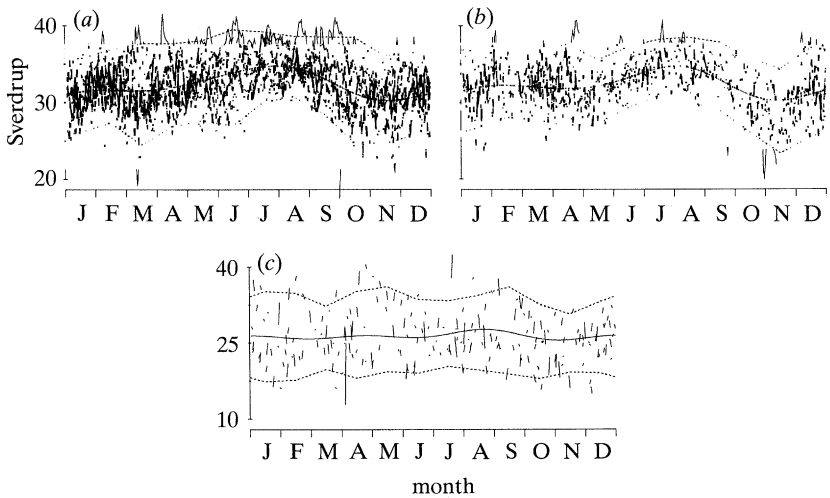

Figure 31. Superposition of yearly segments of daily mean transports. (*a*) 1981 to 1990 BK–SP voltage-derived transports. (*b*) 1969 to 1974 JI–SP voltage-derived transports. (*c*) 1952 to 1961 and 1972 to 1973 KW–HV voltage-derived transports. 95% confidence limits (pair of dashed curves) are based on monthly means. Annual variation (solid smooth curve) is based on frequencies 1, 2 and 3 cpy. The BK–SP and JI–SP voltage-derived transport values have a similar spread in values and similar annual cycle.

each segment divided by the average spectrum are plotted (figure 30) at a contour interval of 0.2 that is roughly equivalent to a 20% change in the spectrum.

The changes in the spectra as a function of time (figure 30) show that the variations are not locked to the yearly cycle, that the changes range from −100 to 60%, that the largest variations occur in the frequency range 0.14 to 0.5 cpd (2-day to 7-day periods), and that the annual variation is relatively constant.

(i) *Events*

The daily transport variations (figures 23–26) contain events that are as large as 10 Sv over time spans as small as a few days. The event during June 1982 showed, for example, an increase of 8 Sv over seven days. The event during October 1987 showed a decrease of 10 Sv over six days.

The superposition of the 10 yearly segments of the 1981–1990 BK–SP voltage-derived transports (figure 31*a*) shows that the transport has a range of 10.8 Sv at the 95% confidence level. Thus a few yearly segments of the transport cannot give a reliable estimate of the transport or its variability. A similar sized range of 9.6 Sv in transport is found for the 1969–1974 JI–SP voltage-derived transports (figure 31*b*).

The KW–HV voltage-derived transports yield a range of 14.8 Sv (figure 31*c*) for a voltage calibration factor $C_0 = 26.0\ \mathrm{Sv\ V^{-1}}$. The variation in the daily values is about 37% larger than the variation in the BK–SP voltage-derived daily transports. The large variability in the KW–HV voltage-derived transports compared with the BK–SP voltage-derived transports and the fairly low correlation squared of 0.61 between the KW–HV and JI–SP voltages for 1972–1973 suggests that the KW–HV voltages are contaminated by meanders flowing across the wide shelf south of Key West. These will increase the variability in the KW–HV voltages and reduce the correlation between the KW–HV and BK–SP voltages.

The circuit model (§2*c*) indicates that meandering effects could cause the calibration factor to be as small as 22.9 Sv $\mathrm{V^{-1}}$. This would reduce the range in daily mean KW–HV voltage-derived transports to 13.0 Sv. Thus, despite the uncertainties in the calibration factor for the KW–HV voltages, the variability of transport east of Jupiter Inlet appears to be smaller than the variability in the transport south of Key West by at least 20%. This indicates that the transport variations undergo a downstream transformation. The downstream decrease in the variations could be caused by some of the variations leaving the Straits via the Old Bahama Channel and the Northwest Providence Channel, or by a nonlinear damping of the variations as the velocity of the stream increases downstream due to the shoaling and narrowing of the Straits. An increase in downstream velocity is known to promote a decrease in the turbulent energy (Hinze 1975).

(ii) *Tidal variation*

Continuity of the tidal transport between Key West and Jupiter Inlet, including sea level changes as deduced from Key West and Jupiter Inlet, indicate that continuity is only satisfied if the tidal calibration factor for the KW–HV voltages has the value $C_\mathrm{T} = 13.0\ \mathrm{Sv\ V^{-1}}$ for the diurnal constituents and the value $C_\mathrm{T} = 9.1\ \mathrm{Sv\ V^{-1}}$ for the semi-diurnal constituents. These values are unrealistically small compared with the estimated value $C_\mathrm{T} = 37.2\ \mathrm{Sv\ V^{-1}}$ derived by the circuit model (§2*c*). Thus the Straits of Florida between Key West and Jupiter Inlet cannot be treated as a closed channel.

The transport values through Old Bahama Channel north of Cuba and the

PHILOSOPHICAL TRANSACTIONS OF THE ROYAL SOCIETY A MATHEMATICAL, PHYSICAL & ENGINEERING SCIENCES

Table 12. *Seasonal variation in transport and heat flux of the Florida Current east of Jupiter Inlet based on 1969–1974 and 1981–1990 voltage-derived transport*
(Heat flux assumes constant flow temperature $\tilde{\theta}_{FC} - \tilde{\theta}_{NA} = 9.61$ °C.)

month	days	transport (Sv)	std (Sv)	heat flux (PW)	std (PW)
Jan	378	31.2	2.6	1.23	0.10
Feb	303	32.3	2.7	1.28	0.11
Mar	364	31.3	3.2	1.24	0.12
Apr	374	32.0	2.8	1.27	0.11
May	364	32.0	2.5	1.26	0.10
Jun	345	32.9	2.9	1.30	0.12
Jul	378	34.5	2.3	1.37	0.09
Aug	362	34.6	2.2	1.37	0.09
Sep	303	33.6	2.8	1.33	0.11
Oct	301	31.3	3.5	1.24	0.14
Nov	330	29.9	3.3	1.18	0.13
Dec	390	31.2	3.0	1.23	0.12
mean	4170	32.2	2.8	1.27	0.11

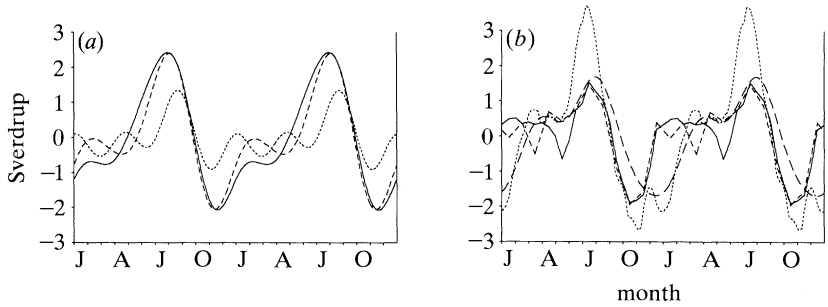

Figure 32. Annual variation in transport based on frequencies 1, 2 and 3 cpy. (*a*) 1981 to 1990 BK–SP voltages (solid curve), 1969 to 1974 JI–SP voltages (dashed curve), 1952 to 1961 KW–HV voltages (dotted curve). (*b*) CME model transport (solid curve), NORDA model transport (long dashed curve), AC model transport (short dashed curve), Kiel model transport (dotted curve).

Northwest Providence channel south of Grand Bahama Island for the tidal constituents (Q_1, O_1, N_2, M_2) are estimated by continuity to be (0.2, 1.1, 0.9, 4.1) Sv for $C_T = 26.0$ Sv V^{-1} applied to the KW–HV voltage whereas the tidal transport values east of Jupiter Inlet are (0.26, 1.15, 0.28, 1.11) Sv. Thus the semi-diurnal tidal transport through the side channel appears to exceed the semi-diurnal tidal transport east of Jupiter Inlet. The combined cross-sectional area of these side channels is estimated to be 41 km^2. This is nearly equal to the cross-sectional area of 43.3 km^2 for the Straits east of Jupiter Inlet. It is thus possible for a significant amount of tidal transport to exit the Straits of Florida through the Old Bahama Channel and Northwest Providence Channel. The existence of these side channels could therefore explain why the non-tidal transport variations east of Jupiter Inlet are different from the transport variations south of Key West.

(iii) *Seasonal and annual variations*

The seasonal variation, based on the monthly mean values of the BK–SP and JI–SP voltage-derived transports, has a 4.6 Sv range with a maximum transport of 34.5 Sv in July and August and a minimum transport of 29.9 Sv in November (table

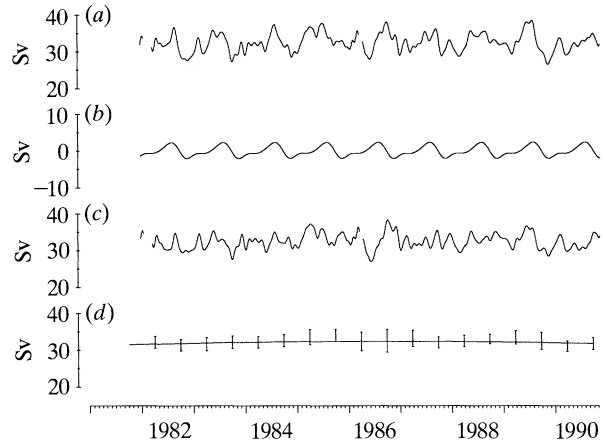

Figure 33. Monthly mean BK–SP voltage-derived transports. (*a*) Monthly mean values. (*b*) Annual variation. (*c*) Monthly mean values minus annual variation. (*d*) Mean and standard deviation of yearly segments advanced by six-month increments (bars). The long-term linear change in the transport is -0.4 ± 1.0 Sv.

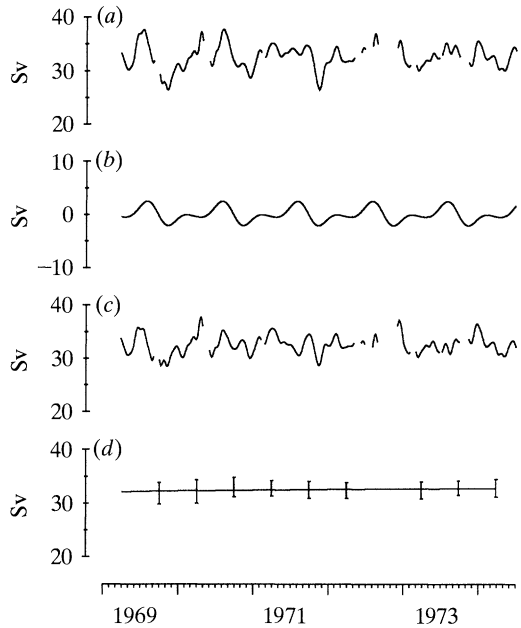

Figure 34. Monthly mean JI–SP voltage-derived transports. (*a*) Monthly mean values. (*b*) Annual variation. (*c*) Monthly mean values minus annual variation. (*d*) Mean and standard deviation of yearly segments (bars). The long-term linear change in the transport is 0.5 ± 0.5 Sv.

12). The annual variation (figure 32*a*), determined by a robust least squares fit of the frequencies 1, 2 and 3 cpy to the voltage-derived transports, has a range of 4.4 Sv for the BK–SP voltage-derived transports, a range of 4.4 Sv for the JI–SP voltage-derived transports, and a range of 2.2 Sv for the KW–HV voltage-derived transports. Thus the annual variation is the same for the BK–SP and JI–SP voltage-derived transports but is larger than the annual variation south of Key West by at least 47 %

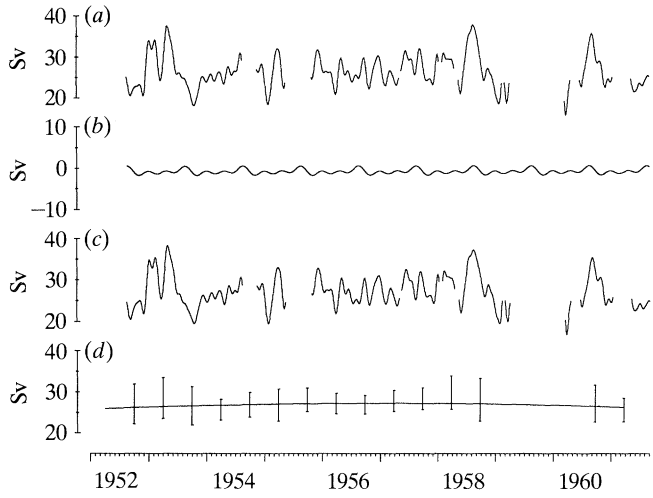

Figure 35. Monthly mean KW–HV voltage-derived transports for $C_0 = 26.0$ Sv V^{-1}. (*a*) Monthly mean values. (*b*) Annual variation. (*c*) Monthly mean values minus annual variation. (*d*) Mean and standard deviation of yearly segments (bars). The long-term linear change in the transport is -0.2 ± 3.0 Sv. The estimated transport variations south of Key West are larger than the transport variations east of Jupiter Inlet.

even if the annual variation is assumed to be confined to the central part of the Florida Straits and therefore has a maximum calibration factor of 35.4 Sv V^{-1} (§2*c*).

The annual variation in transport east of Jupiter Inlet compared with the NORDA model, Anderson–Corry model (Anderson & Corry 1985) community modelling effort (Bryan & Holland 1989), and the Kiel model (Böning *et al.* 1991) (figure 32*b*) shows that the NORDA, Anderson–Corry (AC), and community modelling effort (CME) transports are about 25% too small but that the timing of the minimum and maximum values are in agreement. The seasonal variation in the Kiel model transports are about 40% too large with the maximum occurring about one month earlier than the observed maximum. The Kiel model is the same as the CME model but it is driven by a revised climatological wind based on a revised drag coefficient (20% smaller) and an improved conversion of the Beaufort scale to winds (Böning *et al.* 1991). The AC and CME model transports are nearly identical but are inconsistent with the observed springtime value of the annual variation. The NORDA and Kiel model transports are, however, in closer agreement with the observed springtime values. The conclusion is that all the models need improvements.

The annual variation in the transport south of Key West (figure 32*a*) has a smaller range and smaller springtime transports than the transport east of Jupiter Inlet. This suggests that the annual variation in transport may have a downstream transformation caused by an annual variation in the transports of a few Sverdrups through the Northwest Providence Channel or the Old Bahama Channel. Interestingly, the AC and CME models yield an annual transport variation that is consistent in amplitude and phase with the annual variation in the voltage-derived transport south of Key West (figure 32).

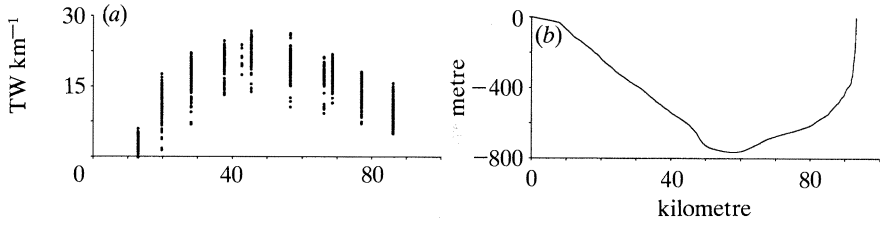

Figure 36. Profiling-derived heat flux for the Straits of Florida east of Jupiter Inlet, assuming the southward flow in the North Atlantic has a constant flow temperature of 9.4 °C. (*a*) Estimated heat flux per kilometre width. (*b*) Channel depth east of Jupiter Inlet to Grand Bahama Island.

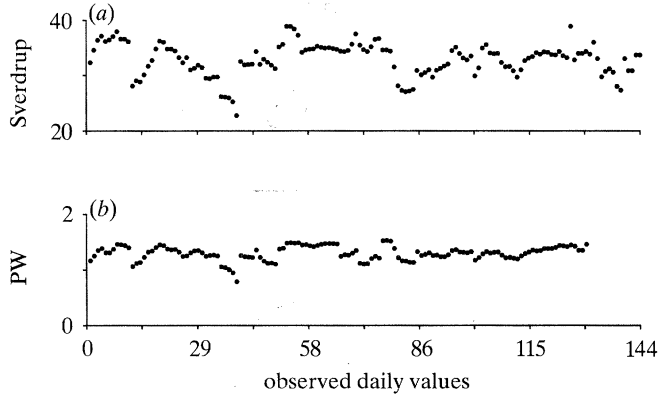

Figure 37. Profiling-derived transport and heat flux listed sequentially with data gaps excluded. There is no apparent long term change in the heat flux from 1982 to 1985.

(iv) *Mean and long-term trend*

The annual mean of the transport for 1981 to 1990 (figure 33*d*), 1969 to 1974 (figure 34*d*), and 1952 to 1961 (figure 35*d*) indicates that the long-term change in transport is less than 0.5 Sv for each time series. A comparison of the profiling-derived transport between 1969–1974 and 1982–1984 together with the spread in values for the 1981–1990 voltage-derived transports (figure 5) suggests that the mean transport east of Miami could be a few Sverdrups smaller than the transport east of Jupiter Inlet. This could be caused by an inadequate sampling of transport or by a downstream increase in the transport due to flow through the Northwest Providence channel.

The mean transport east of Jupiter Inlet, after removing the annual variation, is 32.3 ± 3.2 Sv and the median value is 32.4 Sv based on 4862 daily values from the 1969 to 1990 voltage-derived transports.

(*b*) *Heat flux*

The heat flux into the North Atlantic can be summarized by

$$Q(t) = \rho C_p [\tilde{\theta}_{\mathrm{FC}}(t) - \tilde{\theta}_{\mathrm{NA}}(t)]\, T(t), \tag{5.1}$$

where $\tilde{\theta}_{\mathrm{FC}}(t)$ is the flow temperature of the northward moving Florida Current, $\tilde{\theta}_{\mathrm{NA}}(t)$ is the flow temperature of the southward moving North Atlantic east of the Straits of Florida, and $T(t)$ is the transport of the Florida Current. It is assumed here that $\tilde{\theta}_{\mathrm{NA}}$

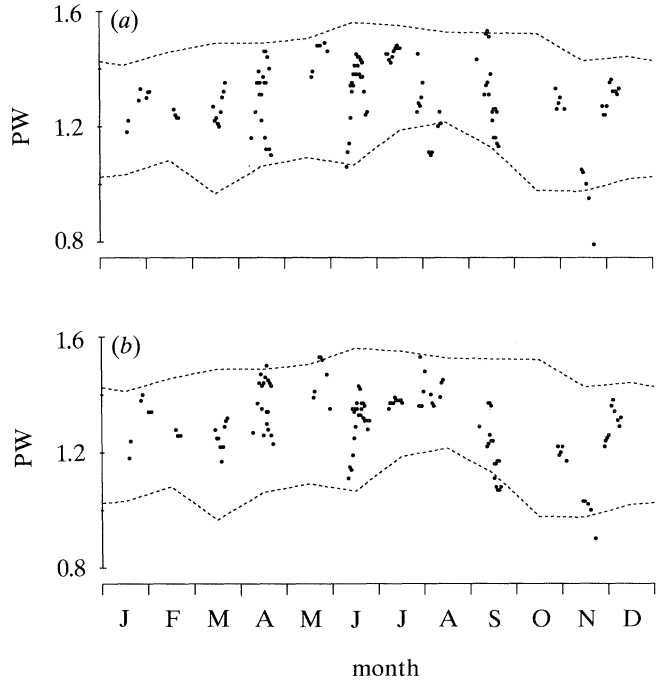

Figure 38. Profiling-derived heat flux estimates assuming the southward flow in the North Atlantic has a constant flow temperature of 9.4 °C. (*a*) Heat flux based on time varying flow temperature and transport of Florida Current. (*b*) Heat flux based on a constant flow temperature of 19.1 °C for Florida Current and a time varying transport. The consistency of the two different estimates confirms the assumption of a constant flow temperature for the Florida Current. Pair of dashed curves are 95% confidence limits based on the 1981–1990 voltage-derived heat flux.

has the constant value 9.43 °C. This value is derived from the heat flux estimated for the Atlantic (Molinari *et al.* 1990). The factor ρC_p is essentially a constant equal to 0.00409 PW °C^{-1} Sv^{-1} (Cox & Smith 1959). The heat flux estimates and conductivity values are based on *in situ* temperatures. Estimates of the total energy flux are based on potential temperatures (Bryan 1962) but since the Florida Current is shallow the difference between *in situ* and potential temperature will be small and negligible.

The flow temperature observed at the various profiling sites (figure 7*a*) shows that most of the temperature variations occur in the coastal region but that the dominant contribution to the heat flux per kilometre width comes from the central portion of the Florida Current (figure 36*a*). Hence it is only necessary to observe the heat flux variations from the central portion of the stream. The profiling data yield a flow temperature of 19.10 ± 0.63 °C and a strait temperature of 16.88 ± 0.66 °C (§3*a*). The Florida Current is therefore a warm current of nearly constant temperature (figure 8) which means that the variations in heat flux are caused mainly by variations in the volume transport. The heat flux can therefore be approximated by

$$Q(t) = \rho C_p [\tilde{\theta}_{\mathrm{FC}} - \tilde{\theta}_{\mathrm{NA}}] T(t), \tag{5.2}$$

where $\tilde{\theta}_{\mathrm{FC}} - \tilde{\theta}_{\mathrm{NA}}$ is a constant equal to 9.61 °C = 19.10 − 9.43 °C.

The mean heat flux estimated by (5.1) and (5.2) for 130 days of profiling data from 1982–1985 is 1.30 ± 0.13 PW and 1.30 ± 0.12 PW respectively. The correlation squared between the variations in the two heat flux estimates is 0.64 and the rms misfit is

0.08 PW. Thus (5.2) for a constant Florida Current flow temperature is a reasonably good approximation of (5.1). The heat flux by (5.2) for the 1981–1990 voltage-derived transports is 1.27 ± 0.15 PW for mean transport 32.3 Sv. The above estimates of the mean heat flux agree with the 1.22 PW heat flux determined by Hall & Bryden (1982) and the 1.21 ± 0.34 PW determined by Molinari *et al.* (1990). A sequential plot of the profiling-derived heat flux, with data gaps excluded (figure 37), shows that there is no long-term trend. Most of the variability occurs on a timescale of a few days.

The seasonal variation in the heat flux is barely detectable (figure 38) with a suggestion of slightly higher heat flux occurring during September and slightly smaller values occurring from November through March. This is consistent with the seasonal variation in heat flux based on the voltage-derived transports (table 12) but is not consistent with the seasonal heat flux variation derived by Molinari *et al.* (1990). Their heat flux estimates imply that $\tilde{\theta}_{\mathrm{FC}} - \tilde{\theta}_{\mathrm{NA}}$ has a range of 7.8 °C and a rms deviation of 2.3 °C. This seems excessively large and is probably caused by uncertainty in their estimate of the heat flux for the geostrophic baroclinic motion. Their baroclinic heat flux estimates account for about 70% of the estimated rms deviation in $\tilde{\theta}_{\mathrm{FC}} - \tilde{\theta}_{\mathrm{NA}}$.

The effect of changes in heat flux on the North Atlantic can be evaluated by estimating the temperature change in the North Atlantic corresponding to a typical Florida Current transport variation, assuming the Florida Current mixes with the North Atlantic surface waters down to the thermocline. A transport change of ΔT, for a duration of Δt at a constant flow temperature difference of $\tilde{\theta}_{\mathrm{FC}} - \tilde{\theta}_{\mathrm{NA}}$, will then produce a temperature change in the North Atlantic Ocean of

$$\Delta\theta = \Delta T [\tilde{\theta}_{\mathrm{FC}} - \tilde{\theta}_{\mathrm{NA}}] \Delta t / V_{ol}$$

where V_{ol} is the volume of the near surface water. If the Florida Current mixes with the water of the North Atlantic lying between 35.5 and 36.0 ppt, then this volume is approximately 10° latitude by 80° longitude by 100 m depth yielding $V_{ol} = 8 \times 10^{14}$ m^3. Thus if $\Delta T = 10$ Sv for $\Delta t = 30$ days, then $\Delta\theta = 0.3$ °C; if $\Delta T = 5$ Sv for $\Delta t = 4$ months, then $\Delta\theta = 0.6$ °C; and if $\Delta T = 1$ Sv for $\Delta t = 1$ year, then $\Delta\theta = 0.4$ °C. These crude estimates suggest that the observed changes in the transport of the Florida Current could cause significant climatic changes in the North Atlantic if this heat is transferred to the atmosphere and not recirculated.

6. Conclusions

Observations of the voltage across the Straits of Florida at 27° N yield estimates of the transport variations with a rms accuracy of 0.8 Sv that is consistent with the error estimate of 0.9 Sv based on the profiling data and the circuit model. The voltage calibration factor for the BK–SP voltages is $C_0 = 24.42 \pm 0.56$ Sv V^{-1} based on a comparison of the voltages with the profiling-derived transports.

The excellent agreement found between the transport variations derived from the voltages, the velocity profiling data, and the current meter data shows that the voltage variations caused by the meandering of the Florida Current are not important at 27° N. This is because the cable weighting factor is relatively constant across the stream (figure 4*b*, *d*). The BK–SP voltages can therefore be used for long term monitoring of the transport variations.

The meandering of the Florida Current makes it impossible to monitor the

transport by a few current meter moorings and the variations in the downstream wavelengths of the flow make it impossible to monitor the transport by a shore-based electric field site.

The KW–HV site is likely to be contaminated by meanders due to the wide shelf south of Key West. Model studies show that the meandering effect can be reduced somewhat if the Key West cable–ocean contact is moved out beyond the 30 km wide shelf. The wide channel and variable bathymetry requires, however, an array of shortspan voltage measurements to remove the spatially varying cable weighting factor W so that accurate transport measurements can be made.

The interpretation of the motion-induced voltages is facilitated because the theory is expressed in terms of the velocity weighted temperature, salinity and conductivity. This yields the voltage-transport equation (2.33) that is interpretable in terms of volume transport, temperature flux, and salinity flux; and a voltage calibration factor C (2.34) with an error interpretable in terms of changes in the temperature, salinity, and electric currents through the terms ϵ and $\tilde{\epsilon}^*$, where ϵ is caused by time changes in the temperature and salinity of sea water and $\tilde{\epsilon}^*$ is caused by the horizontal electric currents I^* that depend critically on the downstream wavelength of the transport variations. The calibration factor will therefore only be a time invariant constant when the variations of the temperature and salinity of the Straits of Florida are small and when the downstream wavelengths are relatively time invariant and much larger than the stream width.

The experimental results show that the best cross-stream voltage sites are those, such as the BK–SP site, where the stream is locally straight over a nearly uniform bottom topography, the sediment conductance is relatively large, the voltages are measured perpendicular to the stream, the cable–ocean contacts are close to the boundaries of the stream but outside the shelf regions, and the cable–ocean contacts are Ag–AgCl electrodes.

Voltages measured from a long cable will not be suitable for observing the transport variations of narrow streams when the cable–ocean contacts are far from the edges of the stream because the horizontal electric current I^* will short out the voltage variations. Voltages from a long cable may be useful, however, for observing variations in volume transport and heat flux of broad scale flows.

A comparison of the tidal variations in the cross-stream voltages and the electric field from a land site indicates that there are significant differences in I^* between the diurnal and semi-diurnal constituents. The I^* is much smaller for the diurnal constituents because its downstream wavelength is much larger than the downstream wavelength for the semi-diurnal constituents. The effect of I^* for the dominant tidal constituents is, however, less than $10 \pm 1\,\%$ for the BK–SP voltages indicating that the voltage effect of I^* is probably minor for the BK–SP voltage-derived transport. The voltage effect of I* dominates the JI–BK voltages, however, which means that I^* needs to be considered when interpreting ocean electric fields measured in regions adjacent to strong ocean streams.

The various wind-generated general circulation models yield annual variations that are only roughly consistent with the annual variation in the voltage-derived transport of the Florida Current east of Jupiter Inlet at 27° N. This indicates the need for further improvements in the models and the wind estimates. The annual variation in transport south of Key West appears to be different but more observations are needed of the KW–HV voltages together with profiling derived transports before the transport variations south of Key West can be accurately

PHILOSOPHICAL TRANSACTIONS OF THE ROYAL SOCIETY A MATHEMATICAL, PHYSICAL & ENGINEERING SCIENCES

established. The accuracy of transports derived from the KW–HV voltages are likely, however, to be inferior to the transports derived from the BK–SP voltages because the KW–HV voltages are likely to be contaminated by meandering effects.

The mean voltage-derived transport east of Jupiter Inlet is 32.3 ± 3.2 Sv based on 4862 daily mean values from 1969 to 1990. There has been no detectable trend to within ± 0.5 Sv over the past two decades. The seasonal variation has a range of 4.4 Sv, which is only 14% of the mean. The transport is, however, highly variable on shorter timescales with month-to-month changes as large as 15 Sv or 50% of the mean. The tidal transport has a maximum range of 7 Sv and the constituents O_1, K_1, and M_2 each have a range of about 2 Sv in transport.

The heat flux is 1.27 ± 0.15 PW based on the mean transport of 32.3 Sv, a Florida Current flow temperature of 19.1 °C, and a North Atlantic flow temperature of 9.43 °C. This value is consistent with the heat flux of 1.30 ± 0.13 PW based on 130 days of profiling temperature and velocity. Because the flow temperature has a nearly constant value of 19.10 ± 0.62 °C, the heat flux variations are caused mostly by transport variations.

Despite the uncertainty in the KW–HV voltage calibration factor, the voltage-derived transport variations south of Key West and east of Jupiter Inlet show that the variation in the daily values decreases downstream by at least 20% and the annual variation increases downstream by at least 47%.

This project was successful because of the dedicated support of numerous co-workers. I thank Tom Sanford for lending me his Jupiter Inlet minus Settlement Point 1969–1974 and Key West minus Havana 1972–1973 voltage recordings, Mark Bushell, Robert Molinari and Kevin Leaman for the use of their profiling data, Rainer Zantopp and Friedrich Schott for their transport values derived from the mooring data, George Maul and Dennis Mayer for their sea level data, Dana Thompson for the NORDA model transports of the Florida Current, Claus Böning for model seasonal transports of the Florida Current, William Woodward, Hugh Milburn, Roy Newman and Alex Nakamura for engineering support, Ansley Manke for programming support, Dai McClurg and Agusta Flosadottir for reviewing the manuscript, and Allison McLean and Ryan Whitney for typing the manuscript.

References

Anderson, D. L. T. & Corry, R. A. 1985 Seasonal transport variations in the Florida Straits: A model study. *J phys. Oceanogr.* **15**, 773–786.

Baines, P. G. & Bell, R. C. 1987 The relationship between ocean current transports and electric potential differences across the Tasman Sea, measured using an ocean cable. *Deep-Sea Res.* **34**, 531–546.

Böning, C. W., Döscher, R. & Isemer, H. 1991 Monthly mean wind stress and Sverdrup transports in the North Atlantic: A comparison of the Hellerman-Rosenstein and Isemer-Hasse climatologies. *J. phys. Oceanogr.* **21**, 221–235.

Broida, S. 1962 Florida Straits transports, April 1960–January 1961. *Bull. Mar. Sci. Gulf Carib.* **12**, 168.

Broida, S. 1963 Florida Straits transports, May 1961–September 1961. *Bull. Mar. Sci. Gulf Carib.* **13**, 58.

Brooks, I. H. 1979 Variations in the transport of the Florida Current at periods between tidal and two weeks. *J. phys. Oceanogr.* **9**, 1048–1053.

Brooks, I. H. & Niiler, P. P. 1975 The Florida Current at Key West: Summer 1972. *J. Mar. Res.* **33**, 83–92.

Bryan, F. O. & Holland, W. R. 1989 A high-resolution simulation of the wind- and thermohaline-driven circulation in the North Atlantic Ocean. In *Proc. 'Aha Huliko'a*, Hawaiian Winter Workshop, University of Hawaii. Hawaii Institute of Geophysics Special Publication.

PHILOSOPHICAL TRANSACTIONS OF THE ROYAL SOCIETY A MATHEMATICAL, PHYSICAL & ENGINEERING SCIENCES

Bryan, K. 1962 Measurements of meridional heat transport by ocean currents. *J. geophys. Res.* **67**, 3403–3414.

Chapman, S. & Bartels, J. 1940 *Geomagnetism*, vol. 1. Oxford: Clarendon Press.

Chave, A. D., Filloux, J. H., Luther, D. S., Law, L. K. & White, A. 1989 Observations of motional electromagnetic fields during EMSLAB. *J. geophys. Res.* **94**, 14153–14166.

Chave, A. D., Flosadottir, A. H. & Cox, C. S. 1990 Some comments on seabed propagation of ULF/ELF electromagnetic fields. *Radio Science* **25**, 825–836.

Chave, A. D. & Luther, D. S., 1990 Low-frequency, motionally induced electromagnetic fields in the ocean. 1. Theory. *J. geophys. Res.* **95**, 7185–7200.

Cox, C. S. 1980 Electromagnetic induction in the oceans and inferences on the constitution of the earth, *Geophys. Surveys* **4**, 137–156.

Cox, C. S., Constable, S. C., Chave, A. D. & Webb, S. C. 1986 Controlled-source electromagnetic sounding of the oceanic lithosphere. *Nature, Lond.* **320**, 52–54.

Cox, C. S., Filloux, J. H. & Larsen, J. C. 1970 Electromagnetic studies of ocean currents and electrical conductivity below the ocean-flow. *The seas* (ed. A. Maxwell), vol. 4, ch. 17, pp. 637–693. New York: John Wiley and Sons.

Cox, R. A. & Smith, N. D. 1959 The specific heat of seawater. *Proc. R. Soc., Lond.* **252**, 51–62.

Dunbar, M. J. 1962 The living resources of northern Canada. In *Proc. R. Soc. Can. Symp. on Canadian population and northern colonization* (ed. Bulden), pp. 125–135. University of Toronto Press.

Emery, K. O. & Uchupi, E. 1984 *The geology of the Atlantic Ocean*. New York: Springer-Verlag.

Faraday, M. 1832 Bakerian Lecture: Experimental researches in electricity – second series. *Phil. Trans. R. Soc. Lond.* **122**, 163–194.

Filloux, J. H. 1987 Instrumentation and experimental methods for oceanic studies. In *Geomagnetism* (ed. J. Jacobs), vol. 1, ch. 3, pp. 143–248. London: Academic Press.

Fofonoff, N. P. & Millard, R. C. 1983 Algorithms for computation of fundamental properties of seawater. *UNESCO Tech. Pap. Mar. Sci.* **44**, 6–14.

Hall, M. M. & Bryden, H. L. 1982 Direct estimates and mechanisms of ocean heat transport. *Deep Sea Res.* **29**, 339–359.

Harvey, R. R., Larsen, J. C. & Montaner, R. 1977 Electric field recording of tidal currents in the Strait of Magellan. *J. geophys. Res.* **82**, 3472–3476.

Hinze, J. O. 1975 *Turbulence*, 2nd edn. New York: McGraw-Hill.

Johns, W. E. & Schott, F. A. 1987 Meandering and transport variations of the Florida Current. *J. phys Oceanogr.* **17**, 1128–1147.

Larsen, J. C. 1968 Electric and magnetic fields induced by deep sea tides. *Geophys. J. R. astr. Soc.* **16**, 47–70.

Larsen, J. C. 1973 An introduction to electromagnetic induction in the ocean. *Phys. Earth Planet. Inter.* **7**, 389–398.

Larsen, J. C. 1974 Note on determining hourly mean values. *J. Geophys.* **40**, 255–257.

Larsen, J. C. 1980 Electromagnetic response functions from interrupted and noisy data. *J. Geomag. Geoelectr.* **32**, suppl. I, 89–103.

Larsen, J. C. 1989 Transfer functions: smooth robust estimates by least-squares and remote reference methods. *Geophys. J. Int.* **99**, 645–663.

Larsen, J. C. 1991 Transport measurements from in-service undersea telephone cables. *IEEE J. Oceanic Engng* **16**, 313–318.

Larsen, J. C. & Sanford, T. B. 1985 Florida Current volume transport from voltage measurements. *Science* **227**, 302–304.

Leaman, K. D., Molinari, R. L. & Vertes, P. S. 1987 Structure and variability of the Florida Current at 27° N: April 1982–July 1984. *J. phys. Oceanogr.* **17**, 566–583.

Lilley, F. E. M., Filloux, J. H., Bindoff, N. L., Ferguson, I. J. & Mulhearn, P. J. 1986 Barotropic flow of a warm-core ring from seafloor electric measurements. *J. geophys. Res.* **91**, 12979–12984.

PHILOSOPHICAL TRANSACTIONS OF THE ROYAL SOCIETY A MATHEMATICAL, PHYSICAL & ENGINEERING SCIENCES

Longuet-Higgins, M. S. 1949 The electrical and magnetic effect of tidal streams. *Mon. Not. R. astr. Soc.* **5**, 285–307.

Longuet-Higgins, M. S., Stern, M. E. & Stommel, H. 1954 The electrical field induced by ocean currents and waves, with applications to the method of towed electrodes. *Pap. Phys. Oceanogr. Met.* **13**, 1–37.

Luther, D. S., Chave, A. D. & Filloux, J. H. 1987 BEMPEX: A study of barotropic ocean currents and lithospheric electrical conductivity. *EOS* **68**, 618–619, 628–629.

Malkus, W. V. R. & Stern, M. E. 1952 Determination of ocean transport and velocities by electromagnetic effects. *J. Mar. Res.* **11**, 97–105.

Maul, G. A., Mayer, D. A. & Bushnell, M. 1990 Statistical relationships between local sea level and weather with Florida-Bahamas Cable and Pegasus measurements of Florida Current volume transport. *J. geophys. Res.* **95**, 3287–3296.

Molinari, R. L., Johns, E. & Festa, J. F. 1990 The annual cycle of meridional heat flux in the Atlantic Ocean at 26.5° N. *J. phys. Oceanogr.* **20**, 476–482.

Niiler, P. P. & Richardson, W. S. 1973 Seasonal variability of the Florida Current. *J. Mar. Res.* **31**, 144–167.

Parker, R. L. 1980 The inverse problem of electromagnetic induction: existence and construction of solutions based on incomplete data. *J. geophys. Res.* **85**, 4421–4428.

Parker, R. L. & Whaler, K. A. 1981 Numerical methods for establishing solutions to the inverse problem of electromagnetic induction. *J. geophys. Res.* **86**, 9574–9584.

Richardson, W. S. & Schmitz, W. J. 1965 A technique for the direct measurement of transport with application to the Straits of Florida. *J. Mar. Res.* **23**, 172–185.

Robinson, I. S. 1976 A theoretical analysis of the use of submarine cables as electromagnetic oceanographic flowmeters. *Phil. Trans. R. Soc. Lond.* A **280**, 355–396.

Robinson, I. S. 1977 A theoretical model for predicting the voltage response of the Dover-Sangatte cable to typical tidal flows. In *A voyage of discovery* (suppl. to *Deep Sea Res.*, ed. M. Angel), pp. 367–39. Oxford: Pergamon Press.

Rosenfeld, L. K., Molinari, R. L. & Leaman, K. D. 1989 Observed and modelled annual cycle of transport in the Straits of Florida and east of Abaco Island, the Bahamas (26.5° N) *J. geophys. Res.* **94**, 4867–4878.

Sanford, T. B. 1967 Measurement and interpretation of motional electric fields in the sea. Ph.D. thesis, Massachussetts Institute of Technology.

Sanford, T. B. 1971 Motionally-induced electric and magnetic fields in the sea. *J. geophys. Res.* **76**, 3476–3492.

Sanford, T. B. 1982 Temperature transport and motional induction in the Florida Current. *J. Mar. Res.* **40**, suppl., 621–639.

Sanford, T. B. & Flick, R. E. 1975 On the relationship between transport and motional electric potentials in broad, shallow currents. *J. Mar. Res.* **33**, 123–139.

Sanford, T. B. & Schmitz, W. J., Jr. 1971 A comparison of direct measurements and G.E.K. observations in the Florida Current off Miami. *J. Mar. Res.* **29**, 347–359.

Schmitz, W. J. Jr. & Richardson, W. S. 1968 On the transport of the Florida Current. *Deep Sea Res.* **15**, 679–693.

Schott, F. A., Lee, T. N. & Zantopp, R. 1988 Variability of structure and transport of the Florida Current in the period range of days to seasonal. *J. phys. Oceanogr.* **18**, 1209–1230.

Spain, P. & Sanford, T. B. 1987 Accurately monitoring the Florida Current with motionally-induced voltages. *J. Mar. Res.* **45**, 843–870.

Stommel, H. 1948 The theory of the electric field induced in deep ocean currents. *J. Mar. Res.* **7**, 386–392.

Stommel, H. 1957 Florida Straits transports: 1952–1956. *Bull. Mar. Sci. Gulf Carib.* **7**, 252–254.

Stommel, H. 1959 Florida Straits transports: June 1956–July 1958. *Bull. Mar. Sci. Gulf Carib.* **9**, 222–223.

Stommel, H. 1961 Florida Straits transports: July 1958–March 1959. *Bull. Mar. Sci. Gulf Carib.* **11**, 318.

PHILOSOPHICAL TRANSACTIONS OF THE ROYAL SOCIETY A MATHEMATICAL, PHYSICAL & ENGINEERING SCIENCES

Wertheim, G. K. 1954 Studies of the electrical potential between Key West, Florida and Havana, Cuba. *Trans. Am. geophys. U.* **35**, 872–882.

Wunsch, C., Hansen, D. V. & Zetler, B. D. 1969 Variations of the Florida Current inferred from sea level records. *Deep Sea Res.* **16**, suppl. 447–470.

Weidelt, P. 1972 The inverse problem of geomagnetic induction. *Z. Geophysik.* **38**, 257–289.

Received 14 November 1990; accepted 21 March 1990

PHILOSOPHICAL TRANSACTIONS OF THE ROYAL SOCIETY A MATHEMATICAL, PHYSICAL & ENGINEERING SCIENCES